

UNIVERSITÀ DEGLI STUDI DI MILANO
Facoltà di Scienze Matematiche, Fisiche e Naturali
Corso di laurea magistrale in Fisica



THE GLUEBALL SPECTRUM IN THE LARGE- N LIMIT

Relatore: Prof. Sergio Caracciolo
Relatore est.: Dott. Biagio Lucini
Correlatore est.: Dott. Antonio Rago

PACS: 11.15.*Ha*, 11.15.*Pg*
12.38.*Gc*, 12.39.*Mk*

Tesi di laurea di
Rinaldi Enrico
matricola 733530

Anno Accademico 2008 – 2009

Contents

| | |
|--|------------|
| Introduzione | iii |
| 1 Introduction to Lattice Gauge Theories (LGT) | 1 |
| 1.1 Feynman Path Integral and Euclidean Field Theory | 1 |
| 1.1.1 A quantum mechanics example | 1 |
| 1.1.2 Functional integrals in Quantum Field Theory | 3 |
| 1.1.3 Euclidean Field Theory | 5 |
| 1.1.4 Lattice discretization | 6 |
| 1.2 Gauge theories on the lattice | 9 |
| 1.2.1 Pure Yang–Mills (YM) theories: continuum formulation | 9 |
| 1.2.2 Pure Yang–Mills (YM) theories: lattice formulation | 13 |
| 1.2.3 Gauge–invariant lattice path integral | 17 |
| 1.3 Critical points and the <i>quantum</i> continuum limit | 19 |
| 1.3.1 β function and asymptotic freedom | 19 |
| 1.4 Finite temperature lattice gauge theories | 21 |
| 2 Motivations for a large-N study | 23 |
| 2.1 Pure YM and QCD in $3 + 1$ dimensions | 23 |
| 2.2 $1/N$ expansion and planar graphs | 24 |
| 2.3 The gauge/gravity correspondence | 28 |
| 3 Setting the physical scale | 33 |
| 3.1 Fixing the lattice spacing | 33 |
| 3.2 The deconfinement transition in LGT | 34 |
| 3.2.1 Center symmetry and the order parameter | 35 |
| 3.2.2 Description of the phase transition | 36 |
| 3.3 Locating the phase transition | 39 |
| 3.3.1 Finite size study | 40 |

| | | |
|----------|---|------------|
| 3.4 | Results for SU(5) and SU(7) | 41 |
| 3.4.1 | Reweighting and error estimation | 47 |
| 3.4.2 | The thermodynamic limit | 53 |
| 4 | Glueballs operators methodology | 57 |
| 4.1 | Glueballs masses on the lattice | 57 |
| 4.1.1 | Euclidean correlators: effective masses | 57 |
| 4.1.2 | Operators with a physical size | 60 |
| 4.1.3 | Effective mass minimization | 64 |
| 4.2 | Constructing glueballs operators | 66 |
| 4.2.1 | Cubic group rotations | 66 |
| 4.2.2 | Operators for glueball states | 69 |
| 4.3 | Mixing with other states | 74 |
| 4.3.1 | Two glueballs scattering states | 74 |
| 4.3.2 | Torelon pairs mixing | 76 |
| 5 | Numerical simulations and data analysis | 81 |
| 5.1 | Monte–Carlo simulations | 81 |
| 5.2 | Diagonalization and numerical issues | 83 |
| 5.3 | The glueball spectrum | 84 |
| 5.3.1 | A general overview | 86 |
| 5.3.2 | Scattering states | 95 |
| 5.4 | Large- N extrapolation | 99 |
| 6 | Conclusions and perspectives | 113 |
| | Ringraziamenti | 115 |
| | Bibliography | 122 |

Introduzione

Le teorie di Yang–Mills [1] furono originariamente introdotte per estendere l'elettrodinamica quantistica (QED) con lo scopo di includere gruppi di simmetria non abeliani, in particolare il gruppo di isospin. Si cercava allora una teoria di gauge che spiegasse le proprietà degli adroni a partire dalle simmetrie fondamentali del sistema. Dopo l'introduzione del modello a quark da parte di Gell–Mann e Zweig nel 1964 fu sviluppata la cromodinamica quantistica (QCD), che nel 1972 divenne la teoria fondamentale alla base della fisica adronica [2]. Tuttavia, per rendere conto dello spettro di particelle osservate negli esperimenti, fu necessario assumere che in qualche modo i costituenti elementari della QCD, quark e gluoni, non potessero esistere come stati asintoticamente liberi dello spettro. Quest'ultima affermazione va sotto il nome di *confinamento* ed è una caratteristica della QCD a basse energie (o, equivalentemente, grandi distanze) di cui ancora non si conosce una spiegazione definitiva a partire da principi primi.

Il confinamento può anche essere definito in modo più formale usando argomenti di teoria dei gruppi, la forma del potenziale statico tra una coppia di quark e antiquark, oppure il fatto che i mesoni seguono le traiettorie di Regge. La QCD ha gruppo di gauge $SU(3)$ e i campi che rappresentano i quark (antiquark) trasformano sotto la rappresentazione fondamentale (antifondamentale), mentre i campi di gauge (gluoni) trasformano nella rappresentazione aggiunta. Di conseguenza ai quark è associato un indice di carica (che in QCD si chiama "colore") mentre ai gluoni ne sono associati due. Si può riformulare il confinamento in termini del "colore" delle particelle osservate nello spettro: esse devono trasformare nella rappresentazione banale (per questo vengono anche chiamate singoletti) e devono quindi essere invarianti di gauge. Tra i singoletti di colore ci sono, per esempio, i barioni (composti da 3 quark) e i mesoni (coppie di quark e antiquark), ma anche i gluoni possono essere combinati insieme per creare stati invarianti di gauge. Questi stati legati che contengono solo gradi di libertà gluonici sono le **glueballs**. Lo studio delle glueballs è interessante per approfondire il ruolo giocato dalla dinamica dei campi di gauge nel fenomeno del confinamento.

A causa del confinamento, la costante di accoppiamento diventa sempre maggiore all'aumentare della distanza tra le particelle che interagiscono e al diminuire dell'energia. Per questo motivo, i metodi perturbativi impiegati per analizzare le soluzioni delle teorie di campo, non sono utilizza-

bili nel regime di bassa energia della QCD: la serie perturbativa nella costante di accoppiamento non converge. Al contrario, ad alte energie e piccole distanze, come dentro un protone ad esempio, i quark e i gluoni si comportano come particelle quasi-libere e interagiscono debolmente tra loro. Questo comportamento è dovuto alla cosiddetta libertà asintotica che caratterizza la QCD ad alta energia, ed è legato alla struttura non-abeliana del gruppo di gauge $SU(3)$. La costante di accoppiamento decresce all'aumentare dell'energia ed è possibile, in quel regime, utilizzarla come parametro di espansione della serie perturbativa.

Ne consegue, dunque, che la tradizionale analisi dei diagrammi di Feynman, è in grado di fornire una descrizione solo di un regime della QCD. La fisica dei collider, caratterizzata da una scala di energia elevata, appartiene al regime perturbativo della teoria, mentre il confinamento e le glueballs sono fenomeni non-perturbativi e richiedono lo sviluppo di diversi metodi di analisi.

Per lo studio delle glueballs, prendiamo in esame la Lagrangiana della QCD che si ottiene dopo aver fatto il limite $m_q \rightarrow \infty$, dove m_q è la massa dei quark. In questo modo stiamo studiando una teoria di pura gauge, ma non stiamo eliminando dal sistema informazioni rilevanti per le glueballs: la dinamica contiene ancora i gradi di libertà gluonici a cui siamo interessati. Possiamo ottenere una giustificazione teorica all'esclusione della parte fermionica della Lagrangiana considerando $SU(3)$ come caso particolare di $SU(N)$. È stato dimostrato da 't Hooft [3] che una teoria di gauge con gruppo $SO(N)$, $U(N)$ o $SU(N)$ ha un naturale parametro in cui è possibile fare un'espansione perturbativa della soluzione. Questo parametro è $1/N$. Nel limite $N \rightarrow \infty$ i primi termini dell'espansione danno il contributo dominante alla serie e, in prima approssimazione, si possono scartare quelli successivi. Per ottenere un limite non banale, è necessario che rimanga costante il parametro di 't Hooft che nel caso di $SU(N)$ è $\lambda_0 = g_0^2 N$, dove g_0 è la costante di accoppiamento bare della teoria. Inoltre, nel limite di 't Hooft, è possibile riarrangiare l'usuale serie perturbativa, in g_0^2 , nella serie in $1/N$, sfruttando le caratteristiche topologiche dei diagrammi di Feynman. L'espansione in $1/N$ può infatti essere vista come un'espansione topologica in grafici di Feynman, dove un grafico di gene h contribuisce all'ordine $(\frac{1}{N^2})^h$. Per esempio i diagrammi dominanti, $O(1)$, nel caso di $SU(N)$ di pura gauge, sono tutti quelli planari (possono essere disegnati su un foglio senza alcuna intersezione tra le linee); è possibile dimostrare che il contributo dei fermioni è soppresso di un fattore $1/N$ rispetto al contributo gluonico. Esistono in letteratura diversi studi che evidenziano come la serie in $1/N$ descriva correttamente la fisica di $SU(3)$ con un numero limitato di correzioni. Ad esempio, limitandosi ai termini $O(1/N^2)$, si ottiene una descrizione approssimata con un errore dell'ordine del 5 – 10%.

Oltre al fatto che il limite di grande N possa essere studiato con una serie perturbativa, c'è anche un'altra ragione per cui è interessante affrontarne lo studio, e proviene dalla teoria delle stringhe. Si tratta della corrispondenza di gauge-gravità (AdS/CFT), basata sulla famosa congettura di

Maldacena [4] e sviluppata nel successivo lavoro di Witten [5]. Questa corrispondenza mette in relazione teorie di stringhe su appropriate varietà Anti-de Sitter (varietà multidimensionali con una curvatura costante negativa) con teorie di campo conformi le cui simmetrie dipendono dalla geometria della varietà. In particolare la congettura di Maldacena afferma la dualità tra una teoria di stringa in $\text{AdS}_{d+1} \otimes \mathbf{X}$ e il limite di grande N di una teoria di campo conforme in d dimensioni e il cui gruppo di simmetria (o super-simmetria) dipende dalla scelta della varietà \mathbf{X} . Sono ormai moltissimi gli studi che confermano la validità di questa congettura per diverse geometrie dal lato della teoria delle stringhe e corrispondenti diversi gruppi di simmetria per le teorie di campo. Chiaramente il nostro interesse non è in una teoria di campo conforme, ma nella QCD. È possibile includere teorie non conformi in diversi modi, ma quello più semplice è stato proposto da Witten [6]. Compattificando una dimensione della varietà su cui è definita la teoria conforme si introduce una scala che rompe automaticamente l'invarianza conforme e questa scala è data dal raggio di curvatura R_0 della compactificazione. Affinchè gli approcci ispirati dalla corrispondenza AdS/CFT, abbiano un potere predittivo per la QCD, una condizione necessaria è che il limite di grande N sia una descrizione accurata di tale teoria. Il confronto di osservabili, come le masse delle glueball, in teorie di gauge $\text{SU}(N)$ con N grande rispetto a $N = 3$ ci permette di studiare le correzioni con cui la QCD è approssimata dal suo limite per $N \rightarrow \infty$.

Con queste motivazioni, in questo lavoro di tesi, abbiamo preso in considerazione una teoria di Yang-Mills con gruppo di gauge $\text{SU}(N)$ per N compreso nell'intervallo di numeri interi (3,8). Il nostro scopo finale è quello di ottenere il valore delle masse degli stati più bassi dello spettro e di alcune eccitazioni, per tutti i valori dei numeri quantici J^{PC} , spin, parità e carica, e per diversi valori di N . Non potendo usare, per il nostro studio, regolarizzatori basati sull'espansione perturbativa in diagrammi di Feynman, abbiamo scelto di definire la teoria su un **reticolo** euclideo quadri-dimensionale. L'uso del reticolo come regolarizzatore fu introdotto da Wilson [7] nel 1974 ed è oggi uno degli strumenti più usati per lo studio di fenomeni non-perturbativi. La presenza di una lunghezza minima, il passo reticolare, impone un "cutoff" agli impulsi (in trasformata di Fourier) e impedisce la divergenza degli integrali; inoltre gli integrali funzionali sono matematicamente ben definiti perchè i cammini sono numerabili su un reticolo finito. Una teoria di gauge definita su reticolo ha il vantaggio di assomigliare sotto certi aspetti ad un sistema di meccanica statistica e può essere analizzata con gli stessi strumenti: per esempio un metodo come l'espansione di alta temperatura in meccanica statistica si traduce in un'espansione nell'inverso della costante di accoppiamento per la teoria di gauge. È dunque possibile in questa formulazione studiare fenomeni nella regione di "strong coupling" della teoria, come il confinamento. Per quanto riguarda le glueballs, la presenza di un mass gap m tra lo stato di vuoto e il resto dello spettro, in teorie di gauge su reticolo, è stato per la prima volta mostrato

da Osterwalder e Seiler [8]. Come ogni altro regolarizzatore, il reticolo è da considerarsi un puro strumento di calcolo: la fisica compare nel momento in cui viene eliminato il regolarizzatore e vengono fissate quantità osservabili attraverso la procedura di rinormalizzazione. La presenza delle glueballs nello spettro del continuo, è subordinata al fatto che m , calcolata su reticolo, scali nel modo corretto seguendo le equazioni del gruppo di rinormalizzazione. Una massa su reticolo è l'inverso di una lunghezza di correlazione e può essere misurata per esempio studiando l'andamento di una funzione di Green a due punti. Come vedremo, le funzioni di correlazione possono essere scritte nella forma

$$C(t) = \langle \Phi^\dagger(t)\Phi(0) \rangle = \sum_n \left| \langle 0 | \Phi^\dagger | n \rangle \right|^2 e^{-E_n t} = \sum_n |c_n|^2 e^{-a_t E_n n t} \quad ,$$

dove abbiamo inserito gli autostati dell'Hamiltoniana $H|n\rangle = E_n|n\rangle$ ($|0\rangle$ è lo stato di vuoto) e scritto la coordinata temporale in unità del passo reticolare $t = a_t n t$.

La procedura usuale [9, 10] per estrarre la massa di una glueball tramite una simulazione di Monte-Carlo consiste nel costruire operatori Φ a partire da prodotti gauge invarianti di campi di gauge sul reticolo; tali operatori devono avere proiezione non nulla sullo stato dello spettro corrispondente alla glueball in esame ($|n\rangle$), e quindi avere gli stessi numeri quantici di $|n\rangle$. Per estrarre più facilmente la massa dallo studio dei correlatori abbiamo scelto di calcolare operatori a impulso nullo $\vec{p} = 0$ ($E_n^2 = |\vec{p}_n|^2 + m_n^2$). Tuttavia, questa procedura può dare informazioni solo sullo stato più basso nello spettro del canale studiato, questo perchè, a grande distanza ($t \rightarrow \infty$) l'unico contributo rilevante nella sommatoria proviene dal termine con la massa più piccola. D'altro canto l'utilizzo di un metodo variazionale ci offre la possibilità di estrarre anche la massa dei primi stati eccitati. Un altro aspetto da tenere in conto è che sul reticolo siamo in grado di misurare $C(t)$ solo per pochi valori di t , prima che il rumore diventi più grande del segnale. Di conseguenza risulta fondamentale che lo stato Φ abbia la massima proiezione possibile sullo stato di glueball $|n\rangle$, $|\langle 0 | \Phi^\dagger | n \rangle|^2 \sim 1$, per poter estrarre informazioni dalla funzione di correlazione anche a piccole distanze temporali: questo incrementa il segnale della misura [11] per piccoli t prima che il rumore statistico, indipendente da t , cominci a prevalere.

La misura dei correlatori sarà effettuata usando metodi numerici. Questo perchè una teoria di gauge su reticolo ha anche la caratteristica di poter essere simulata al calcolatore, grazie alla sua natura intrinsecamente discreta. Come in meccanica statistica, possono essere usati i metodi Monte-Carlo. Fu Creutz [12] per la prima volta nel 1980 a cominciare questi studi numerici che oggi dominano quasi ogni tipo di calcolo su reticolo.

Va fatto notare, che su reticolo, il gruppo di simmetria dello spazio-tempo non è il gruppo di Lorentz, dunque gli stati creati non saranno identificabili con gli autovalori dello spin: gli stati a momento nullo trasformeranno sotto il gruppo delle rotazioni del cubo O (a cui sono aggiunte coniugazione di carica e parità) e saranno identificati dai valori di R^{PC} , dove R gioca un ruolo

analogo allo spin ed indica una delle 5 rappresentazioni irriducibili (A_1, A_2, E, T_1, T_2) del gruppo. Nel continuo, gli stati di spin J^{PC} possono essere ricostruiti dagli stati in R^{PC} studiando le rappresentazioni di O incluse in $SO(3)$, che è il gruppo delle rotazioni continue dello spazio.

Per $SU(3)$ i risultati numerici sono ormai consolidati da tempo [13, 14], ma non esiste ancora uno studio a grande N che abbia indagato tutti i canali R^{PC} sistematicamente. Il risultato originale di questo lavoro di tesi è di effettuare tale studio. Utilizziamo, inoltre, una nuova metodologia per creare gli operatori di glueball Φ . Come abbiamo già detto, la procedura per calcolare le masse si basa fundamentalmente sulla possibilità di creare operatori Φ che trasformano sotto le rappresentazioni irriducibili A_1, A_2, E, T_1, T_2 , e che proiettano con un coefficiente di ordine 1 su almeno uno stato dello spettro. A partire dal prodotto di campi di gauge lungo un percorso chiuso di lunghezza L (in unità di passo reticolare), costruiamo, in maniera automatica, una combinazione lineare delle sue trasformazioni sotto il gruppo cubico tale che essa appartenga ad una rappresentazione irriducibile: prendendone la traccia della parte reale o della parte immaginaria otteniamo un operatore gauge invariante in grado di creare dal vuoto uno stato con i numeri quantici R^{P+} o R^{P-} . Usando percorsi di diversa lunghezza L e di diversa forma riusciamo a costruire operatori per stati in tutte le rappresentazioni irriducibili di O . Questi operatori vengono usati per misurare i correlatori per tutte le 20 combinazioni dei numeri quantici R^{PC} ; mediante una procedura variazionale e poi possibile estrarre la massa dello stato fondamentale e di alcuni stati eccitati.

Dalla nostra analisi abbiamo ottenuto lo spettro delle teorie di gauge da $SU(3)$ fino ad $SU(8)$, e questo ci ha permesso di estrapolare, mediante un fit, il valore delle masse degli stati dello spettro a $N = \infty$. Per quanto riguarda le teorie di gauge in 3+1 dimensioni, questo è il primo studio di grande N compiuto in modo completo su tutte le rappresentazioni. Inoltre, abbiamo cercato di determinare, con maggiore precisione rispetto agli studi precedenti presenti in letteratura, le possibili contaminazioni nello spettro misurato da parte di stati spuri, non corrispondenti alla propagazione di singole particelle. Tuttavia, sebbene sia stato possibile riconoscere alcune di queste contaminazioni, ulteriori analisi sono necessarie per approfondire la natura dei nostri risultati a riguardo.

1. Introduction to Lattice Gauge Theories (LGT)

The Lattice Gauge Theory (LGT) formalism [7], is one of the few known non-perturbative regularization of quantum field theory. It is mainly based on three essential concepts: the Feynman path integral, or functional integral, the Euclidean formulation obtained by continuing the real time variable to imaginary time, and the regularization of Euclidean functional integrals through a space-time lattice. The material presented in this chapter does not pretend to be original and can be found in many good textbooks on the subject [15, 16]. However, this introduction makes this thesis work self-consistent.

1.1 Feynman Path Integral and Euclidean Field Theory

1.1.1 A quantum mechanics example

Let's start with a simple example, given by the quantum mechanical description of a non-relativistic particle in one space dimension, to elucidate the construction of the path integral formulation. The path integral representation, as we will see, is perhaps the most intuitive picture one can make to explain quantum mechanical transition amplitudes. Given the Hamiltonian H of the system, a transition amplitude is

$$\langle x', t' | x, t \rangle = \langle x' | e^{-iH(t'-t)} | x \rangle \quad , \quad (1.1)$$

where x label the position of the particle in the space and it is the only degree of freedom of the system. It is related to the probability of the particle going from the space-time point (x, t) to (x', t') under the dynamics dictated by H . Now we would like to expand this expression inserting a complete set of coordinate eigenstates (resolution of the identity)

$$1 = \int dx_1 |x_1\rangle \langle x_1| \quad , \quad (1.2)$$

and dividing the temporal interval $T = (t' - t)$ in $T - \Delta t = (t' - t_1)$ and $\Delta t = (t_1 - t)$; thus we obtain

$$\langle x', t' | x, t \rangle = \int dx_1 \langle x' | e^{-iH(t'-t_1)} | x_1 \rangle \langle x_1 | e^{-iH(t_1-t)} | x \rangle \quad . \quad (1.3)$$

This simply means that we are summing over all the x_1 positions the particle can occupy at time t_1 .

Proceeding this way, using other positions x_2, \dots, x_n , results in cutting the initial time interval in n parts which we can choose to be equal to $\Delta t = \frac{T}{n}$. The resulting expression is a sum (integral) over all the positions that the particle can occupy at discrete time intervals and so we end up with a discretized time direction:

$$\langle x', t' | x, t \rangle = \int dx_1 \dots dx_{n-1} \langle x_n | e^{-iH\Delta t} | x_{n-1} \rangle \langle x_{n-1} | e^{-iH\Delta t} | x_{n-2} \rangle \dots \langle x_1 | e^{-iH\Delta t} | x_0 \rangle \quad , \quad (1.4)$$

where we set $x' \equiv x_n$ and $x \equiv x_0$ because they are the positions at time $T = n\Delta t$ and at time $t = 0$.

If Δt is small enough and the potential part of the Hamiltonian is only position dependent, every matrix element in the multiple integral (1.4) can be approximated using the Baker–Campbell–Hausdorff formula. Using the Fourier transformation of the kinetic part in the Hamiltonian leads to

$$\langle x' | e^{-iH(t'-t)} | x \rangle \approx \int dx_1 \dots dx_{n-1} \exp i \sum_{k=0}^{n-1} \Delta t \left\{ \frac{m}{2} \left(\frac{x_{k+1} - x_k}{\Delta t} \right)^2 - V(x_k) \right\} \quad . \quad (1.5)$$

The exponent is just the classical action in the limit $n \rightarrow \infty$ for a classical trajectory from x to x' and with intermediate positions $x_k = x(k\Delta t)$,

$$\begin{aligned} & \sum_{k=0}^{n-1} \Delta t \left\{ \frac{m}{2} \left(\frac{x_{k+1} - x_k}{\Delta t} \right)^2 - V(x_k) \right\} \\ & \longrightarrow \int_0^T dt \left\{ \frac{m}{2} \left(\frac{dx}{dt} \right)^2 - V(x) \right\} = \int_0^T dt L(x, \dot{x}; t) \equiv \mathcal{S} \quad . \end{aligned} \quad (1.6)$$

If we write the integrations over the x_k in the continuum time limit, the integral can be interpreted as an integration over a continuous path; therefore we can write (1.5) as

$$\langle x' | e^{-iH(t'-t)} | x \rangle = \int_x^{x'} \mathcal{D}x e^{i\mathcal{S}} \quad . \quad (1.7)$$

The meaning of (1.7) is that, if we want to evaluate a *quantum* transition amplitude, we have to sum over all possible *classical* paths from x to x' , each weighted with the exponential of i times the correspondent *classical* action. Quantum mechanical operators have been eliminated

in favour of an infinite-dimensional integral, often called *functional integral*. Although it is a physically beautiful result, it is difficult to give the expression above a satisfactory mathematical meaning as an integral over some space of functions: this is due to the fact that the integrand is complex and strongly oscillating. We will return on this key point after reviewing the main lines of the path integral applied to quantum field theory.

1.1.2 Functional integrals in Quantum Field Theory

The language of the path integral can be translated from quantum mechanics to quantum field theory, and indeed it turned out to be one of the most useful tools in field theory, because many results can be derived in a compact and easy way through formal manipulations of functional integrals.

In a quantum field theory, one of the tasks is to calculate the Green functions for the fields, which provide all the physical information for the system (like scattering matrix elements via reduction formula, or decay rates). Let's try to be more precise introducing the path integral formalism for a real scalar field $\phi(x)$, where $x = (\vec{x}, t)$ labels the space-time coordinates. Now the field $\phi(x)$ is an operator in the Heisenberg representation: the space-time continuous coordinates are the degrees of freedom of the theory.

A Green function (or n -points correlation function) is the vacuum expectation value of a time-ordered products of n Heisenberg fields (indicated by the subscript H),

$$\begin{aligned} G(\phi(x_1), \dots, \phi(x_n)) &= \langle 0 | \phi(x_1) \dots \phi(x_n) | 0 \rangle \quad (t_1 > \dots > t_n) \\ &= \langle 0 | \mathcal{T} \{ \phi_H(x_1) \dots \phi_H(x_n) \} | 0 \rangle \quad . \end{aligned} \quad (1.8)$$

\mathcal{T} is the time-ordering operator and the time evolution of each field is given by the Hamiltonian H as

$$\phi_H(\vec{x}, t) = e^{iHt} \phi_H(\vec{x}, t=0) e^{-iHt} \quad . \quad (1.9)$$

In the quantum mechanical example we have seen that, using the path integral, the action \mathcal{S} of the system acquires a central role and so does the Lagrangian. Thus we decide to abandon the Hamiltonian formalism in favour of the Lagrangian one; furthermore, every symmetry the Lagrangian may have is explicitly preserved by the functional integral and the role of symmetries will be increasingly important as we proceed in our study of quantum field theory.

For a field theory we write the action as

$$\mathcal{S} = \int d^4x \mathcal{L}(x) \quad , \quad (1.10)$$

where $\mathcal{L}(x)$ is the Lagrangian density. Now, just by translating what we have seen in Sec. 1.1.1, we know how a field transition amplitude looks like using the functional integral: the basic

variables $x_k(t)$ become the fields $\phi(x)$, the measure over the paths become a measure over field configurations in the space, $\prod_{t,\vec{x}} d\phi(\vec{x}, t) \equiv \mathcal{D}\phi$. Thus our formula becomes

$$\langle \phi_f(\vec{x}) | e^{-i\text{HT}} | \phi_i(\vec{x}) \rangle = \int \mathcal{D}\phi \exp \left[i \int_0^T d^4x \mathcal{L} \right] , \quad (1.11)$$

where the functions $\phi(x)$ over which we integrate are constrained to the specific configurations $\phi_i(\vec{x})$ at $t = 0$ and $\phi_f(\vec{x})$ at $t = T$. However, a Green function is a vacuum expectation value: it is a different object from a transition amplitude. To find the functional expression for a Green function we can start from the following integration

$$\int \mathcal{D}\phi \phi(x_1) \phi(x_2) \dots \phi(x_n) \exp \left[i \int_{-T}^T d^4x \mathcal{L}(\phi) \right] , \quad (1.12)$$

where the boundary conditions on the path integral $\int \mathcal{D}\phi$ are $\phi(\vec{x}, -T) = \phi_i(\vec{x})$ and $\phi(\vec{x}, T) = \phi_f(\vec{x})$ for some $\phi_i(\vec{x}), \phi_f(\vec{x})$. Here we should remark that, whereas the ϕ 's in (1.12) are classical fields (and then $\phi(x)$ are numbers), the ones in (1.8) are Heisenberg operators. Starting from (1.12) and introducing completeness relations, we can relate it to a field transition amplitude of a \mathcal{T} -ordered product of fields

$$\langle \phi_f(\vec{x}) | e^{-i\text{HT}} \mathcal{T} \{ \phi_H(x_1) \dots \phi_H(x_n) \} e^{-i\text{HT}} | \phi_i(\vec{x}) \rangle . \quad (1.13)$$

This expression is almost equal to the n -point correlation function. To make it more nearly equal, we take the limit $T \rightarrow \infty(1 - i\epsilon)$, to project out the vacuum state $|0\rangle$ from $|\phi_i\rangle$ and $|\phi_f\rangle$ (provided that these states have some overlap with $|0\rangle$, which we assume). This can be shown, for example, inserting a complete set of energy eigenstates

$$e^{-i\text{HT}} | \phi_i \rangle = \sum_n e^{-iE_n T} | n \rangle \langle n | \phi_i \rangle , \quad (1.14)$$

and isolating the contribution of $|0\rangle$ from the sum

$$e^{-i\text{HT}} | \phi_i \rangle = e^{-iE_0 T} | 0 \rangle \langle 0 | \phi_i \rangle \sum_{n \neq 0} e^{-iE_n T} | n \rangle \langle n | \phi_i \rangle , \quad (1.15)$$

where E_0 is the vacuum energy (and we are assuming $\langle 0 | \phi_i \rangle > 0$). Since $E_n > E_0$ for all $n \neq 0$, we can get rid of all the $n \neq 0$ terms in the series by sending $T \rightarrow \infty$ in a slightly imaginary direction: then the exponential factor $e^{-iE_n T}$ dies slowest for $n = 0$, and we have

$$e^{-i\text{HT}} | \phi_i \rangle = \lim_{T \rightarrow \infty(1-i\epsilon)} \langle 0 | \phi_i \rangle e^{-iE_0 \cdot \infty(1-i\epsilon)} | 0 \rangle . \quad (1.16)$$

The overlap $\langle 0 | \phi_i \rangle$ and the awkward phase factor $e^{-iE_0 \cdot \infty(1-i\epsilon)}$ cancel if we divide (1.13) by the same expression, but without the T -ordered product of n fields, and, if we use the same trick

to project out the vacuum state in that field transition amplitude as well. In the end, we obtain the path integral formula for a n -point Green function:

$$\langle 0 | \mathcal{T} \{ \phi_H(x_1) \dots \phi_H(x_n) \} | 0 \rangle = \lim_{T \rightarrow \infty(1-i\epsilon)} \frac{\int \mathcal{D}\phi \phi(x_1) \phi(x_2) \dots \phi(x_n) \exp \left[i \int_{-T}^T d^4x \mathcal{L} \right]}{\int \mathcal{D}\phi \exp \left[i \int_{-T}^T d^4x \mathcal{L} \right]} . \quad (1.17)$$

We remark here again that the infinite dimensional integration over all classical field configurations is not mathematically well defined, despite the fact that it has a formal meaning.

1.1.3 Euclidean Field Theory

In the previous section we used a trick to relate quantum field amplitudes to Green functions; the key reason for this to work, is that the exponential factor is no more an oscillating phase if the time is an imaginary number, but it dies out when the exponent is strictly positive (as the energy of states above the vacuum).

With this in mind, let us choose all time variables to be purely imaginary

$$t = -i\tau, \quad \tau \in \mathbb{R} . \quad (1.18)$$

This imaginary time analytic continuation (which is often referred to as the *Wick rotation*, because the time coordinate is rotated by 90 degrees in the complex plane, going from the real, to the imaginary axis) transforms the real time Green functions in *Euclidean* Green functions (or *Schwinger functions*)

$$G(\phi(\vec{x}_1, -i\tau_1), \dots, \phi(\vec{x}_n, -i\tau_n)) = G_E(\phi(\vec{x}_1, \tau_1), \dots, \phi(\vec{x}_n, \tau_n)) . \quad (1.19)$$

The name "Euclidean" is understood looking at the space-time metric for $x = (\vec{x}, \tau)$ which is now a Kronecker δ :

$$ds^2 = -dt^2 + dx_1^2 + dx_2^2 + dx_3^2 \quad (1.20)$$

has changed in

$$ds^2 = d\tau^2 + dx_1^2 + dx_2^2 + dx_3^2 , \quad (1.21)$$

and the Euclidean symmetry between space and time is manifest. The path integral functional for a Euclidean Green function can be written, starting from (1.17) and substituting (1.18). Then the $T \rightarrow \infty(1-i\epsilon)$ limit becomes a limit on the imaginary axis alone. Thus we obtain

$$G_E(\phi(\vec{x}_1, \tau_1), \dots, (\vec{x}_n, \tau_n)) = \lim_{\tau \rightarrow \infty} \frac{\int \mathcal{D}\phi \phi(x_{1E}) \phi(x_{2E}) \dots \phi(x_{nE}) \exp \left[- \int_{-\tau}^{\tau} d^4x_E \mathcal{L}_E \right]}{\int \mathcal{D}\phi \exp \left[- \int_{-\tau}^{\tau} d^4x_E \mathcal{L}_E \right]} , \quad (1.22)$$

where we used the subscript E to remind us the fact that we are in a Euclidean space–time. The exponential weight in the integral is now

$$e^{-\mathcal{S}_E} \quad , \quad (1.23)$$

and, if the Euclidean action \mathcal{S}_E is a real valued functional of the fields, bounded from below, this can be interpreted as a "Boltzmann factor". The form of (1.22) then, resembles that of a statistical ensemble average, where the denominator is the partition function

$$\mathcal{Z}[\phi] = \int \mathcal{D}\phi e^{-\mathcal{S}_E[\phi]} \quad (1.24)$$

of the system: the Euclidean fields are no more considered as operators, but as random variables, whose expectation values yield the correlation functions through (1.22). The Euclidean action \mathcal{S}_E is obtained, from the real time action in the Minkowski space–time, just by replacing t with $-i\tau$ in the argument of functions, in the integration measure and in the space–time derivative.

1.1.4 Lattice discretization

As we have pointed out in the previous sections, the path integral expressions for Green functions have only a well defined meaning for systems with a numerable number of degrees of freedom. In field theory, however, where one is dealing with an infinite number of degrees of freedom, labelled by the coordinates \vec{x} and, in general, by some additional discrete indices, the multiple integrals are only formally defined. In the quantum mechanical case, the path integral was defined as a limit of a finite–dimensional integral which resulted from a discretization of time. To give the path integrals, in quantum field theory, a precise meaning, we will therefore have to discretize not only time, but also space: we will be forced to introduce a space–time lattice.

Eventually we will have to remove again this lattice structure, and this is quite a non–trivial task, which is related to the renormalization of Green functions. The renormalization program in continuum perturbation theory first requires the regularization of the Feynman path integrals in momentum space. These integrals will then depend on one or more parameters which are introduced in the regularization process (momentum cutoff, Pauli–Villars masses, dimensional regularization parameter). Since the effect of any regularization procedure is to render the momentum integrations in Feynman integrals ultraviolet finite, let us loosely say that the first step in the renormalization program consists in the introduction of a momentum cutoff. If the original Feynman integrals are divergent, the the regularized integrals will be strongly dependent on the cutoff. The second step in the renormalization program now consists in defining renormalized Green functions, which approach a finite limit as the cutoff is removed. This demands that the bare parameters of the theory become cutoff dependent. This dependence is determined

by imposing a set of renormalization conditions, which merely state that such quantities as the physical coupling strength measured at some momentum transfer, and particle masses are to be held fixed as the cutoff is removed.

In the lattice approach this program can be formulated without reference to perturbation theory. The first step (regularization) consists in introducing a space–time lattice at the level of the path integral. This regularization merely corresponds to defining what we mean by a path integral. The second step of the renormalization program the corresponds to removing the lattice structure. This amounts to studying the continuum limit. It is therefore not surprising that the bare parameters of the theory will have to be tuned to the lattice spacing in a very definite way depending, in general, on the dynamics, if physical observables are to become insensitive to the underlying lattice structure. Within the perturbative framework, the introduction of the a space–time lattice corresponds to a particular way of regularizing Feynman integrals, but this regularization does not amount to the naive introduction of a momentum cutoff. Although the momentum space integrals will indeed be cut off at a momentum of the order of the inverse lattice spacing, the integrands of Feynman integrals will not have the usual structure, but are modified in a non–trivial way. For example, in the lattice formulation of gauge theories, new interaction vertices pop up, which have no analogue in the continuum formulation.

Let us define the path integral on a four–dimensional hypercubic lattice; space–time coordinates x_μ are restricted to be discrete lattice sites:

$$x_\mu = a m_\mu, \quad m_\mu \in \mathbb{Z} \quad , \quad (1.25)$$

where a is the *lattice spacing*. We will always use a hypercube of finite extension so that all our functional integral are finite–dimensional. This means we are considering the theory in a finite volume and we shall specify boundary conditions for the functions. Of course, we would like to recover physics in a continuous and infinite space–time eventually. If we define the size of the hypercubic box as $L = na$, then the task is to take the infinite volume limit $n \rightarrow \infty$, which is the easier part in general, and to take the continuum limit $a \rightarrow 0$, which amount to the renormalization program described above. Choosing the size L equal in each of the four directions is just a matter of convention for the moment and the same is true for the lattice spacing; we could also choose different lattice spacing a_s, a_t for the spatial and the temporal directions (even if the choice of the temporal direction is purely conventional due to the Euclidean symmetry) and this breaks the cubic symmetry of the discrete system: a lattice of this kind is called *anisotropic*. Moreover, one can choose also different lattice sizes L_s, L_t and we will see at the end of this chapter that the field theory defined on such lattices can be seen as a thermal field theory if L_t is small (L_t is proportional to the inverse of the temperature, thus the infinite volume limit is equivalent to a zero temperature field theory).

Let’s see now how we can write a discretized action on the lattice. Firstly, on the lattice, integrals

can be replaced by finite sums. We shall use the notation

$$\sum_x \equiv a^4 \sum_{m_1=0}^{n-1} \cdots \sum_{m_4=0}^{n-1} \equiv a^4 \sum_m \quad , \quad (1.26)$$

which leads to

$$\sum_x f(x) \rightarrow \int_0^L d^4x f(x) \quad , \quad (1.27)$$

in the continuum limit for a smooth function $f(x)$. Moreover, derivatives can be replaced by finite differences. We can define, for example, a forward difference

$$\Delta_\mu^f f(x) = \frac{1}{a}(f(x + a\hat{\mu}) - f(x)) \quad , \quad (1.28)$$

and a backward difference

$$\Delta_\mu^b f(x) = \frac{1}{a}(f(x) - f(x - a\hat{\mu})) \quad , \quad (1.29)$$

where $\hat{\mu}$ is a unit vector in the direction μ ; both these differences led to the continuum derivative

$$\Delta_\mu^f f(x) , \Delta_\mu^b f(x) \rightarrow \frac{\partial}{\partial x_\mu} f(x) \quad \text{if } a \rightarrow 0 \quad . \quad (1.30)$$

Different definitions of finite differences can lead to the same continuum limit derivative, but the error in powers of the lattice spacing can be of different order. Usually, if we expand the finite difference of a smooth function in powers of a , the term which is independent of a survives in the continuum limit, whereas the terms $O(a)$, $O(a^2)$, etc... are called *lattice artifacts* and are supposed to vanish. This is indeed only a simple, or classic, interpretation of the continuum limit for a discretized theory: the field configurations, which enter the path integral, are usually not smooth at all on the lattice scale, they can change rather wildly from site to site, and we should treat carefully the continuum limit of the quantum theory. This limit involves the concept of renormalization that we stated above, and the concept of scaling of physical properties. We will return on these concepts with more details in Sec. 1.3.

With finite sums and differences, it is easy to define the discrete analogue of the Euclidean action, which, of course, has to be chosen with the right classical continuum limit (in the sense of power expansion in terms of the lattice spacing). The last piece we need, to write down a well-defined formulation of the path integral, is the integration measure over the paths; in a field theory we know that this is a measure on the field configurations and that we can interpret these fields as random variables. If the hypercubic lattice is finite, then the functional integration is finite dimensional and perfectly defined; for example, the measure of (1.24) is

$$\mathcal{D}\phi = \prod_x d\phi(x) \quad , \quad (1.31)$$

where the product \prod_x is on all the lattice sites defined by (1.25).

Having a well-defined functional integral, we can now try to evaluate it. In perturbation theory, for example, we usually face momentum integrals that have to be regularized in order to proceed with the calculation. A lattice field theory has a natural momentum cutoff which regularizes it, as we have already noticed: the lattice spacing is the minimum distance between two points, thus the wavelengths propagating on the lattice have a maximum frequency. By having a look at the Fourier transform, we can show how the cutoff emerges for a scalar field $\phi(x)$ defined only on $x \in \Lambda$. The Fourier transformed scalar field is

$$\tilde{\phi}(p) = \sum_x e^{-ip \cdot x} \phi(x) \quad , \quad (1.32)$$

where we have used the sum on the lattice sites, and the Euclidean inner product $p \cdot x$; this field is periodic in momentum-space because, if we change p to

$$p_\mu = p_\mu + \frac{2\pi}{a} \quad , \quad (1.33)$$

$\tilde{\phi}(p)$ is unchanged. Every function defined in momentum-space can then be restricted to have values only in the Brillouin zone

$$-\frac{\pi}{a} < p_\mu < \frac{\pi}{a} \quad . \quad (1.34)$$

Therefore, the maximum possible momentum is π/a , and if we specify periodic boundary conditions for the scalar field, the momenta will be also discretized. This last observation implies that momentum-space integration, used in perturbation theory for example, can be replaced by finite sums.

At this point, all functional integrals have turned into regularized and finite expressions. We can then proceed to discuss gauge theories in this framework.

1.2 Gauge theories on the lattice

We would like to start this section with a reminder of gauge theories in a continuum and infinite Euclidean space-time, in order to underline the main differences that we will see in their discrete form. Since we are going to deal with the pure gauge theory for the rest of our work, we will focus on that; however, we will use matter fields, and their transformation laws under the gauge group, to explain concepts such as parallel transport and covariant derivative. We will refer to the pure gauge theory with any gauge group as the Yang-Mills theory [1].

1.2.1 Pure Yang-Mills (YM) theories: continuum formulation

Let's start our discussion on continuum gauge theory in a Euclidean space-time with N complex scalar fields $\phi^i(x)$, $i = 1, \dots, N$. These fields are the components of a complex vector field $\phi(x)$.

For each space–time point x , the vector $\phi(x)$ is an element of a vector space $V(x)$, where a scalar (inner) product is defined by summation over the components of the vectors.

Given the usual continuum scalar field action, with a potential quadratic in $\phi(x)$, like

$$\mathcal{S} = \int d^4x [\phi(x) (\square + m^2) \phi(x) + V(\phi^2(x))] \quad , \quad (1.35)$$

it is easy to show that this is invariant under the transformation

$$\phi(x) \rightarrow \phi'(x) = \Omega \phi(x) \quad , \quad \Omega \in \text{SU}(N) \quad . \quad (1.36)$$

Ω is a $N \times N$ matrix, independent of x , and belongs to the special unitary group $\text{SU}(N)$, i.e.

$$\Omega \Omega^\dagger = \mathbf{1} \quad , \quad \det \Omega = 1 \quad . \quad (1.37)$$

We will always use this group in the following. However, the action (1.35) is also invariant under the more general $\text{U}(N)$ group.

A more general request of invariance on the action, is that physics must be independent of a local change of basis. Applied to our situation, this would demand the modification of the action in order to remain unchanged under the transformations of the form

$$\phi(x) \rightarrow \phi'(x) = \Omega(x) \phi(x) \quad , \quad \Omega(x) \in \text{SU}(N) \quad . \quad (1.38)$$

Since $\Omega(x)$ varies with the space–time point x , these are called *local gauge transformations*, or simply *gauge transformations*. An observation is in order here: the gauge transformation matrices $\Omega(x)$ have to be chosen in a unitary irreducible representation of the gauge group.

As it stands, the continuum action (1.35) is not invariant under (1.38), because the derivative term is applied to the transformation matrix as well. Another way to look at this problem is that a derivative, in general, involves the field ϕ in two distinct points, even if they are infinitesimally close: $\phi(x)$ and $\phi(x + dx)$ can be expressed in two different basis (transform under different Ω 's), therefore they can not be compared.

The solution can be achieved by introducing a "covariant" derivative. By analogy with General Relativity, the covariant derivative can relate quantities which are expressed in different basis, depending on the space–time point.

As we said, we have to subtract vectors at infinitesimal neighbouring points x and $y = x + dx$; as the basis in different points may be chosen arbitrarily, we can compare the vectors only by parallel transporting them to the same point. The parallel transport along a curve is defined in the following way. Let C_{xy} be some curve in space–time from x to y . With C_{xy} we associate a $\text{SU}(N)$ matrix which define a mapping from the vector space in x , $V(x)$, to the one in y , $V(y)$

$$U(C_{xy}) : V(x) \rightarrow V(y) \quad . \quad (1.39)$$

Then the vector

$$U(C_{xy}) \phi(x) \in V(y) \quad , \quad (1.40)$$

is defined to be the vector $\phi(x)$ parallel transported along C_{xy} to the point y . $U(C_{xy})$ is called *parallel transporter*. Under the transformation law (1.38) the parallel transporter transforms as

$$U(C_{xy}) \rightarrow U'(C_{xy}) = \Omega(x)U(C_{xy})\Omega^\dagger(x) \quad . \quad (1.41)$$

Let us consider an infinitesimal straight curve from x to $x + dx$ and its parallel transporter, in order to recover an expression for the covariant derivative. A curve with zero length has a parallel transporter equal to unity, and if the length of the curve is infinitesimal, the parallel transporter deviates from unity only infinitesimally; we can then write

$$U(C_{x,x+dx}) = \mathbf{1} + A_\mu(x)dx^\mu \quad , \quad (1.42)$$

where

$$A_\mu(x) \in \text{su}(N) \quad (1.43)$$

is an element of the Lie algebra of $\text{SU}(N)$: A_μ is a $N \times N$ traceless anti-hermitian matrix and it transforms as a vector under the Lorentz group. If we define the covariant differential of $\phi(x)$ as

$$D\phi(x) = U(C_{x,x+dx})\phi(x + dx) - \phi(x) \quad , \quad (1.44)$$

we obtain

$$D\phi(x) = D_\mu\phi(x)dx^\mu \quad , \quad (1.45)$$

with the covariant derivative given by

$$D_\mu\phi(x) = (\partial_\mu + A_\mu(x))\phi(x) \quad . \quad (1.46)$$

In this context, A_μ is called *gauge field* and transforms with the following law

$$A_\mu(x) \rightarrow A'_\mu(x) = \Omega(x)A_\mu(x)\Omega^\dagger(x) + \Omega(x)(\partial_\mu\Omega^\dagger(x)) \quad . \quad (1.47)$$

It is easy to show that the covariant derivative of $\phi(x)$, then transforms as ϕ , i.e. it is a vector:

$$D_\mu\phi(x) \rightarrow D'_\mu\phi'(x) = \Omega(x)D_\mu\phi(x) \quad , \quad (1.48)$$

because the derivative itself as the same transformation as the parallel transporter.

Replacing ∂_μ with D_μ in the action is then sufficient to guarantee its gauge invariance. However, the gauge field does not transform homogeneously. A function of the gauge fields which transform covariantly, can be found using the commutator of two covariant derivatives. It is the *field*

strength tensor. This tensor is the corresponding quantity of the curvature tensor in General Relativity:

$$F_{\mu\nu}(x) = [D_\mu, D_\nu](x) = \partial_\mu A_\nu(x) - \partial_\nu A_\mu(x) + [A_\mu(x), A_\nu(x)] \quad , \quad (1.49)$$

and in the abelian U(1) case it is exactly the Faraday–Maxwell tensor of the electromagnetic field. The field strength tensor transforms covariantly

$$F_{\mu\nu}(x) \rightarrow F'_{\mu\nu}(x) = \Omega(x)F_{\mu\nu}(x)\Omega^\dagger(x) \quad . \quad (1.50)$$

From this quantity it is easy to construct a scalar, by contracting the indices together; then a scalar and gauge–invariant quantity is the trace

$$\begin{aligned} \text{Tr} [F_{\mu\nu}(x)F_{\mu\nu}(x)] &\rightarrow \text{Tr} [F'_{\mu\nu}(x)F'_{\mu\nu}(x)] = \text{Tr} \left[\Omega(x)F_{\mu\nu}(x)F_{\mu\nu}(x)\Omega^\dagger(x) \right] \\ &= \text{Tr} [F_{\mu\nu}(x)F_{\mu\nu}(x)] \quad , \end{aligned} \quad (1.51)$$

where the Einstein summation convention on repeated indices is used. We will see in a moment how we can use this trace to define an action for the gauge fields, in order to give them a dynamics.

Now, we would like to introduce the component notation which is merely a parametrization of Ω , A_μ , $F_{\mu\nu}$ in terms of the generators of the Lie algebra corresponding to the gauge group SU(N). Every element of a Lie group can be written in terms of the elements of the corresponding algebra via the exponential (canonical) map, and an element of the Lie algebra is a linear combination of its generators. Therefore we can write a gauge transformation matrix as

$$\Omega(x) = e^{i\sum_a \omega^a(x)T_a} \quad , \quad (1.52)$$

where the matrices T_a are the $N^2 - 1$ generators of the algebra $\mathfrak{su}(N)$ and ω^a are real functions of x . This decomposition in terms of the ω^a is unique in a sufficiently small neighbourhood of unity. The generators T_a transform under the adjoint representation of the group which has the same dimension of the group itself, and are usually chosen to be traceless hermitian matrices. Moreover they satisfy the commutation relations

$$[T_a, T_b] = if_{abc}T_c \quad , \quad (1.53)$$

where f_{abc} are real and completely antisymmetric, and are called the *structure constants* of the algebra. Usually they are also normalized as

$$\text{Tr} (T_a T_b) = \frac{1}{2}\delta_{ab} \quad . \quad (1.54)$$

These generators can be used to parametrize the gauge field, which is an element of the algebra. It can be decomposed as

$$A_\mu(x) = \sum_{a=0}^{N^2-1} iA_\mu^a(x)T_a \quad , \quad (1.55)$$

where the A_μ^a 's are the components of the gauge field. The same can be done with the field strength tensor,

$$F_{\mu\nu}(x) = \sum_{a=0}^{N^2-1} iF_{\mu\nu}^a(x)T_a \quad . \quad (1.56)$$

The components of the field strength tensor are related to the ones of the gauge field by the following expression

$$F_{\mu\nu}^a(x) = \partial_\mu A_\nu^a(x) - \partial_\nu A_\mu^a(x) + f_{abc}A_\mu^b(x)A_\nu^c(x) \quad , \quad (1.57)$$

where we have used the definition (1.50) and the relations (1.53).

Now we return to the problem of defining a dynamics for the gauge fields; this will be given by an action which we require to be gauge invariant. We have already seen a function of the gauge fields which is scalar and gauge invariant, and this function is the trace of the scalar quantity obtained by contracting the indices of the field strength tensor (1.51). Usually, a coupling constant g is introduced conventionally to account for the strength of the interaction (the components $A_\mu^a(x)$ are redefined as $-gA_\mu^a(x)$, and the same happens to $F_{\mu\nu}^a(x)$), and the action is

$$\mathcal{S}_{YM} = -\frac{1}{2g^2} \int d^4x \text{Tr} F_{\mu\nu}F_{\mu\nu} = \frac{1}{4} \int d^4x \sum_a F_{\mu\nu}^a F_{\mu\nu}^a \quad . \quad (1.58)$$

This is the pure Yang–Mills action, or pure gauge action, in the continuum and represents the dynamics of the gauge field coupled to itself (we have presented here the Euclidean form of the action). It defines a highly non-trivial interacting continuum theory because, writing down the product of the $F_{\mu\nu}^a$'s, cubic and quartic self-interaction terms for A_μ^a appear. It is thus interesting to study this gauge theory on its own, without the scalar field we used to introduced the basic concepts: we will go more into the details in Chapter 2.

What we have written so far, was a review of the concepts defining a continuum gauge theory. In the next section, we are going to define the same concepts, but in their discretized form on the lattice. At the end we would like to recover also a relation between the lattice variables and the continuum variables, in order to ensure that in the classical continuum limit we are actually recovering the right physics.

1.2.2 Pure Yang–Mills (YM) theories: lattice formulation

Following the lines of the previous section we would like to define a discretized action which is invariant under local gauge transformations. On a Euclidean discrete lattice, the fields and

the gauge matrices are defined only for x being a lattice point. In order to avoid ambiguities between the continuum and the lattice quantities, we will refer to the x -dependence of lattice quantities using a subscript; indeed we can think of a field in x , for example, as it is a variable associated with that point.

The gauge transformation on the scalar field is

$$\phi_x \rightarrow \phi'_x = \Omega_x \phi_x, \quad \Omega_x \in \text{SU}(N) \quad . \quad (1.59)$$

If the action contains bilinears of the fields in different lattice points, then it is not gauge invariant, and a gauge field must be introduced. For example, if we discretize the scalar field action (1.35) using the finite forward difference (1.28), then the kinetic part contains nearest neighbours interactions of the form

$$\phi_x \cdot \phi_y \quad \text{with } y = x + a\hat{\mu} \quad . \quad (1.60)$$

An interaction of this kind is not invariant under transformation (1.59) because the Ω_x and Ω_y are generally different. Let us follow the procedure used in the continuum to create a covariant derivative: the first step is to define a parallel transporter in order to compare ϕ_x with ϕ_y . The shortest parallel transporters on the lattice, different from unity, are those associated with the links (or bonds) b connecting nearest neighbouring points. To denote such a quantity we use the notation

$$U(b) \equiv U(x, x + a\hat{\mu}) \equiv U_{x,\mu} \quad , \quad (1.61)$$

and it can be shown that it is an element of the gauge group in the same irreducible representation of the gauge transformation matrices Ω . Therefore the link variable, as this parallel transporter is always called, transforms following

$$U_{x,\mu} \rightarrow U'_{x,\mu} = \Omega_x U_{x,\mu} \Omega_{x+a\hat{\mu}}^\dagger \quad . \quad (1.62)$$

A lattice covariant derivative can be constructed starting from the forward lattice derivative, and by parallel transporting the field $\phi_{x+a\hat{\mu}}$ to the point x , such that its transformation properties are the same as ϕ_x . By looking at (1.62), it is easy to see that

$$U_{x,\mu} \phi_{x+a\hat{\mu}} \rightarrow \Omega_x \left(U_{x,\mu} \phi_{x+a\hat{\mu}} \right) \quad , \quad (1.63)$$

under a gauge transformation, like ϕ_x , and that we can write

$$D_\mu^f \phi_x = \frac{1}{a} \left(U_{x,\mu} \phi_{x+a\hat{\mu}} - \phi_x \right) \quad , \quad (1.64)$$

for the lattice covariant (forward) derivative. We could have recovered this form for the lattice covariant derivative starting from the forward finite difference (1.28) and adding an auxiliary

discrete field to compensate for the lack of gauge covariance; then, by requiring that $D_\mu^f \phi_x$ should transform covariantly, it can be shown that (1.64) is the only possible form for the lattice covariant derivative.

It is important now to underline one important difference with the continuum formulation: the lattice covariant derivative is defined using $U_{x,\mu}$, which is an element of the gauge *group*, whereas the continuum lattice derivative makes use of $A_\mu(x)$, which belongs to the gauge *algebra*. This means that we will be able to write down an action where the lattice gauge fields are group elements, and the functional integration will be an integration over the group manifold.

Let us deepen our understanding of the link variable by finding the relation between it and the continuum gauge fields (or gauge vector potential). The canonical relation between a Lie group and its algebra is the exponential map and, if we remember the expression (1.42) for an infinitesimal parallel transporter in the continuum, we would then write the link variable as

$$U_{x,\mu} = e^{aA_\mu(x)} \approx \mathbf{1} + a\tilde{A}_\mu(x) \quad . \quad (1.65)$$

In the last expression, $\tilde{A}_\mu(x)$ is defined only on lattice sites and it is a discretized version of the vector potential (can be identified with it only in the continuum limit)

$$A_\mu(x) = \tilde{A}_\mu(x) + O(a) \quad . \quad (1.66)$$

The lattice spacing enters the expression above because it is the natural unit of the lattice, and we see from (1.42) that the vector potential has the dimension of an inverse length. In the continuum we expect that $a\hat{\mu} \approx dx_\mu$.

After having defined the lattice gauge field, we would like to obtain the field strength tensor on the lattice. This can be done easily, starting from the continuum definition in terms of covariant derivatives, and replacing them with the corresponding lattice expressions:

$$G_{x,\mu\nu} = [D_\mu^f, D_\nu^f] = \frac{1}{a^2} (U_{x,\mu} U_{x+a\hat{\mu},\nu} - U_{x,\nu} U_{x+a\hat{\nu},\mu}) \quad . \quad (1.67)$$

The dimension of the lattice field strength is expressed in terms of power of the lattice spacing, and it is $[L^{-2}]$. We should remember, from now on, that on the lattice, every object has a dimension which can always be expressed in terms of the fundamental length given by the lattice spacing a .

Following what we did in the last section, using the field strength tensor, we now define an action for the lattice theory, following (1.51), and noting that

$$\text{Tr } G_{x,\mu\nu} G_{x,\mu\nu}^\dagger \quad , \quad (1.68)$$

is gauge invariant. It is interesting to note that the object we traced can be written as the product of gauge fields around a closed squared path, called the *plaquette*. The plaquette p ,

identified by a lattice site x and two directions (μ, ν) , is the smallest closed loop on the lattice, and we can associate to it a parallel transporter

$$U_p \equiv U_{x,\mu\nu} = U_{x,\mu} U_{x+a\hat{\mu},\nu} U_{x+a\hat{\nu},\mu}^\dagger U_{x,\nu}^\dagger \quad , \quad (1.69)$$

called the *plaquette variable*. This variable is the analogue of the continuum parallel transporter around an infinitesimal dx_μ, dx_ν square, which we have related to the commutator of covariant derivative.

Using the plaquette variable, we can write

$$\text{Tr} [G_{x,\mu\nu} G_{x,\mu\nu}^\dagger] = \frac{1}{a^4} \text{Tr} [2 \cdot \mathbf{1} - U_{x,\mu\nu} - U_{x,\mu\nu}^\dagger] = \frac{2}{a^4} \text{Tr} [\mathbf{1} - \text{Re} U_{x,\mu\nu}] \quad . \quad (1.70)$$

Substituting (1.65) in (1.69), and using the Baker–Campbell–Hausdorff formula, we find

$$U_{x,\mu\nu} = e^{a^2 \tilde{F}_{\mu\nu}(x)} \quad , \quad (1.71)$$

where $\tilde{F}_{\mu\nu}(x)$ is a discretized version of the continuum field strength tensor (it is defined using Δ_μ^f and \tilde{A}_μ , instead of ∂_μ and A_μ) and it is related to the continuum $F_{\mu\nu}$ by

$$F_{\mu\nu}(x) = \tilde{F}_{\mu\nu}(x) + O(a) \quad . \quad (1.72)$$

The lattice action which has been proposed by Wilson [7] for the pure $SU(N)$ lattice gauge theory is defined in terms of the plaquette variables:

$$\mathcal{S}_{LAT} = \beta \sum_p \left[1 - \frac{1}{N} \text{Re Tr } U_{x,\mu\nu} \right] \quad . \quad (1.73)$$

Here, the sum over all plaquettes p is meant to include every plaquette only with one orientation. This action is clearly gauge invariant due to the cyclicity of the trace; furthermore it is real and positive. There are other possibilities for defining a gauge-invariant action, but this is the simplest choice.

A first observation we can make is that, whereas the continuum Yang–Mills action does not depend on the irreducible representation of the gauge transformations (because the algebra generators are always in the adjoint representation), here we are using group elements, and the Wilson action depends explicitly on the representation of the gauge matrices Ω we started with. For our purpose, in this work we are going to use always the fundamental (defining) representation for the matrices Ω (and then for the link and plaquette variables).

The parameter β in front of the plaquette sum is the *coupling constant* of the lattice gauge theory and it is related to the bare coupling g_0 of the continuum Yang–Mills theory. To find this relation, we merely require that, for $a \rightarrow 0$, we recover the action (1.58). Expanding (1.71) in powers of small a and tracing it, as dictated by the Wilson action, we find

$$\beta = \frac{2N}{g_0^2} \quad , \quad (1.74)$$

by comparing the leading term $O(1)$ of the resulting expression with the Yang–Mills continuum action. We can anticipate here that, as a bare coupling, this can vary following the renormalization flow and it becomes a function of the cutoff, i.e. a function of the lattice spacing, $\beta(a)$. We are now ready to define the quantum gauge theory on the lattice using a gauge–invariant functional integral; the last thing we need is to define a gauge–invariant functional measure.

1.2.3 Gauge–invariant lattice path integral

We have already shown how to quantize a field theory using the functional integral formalism; to calculate the expectation value of some observable \mathcal{O} in the pure Yang–Mills theory, we would write the formal expression

$$\langle \mathcal{O} \rangle = \frac{1}{\mathcal{Z}} \int \mathcal{D}A_\mu \mathcal{O} e^{-S_{YM}[A_\mu]} \quad , \quad (1.75)$$

where

$$\mathcal{D}A_\mu = \prod_{x,\mu} dA_\mu(x) \quad . \quad (1.76)$$

This integral is meant to be a functional integral over all configurations of the gauge field A_μ . However, this integral is ill–defined because it is divergent: for every configuration of the gauge fields, we shall count also the infinite gauge–equivalent configurations and with the same weight given by the action, which is gauge invariant. Moreover, if we were to calculate the functional integral by means of perturbation theory, then we would face the problem that some particular configurations of the gauge fields are not allowed: it is then necessary to fix a particular gauge to avoid the zero modes that appear in the quadratic part of the action.

On the lattice we would like to have an integration measure which we require to be gauge invariant not to spoil the gauge symmetry principle that guided us in the construction of the theory from the beginning. In a lattice pure gauge theory, we expect all the observables to be functions of the lattice gauge fields: the link variables define the physical observables. Let us denote a lattice field configuration as a particular set of link variables

$$\{U(b)\} \equiv U \quad , \quad (1.77)$$

where $b = (x, \mu)$ is an oriented link (from x to $x + a\hat{\mu}$) and the set spans all the lattice links. Then the expectation value of a lattice observable can be written as

$$\langle \mathcal{O}_{LAT} \rangle = \frac{1}{\mathcal{Z}_{LAT}} \int \mathcal{D}U \mathcal{O}_{LAT} e^{-S_{LAT}[U]} \quad , \quad (1.78)$$

where

$$\mathcal{D}U = \prod_b dU(b) \quad (1.79)$$

is a finite-dimensional group measure. Here, $dU(b)$ is a volume element in the group manifold. In order to be gauge invariant, the integration measure must satisfy

$$dU = dU' \quad , \quad U'_{x,\mu} = \Omega_x U_{x,\mu} \Omega_{x+a\hat{\mu}}^\dagger \quad , \quad (1.80)$$

which also means that

$$dU = d(U\Omega) = d(\Omega U) \quad . \quad (1.81)$$

On a compact Lie group, such a measure, invariant under left and right translations in the group space, can always be uniquely defined: it is the *Haar measure*.

The problem of equivalent gauge configurations is present in the lattice path integral as well, but with an important difference: here the integration variables belong to the group, whereas in the continuum they are elements of the algebra. Moreover, on a finite lattice, the measure is finite-dimensional, and then well defined (the infinite volume results are obtained taking the limit of finite volume quantities). The difference between the group and the algebra we are interested in at the moment, is that, for a compact group, the gauge volume is finite: the gauge equivalent configurations we need to integrate over, are finite, and their volume can be normalized to unity. However, if we attempt to use perturbation theory starting from (1.78), we will be forced to introduce a gauge-fixing term in the action, right as in the well known continuum case; the reason is that we would like to avoid the zero longitudinal modes in the gauge field propagator. Non-perturbatively, it is possible not to fix any gauge on the lattice, as long as one is interested in gauge-invariant observables: the expectation value of a non gauge-invariant quantity is zero if we do not fix the gauge, whereas, for a gauge-invariant observable, the expectation value is the same in any case, with fixed or unfixed gauge. This is the consequence of having chosen the path integral to be entirely gauge invariant.

Let us now look closely at the partition function which enters the formula (1.78) for an expectation value on the lattice. We can write it as

$$\mathcal{Z}_{LAT} = \int \prod_b dU(b) e^{-S_{LAT}[U]} \quad , \quad (1.82)$$

and we know that this defines the vacuum effects of a regularized gauge theory. We can use this partition function to study the resulting theory without resorting to perturbation theory: lattice formulation of gauge theories is then a powerful tool to explore the non-perturbative regime of such theories. Moreover, we can find an analogy between (1.82) and the partition function of a statistical mechanics system where $\beta = 2N/g_0^2$ is the inverse temperature and $\sum_p [1 - \frac{1}{N} \text{ReTr } U_{x,\mu\nu}]$ gives the energy in the Boltzmann factor; it is possible to use statistical methods to study a lattice theory and the advantages are that these methods are well established and usually easy to apply. For example, a high-temperature expansion of the partition function

in statistical mechanics consists in a small β expansion: since $\beta \propto 1/g_0^2$, this amounts in a strong-coupling expansion of the corresponding gauge theory. Other methods, like mean field approximation or Monte Carlo simulations, can be employed for a lattice gauge theory. We shall make use of numerical Monte Carlo simulations in the following.

1.3 Critical points and the quantum continuum limit

It is important to stress again that, after having obtained a result on the lattice using one of the methods above or by means of perturbation theory, this result has to be "translated" into a physical continuum result. This procedure, called the *continuum limit*, or quantum continuum limit, is not trivial. As we already said in Sec. 1.1.4, the quantum continuum limit can be viewed as a renormalization program, where one has to remove the regularization (the lattice spacing in this case), while keeping fixed some physical observables (like a mass or an energy scale).

Imagine that we have measured a mass in lattice units $\hat{m} = ma$; if we let $a \rightarrow 0$, then $\hat{m} \rightarrow 0$ because we would require the physical dimensionful mass m to remain finite in that limit. At the same time, we can look at \hat{m} as the inverse of a correlation length $\hat{\xi} = 1/\hat{m}$ in the corresponding statistical system. In the continuum limit, the correlation length diverges, which is a sign of a second order phase transition, or critical point of the statistical system. This relation between continuum limit and critical points, can be explained naively with a physically sounding argument; if we want the lattice result to be valid in the continuum physics, we have to require that the system loses memory of the underlining lattice structure: this is just what happens when the correlation length of the system diverges.

The only parameter we have in our lattice theory is the dimensionless coupling constant β , or equivalently g_0^2 . This is the only quantity we can tune to reach the critical point of the theory. What we are saying is that, while sending a to 0, we should let g_0 go to g_{crit} at the same time. This is a typical feature of the renormalization procedure, where bare couplings of a theory acquire a dependence on the cutoff or on the energy scale at which the theory is defined.

1.3.1 β function and asymptotic freedom

Using the renormalization group (RG) equation for g , and considering the lattice spacing a as the inverse of our energy scale, we write

$$-a \frac{dg}{da} = \beta(g) \quad . \quad (1.83)$$

Here $\beta(g)$ is the beta function of the theory. In the perturbative regime $g_0 \ll 1$, the renormalization group equation is well approximated by the first two terms of the beta function:

$$-a \frac{dg_0(a)}{da} = -\beta_0 g_0^3 - \beta_1 g_0^5 \quad , \quad (1.84)$$

where the first two terms of the expansion are universal (do not depend on the choice of renormalization scheme) and read

$$\beta_0 = \frac{11N}{48\pi^2} \quad , \quad \beta_1 = \frac{102}{121}\beta_0^2 \quad , \quad (1.85)$$

for a $SU(N)$ pure gauge theory. The remarkable fact in these formulae is that the beta function in (1.84) is negative in a neighbourhood of the origin (where the perturbative series is reliable), implying that the coupling g_0 becomes smaller as the length scale a decreases. This property, characteristic of non-Abelian gauge theories, is called *asymptotic freedom*. It suggests that perturbation theory becomes reliable at short distances, or high energies, in the continuum as well as in the lattice theory. Moreover, it implies that the point $g_0 = 0$ is a RG-fixed point, and the continuum limit of lattice gauge theory has to be taken sending a to 0, as well as g_0 to 0, if we want physical quantities to remain finite.

Integrating the RG equation (1.84), we obtain the relation between a and g_0

$$a = \Lambda_{LAT}^{-1} e^{-\frac{1}{2\beta_0 g_0^2}} (\beta_0 g_0^2)^{-\frac{\beta_1}{2\beta_0^2}} [1 + O(g_0^2)] \quad , \quad (1.86)$$

and

$$g_0^2 = -\frac{1}{\beta_0 \ln(a^2 \Lambda_{LAT}^2)} \quad , \quad (1.87)$$

which again reveals the vanishing of g_0 in the continuum limit $a \rightarrow 0$. The equations above, also show the appearance of an integration constant Λ_{LAT} which has the dimension of an energy. This is quite interesting, because the pure gauge theory has no dimensional parameters (g_0 is dimensionless and there is no mass term) in its classical action. This phenomenon is associated with *dimensional transmutation* and it is a pure quantum effect.

From the last discussion, we see that, in order to make physical predictions using lattice gauge theories, it is in general necessary to measure a number of physical observables equal to the number of bare parameters on the action. Every physical dimensionful observable on the lattice is then measured in terms of the appropriate power of the lattice lambda parameter Λ_{LAT} . This parameter is completely arbitrary so far and reflects the arbitrariness in the choice of the renormalization scale. What we learn from this is that, on the lattice, we can only determine dimensionless ratios of physical quantities. Moreover, to ensure we are extracting continuum physics, every observable should follow the exponential behaviour in (1.86) called *asymptotic scaling*, which means we are sufficiently close to $g_0 = 0$.

In the following, we would like to calculate masses on the lattice. We should then set a physical scale, and express our masses in terms of that. In Ch. 3, we will see how to practically set the scale for our lattice calculations.

1.4 Finite temperature lattice gauge theories

We are going to explain in this section how to describe a quantum field theory in thermodynamic equilibrium at finite-temperature $T \neq 0$. The natural framework is, again, the Euclidean path integral, and a lattice formulation follow just in the same way as we have described in the previous sections.

The path-integral representation of a finite-temperature quantum field theories starts from the thermal partition function

$$\mathcal{Z}(T, V) \equiv \text{Tr} e^{-\beta H} \equiv \sum_n \langle n | e^{-\beta H} | n \rangle = \sum_n e^{-\beta E_n} \quad , \quad (1.88)$$

where we have written the trace as a sum over a complete set of energy eigenstates. The parameter β is related to the inverse temperature through the Boltzmann constant

$$\beta = \frac{1}{kT} \quad . \quad (1.89)$$

For convenience, we set $k = 1$ in the following.

Following (1.11), which tells us how to write the amplitude for the propagation of a field in the time interval given by T , we can now interpret our temperature as a time variable (after a Wick rotation) writing

$$\langle \phi_f(\vec{x}) | e^{-H/T} | \phi_i(\vec{x}) \rangle = \int \mathcal{D}\phi \exp \left[- \int_0^{1/T} dt \int d^3x \mathcal{L} \right] \quad . \quad (1.90)$$

In order to calculate the trace over states, we should put $\phi_f(\vec{x}) = \phi_i(\vec{x})$, and perform an additional integration over $\phi_i(\vec{x})$. The resulting expression for the partition function is almost equal to (1.24), where the time variable of the action goes from 0 to $1/T$, and where the field ϕ is taken with periodic boundary conditions

$$\phi(\vec{x}, 0) = \phi(\vec{x}, 1/T) \quad , \quad (1.91)$$

$$\mathcal{Z}(T, V) = \int \mathcal{D}\phi \exp \left[- \int_0^{1/T} dt \int_{-\infty}^{\infty} d^3x \mathcal{L} \right] \quad . \quad (1.92)$$

If the field were a fermionic one, instead of bosonic, we would have chosen antiperiodic boundary conditions in order to gain the right Fermi-Dirac statistics. The expression (1.92) reproduces the standard Euclidean formulation of quantum field theory in the limit $T \rightarrow 0$. The point is that nothing depends on real time for a system in thermodynamical equilibrium, and in this formulation we are allowed to calculate only static properties (such as masses or interaction potentials) of the field theory.

As we pass to the lattice regularization of the quantum field theory, the only thing to do is to

define a lattice whose size along the temporal axis is much smaller than along the spatial ones. The spatial volume should remain large to guarantee that we are in the thermodynamic limit, whereas the time direction need to be small in unit of lattice spacing if we want to reproduce a finite temperature:

$$L_t = \frac{1}{aT} \ll L_s \quad , \quad (1.93)$$

where L_t is the size of the temporal direction and L_s the size of the spatial ones. It is then straightforward to consider the temperature on the lattice as

$$T = \frac{1}{aL_t} \quad , \quad (1.94)$$

and to impose periodic boundary conditions as usually by construction. We remind that on a Euclidean lattice, all directions are symmetric, and any of the four can be chosen as the temporal one.

Another important remark is that, since the lattice spacing is related to the coupling constant, as described in Sec. 1.3, we can change the temperature on the lattice by varying either the size along the temporal axis L_t , or the lattice coupling constant β (we are now considering only a pure lattice gauge theory for our convenience).

2. *Motivations for a large- N study*

From the previous chapter, we have learnt that the lattice discretization has the advantage of being a truly non-perturbative regularization of gauge theories. We can apply the lattice approach to study QCD, for example. However, it would be of great importance to have some kind of non-perturbative insight of the theory directly in the continuum to guide numerical studies. The most concrete proposal in this direction is the large- N limit, first proposed by 't Hooft [3]. Another non-perturbative insight of QCD comes from string theories through their conjectured duality with field theories [4]. In this chapter we will briefly review the aforementioned approaches in order to motivate our study of a pure Yang-Mills theory in the large- N limit.

2.1 *Pure YM and QCD in 3 + 1 dimensions*

The analysis we will describe in the next chapters starts from the definition of a pure gauge theory with a generic gauge group $SU(N)$ in 3 + 1 dimension. Such a theory, which is perfectly sensible as a continuum theory, will be discretized on a regular hypercubic 4 dimensional lattice in order to gain information with direct measurements of spectral observables. However, we now want to start from the continuum gauge theory defined by the Lagrangian density

$$\mathcal{L} = -\frac{1}{2}\text{Tr} F_{\mu\nu}F^{\mu\nu} \quad , \quad (2.1)$$

where the field strength tensor $F_{\mu\nu}$ has already been defined in Sec. 1.2.1, but in the following discussion we shall use a slightly different notation. Now the gauge field A_μ is an hermitian $N \times N$ matrix expressed in terms of the $\mathfrak{su}(N)$ algebra generators T_a as

$$[A_\mu(x)]^{ij} = \sum_{a=0}^{N^2-1} A_\mu^a(x)[T_a]^{ij} \quad . \quad (2.2)$$

As we know, the index a in the above expression refers to the adjoint representation of the group (the one of the generators), whereas the two indices i and j of the matrix form $[A_\mu(x)]^{ij}$, refer to the fundamental and anti-fundamental representations respectively. Using the double index notation (or component notation) will help in understanding the index structure of the Feynman

diagrams.

A perturbative evaluation of the dynamics of such a Yang–Mills theory, expressed as a series in powers of the coupling constant or equivalently in the usual diagrammatic expansion with Feynman graphs, is not a valuable tool to investigate the low energy regime of the theory. In that region of the phase space, the theory is supposed to be confining for all values of $N \geq 2$ and signals of confinement, such as a linear increasing of the potential between two static charges at asymptotically large distances, have been observed in numerical simulations. However, a deep understanding of the full large distance/small energy regime of the theory needs still to be reached.

It is important to note that, though the theories defined by (2.1) for all values of N , might have little to do with the physics of the real world described by QCD with gauge group $SU(3)$, their understanding can shed light on the behaviour of the gauge degrees of freedom in QCD and explain their role in the confinement phenomenon. Indeed, a pure $SU(3)$ pure gauge theory can be viewed as the full QCD where the mass of the matter fields (the quarks) has been taken to infinity; this $m_q \rightarrow \infty$ limit corresponds to the impossibility of propagating a quark particle which, being infinitely heavy, does not contribute to the dynamical sector of the theory. Thus, this limit describe the propagation of only gauge fields (the gluons), and from their interactions it is possible to create a full spectrum of bounded excitations called *glueballs*. Glueballs are supposed to be present in the full QCD as well, but their mixing with quark bound states, such as mesons, can hide their contribution in the spectrum.

In the following, we will provide a reason for discarding the quark degrees of freedom, at least for large $SU(N)$ groups and we will show that QCD with a $SU(\infty)$ gauge group is a pure Yang–Mills theory.

2.2 $1/N$ expansion and planar graphs

One might think that letting $N \rightarrow \infty$ would make the analysis of QCD much more complicated because of the larger gauge group and consequent increase of the number of dynamical degrees of freedom. Moreover, one might think that $N = \infty$ has very little to do with $N = 3$. However, $SU(N)$ gauge theories simplifies in the $N \rightarrow \infty$ limit and, more precisely, the solutions to these theories possess an expansion in powers of $1/N$.

This important observation was first pointed out by 't Hooft [3] and it is based on the fact that in such theories, N is another dimensionless parameter besides g_0 ; a sensible $N \rightarrow \infty$ limit is possible when a suitable combination of N and g_0 is held fixed. Moreover, this is true for general field theories with symmetry group $O(N)$, $U(N)$, besides their restriction to the special subgroups. Here we want to give only a brief overview of the arguments and of the consequences

relevant to our work; what follows is based on the treatment of Coleman [17] and on [18, 19]. Let us consider a pure continuum gauge theory as expressed at the beginning of the previous section by (2.1) and (2.2). The propagator of the gluon field A_μ^a with colour index a (using the adjoint notation) is

$$\langle A_\mu^a(x) A_\nu^b(y) \rangle = \delta^{ab} D_{\mu\nu}(x-y) \quad , \quad (2.3)$$

where $D_{\mu\nu}(x-y)$ is the gauge fixed propagator in perturbation theory. We are now only interested in the index structure of the propagator and we will omit the space–time term $D_{\mu\nu}(x-y)$. The index is conserved in the propagation as indicated by the delta function. However, as we have already noticed, general theoretical observations of group theory allow an adjoint index to be written as a pair of fundamental and anti–fundamental indices running, in this case, from 1 to N . In the double index notation we can write the propagator as

$$\langle (A_\mu)^{ij}(x) (A_\nu)^{kl}(y) \rangle \propto \left(\frac{1}{2} \delta^{il} \delta^{kj} - \frac{1}{2N} \delta^{ij} \delta^{kl} \right) \quad , \quad (2.4)$$

where we have used the completeness condition on the generators T_a . Omitting the second term in parentheses on the right hand side of (2.4) at large N because it is subleading, we can depict the gluon propagator by a double line as shown in Fig. 2.1: each line represents the delta function which preserve the index along the line, and each line has an arrow indicating if it is a fundamental (arrow from left to right) or anti–fundamental index (arrow from right to left).

The great advantage of the double line representation is manifest when we have to follow colour indices on Feynman diagrams; to each double–line graph there corresponds a single–line graph with a given assignment of the indices. Every diagram in the usual perturbation expansion can be completely rewritten as a sum of double–line graphs. Each double–line graph gives a particular colour index contractions of the original diagram. For example, the three–gluon interaction vertex is shown in Fig. 2.2.

To compute the N –dependence of each diagram, in order to understand its contribution in the large– N expansion, it is better to define a rescaled Lagrangian where the fields are $g_0 N^{-1/2} A \rightarrow A$

$$\mathcal{L} = \frac{N}{g_0^2} \left[-\frac{1}{2} \text{Tr} F_{\mu\nu} F^{\mu\nu} \right] \quad . \quad (2.5)$$

The theory defined by this Lagrangian admit a smooth non–trivial $N \rightarrow \infty$ limit where there exists loops diagrams which contributes even at the leading order in $1/N$.

One can read off the powers of N in any Feynman graph from (2.5). Every vertex has a factor of N , every propagator a factor $1/N$ and, in addition, every colour index loop gives a factor of N , since it represents a sum over N colours. Moreover, through the double–line notation, we can relate each graph to a two dimensional surface. For simplicity, let us consider only vacuum connected diagrams. Because those graphs has no external lines, every index line must close to

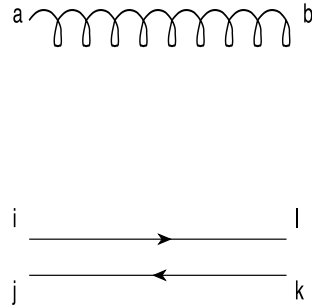


Figure 2.1: The gluon propagator in the single-line representation (above panel) with an index in the adjoint representation which is conserved by the delta function in (2.3). In the double-line representation (lower panel), the index conserved are in the fundamental (right arrow) and in the anti-fundamental (left arrow).

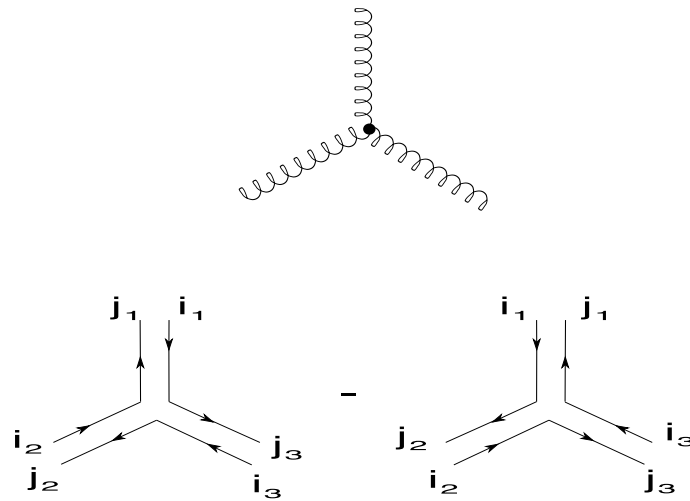


Figure 2.2: The three-gluon interaction vertex in the single-line representation (above panel) and in the double-line representation (lower panel). The subscripts in the line indices refer to each of the three gluons. The relative minus sign can be calculated directly from the cubic A term in the Lagrangian (2.1) written in the components notation.

form a loop: this loop can be considered as the perimeter or edge of a polygon. Hence, a double line is a prescription for fitting together these polygons to form a two dimensional surface. Since the edge of the polygons are oriented by the arrows on the index lines, the resulting surface corresponding to a graph will be oriented.

We know that every two dimensional oriented surface is topologically equivalent to a sphere with some number of holes cut out of it and some number of handles stuck on it. It can be shown that the diagrammatic expansion can be rearranged in a topological expansion. In fact, a graph with V vertices, E edges and F faces (where a face is an index loop) is proportional to

$$N^{V-E+F} \equiv N^\chi \quad , \quad (2.6)$$

where χ is the Euler character of the surface and it is a topological invariant. For the kind of surfaces we can construct starting from the double-line diagrams, the Euler character can be defined using the number of holes (boundary in mathematical language) b and handles h (which is called the *genus* of the surface) as

$$\chi = 2 - 2h - b \quad . \quad (2.7)$$

Therefore, the maximum power of N carried by a diagram can be 2, when $h = 0$ and $b = 0$ and the surface is equivalent to a sphere. In the $N \rightarrow \infty$ limit, these graphs contribute to the leading term. In terms of the single-line original graphs this means that they are planar graphs, that is graphs that can be written with no intersections between the lines but interaction vertices. Non-planar diagrams have genus $h > 0$ and then are subleading.

Moreover, the number of holes b can be different from zero only if we allow quarks to propagate, because a boundary in the surface comes from a loop of unpaired index lines. As we can see from (2.6) and (2.7), planar diagrams with one quark loop forming the boundary of the graph are subleading because they carry a power N .

Any diagram in perturbation theory is proportional to the coupling constant and we insert it in our previous counting rules. Let us consider the simplest radiative correction in the pure gauge theory, the one-loop correction to the gluon propagator shown in Fig. 2.3. There are 2 three-gluons vertices, each with a power of g_0 , and a gluon loop where a sum over the colour must be performed giving a contribution of order N . Therefore, the contribution of this diagram is $\sim g_0^2 N$. If we want the large- N limit to be non-trivial, the coupling constant should satisfy the scaling

$$g_0^2 \sim \frac{1}{N} \quad . \quad (2.8)$$

A sensible $N \rightarrow \infty$ limit is then performed by keeping fixed

$$\lambda \equiv g_0^2 N \quad , \quad (2.9)$$

the so called 't Hooft coupling, which is $O(1)$. Hence, the pure gauge theory has a genus expansion in diagrams which contribute at order

$$\left(\frac{1}{N^2}\right)^h, \quad (2.10)$$

whereas a gauge theory with quarks has diagrams at order

$$\left(\frac{1}{N^2}\right)^h \left(\frac{1}{N}\right)^b. \quad (2.11)$$

We can then draw the conclusion that neglecting quark degrees of freedom by sending $m_q \rightarrow \infty$ gives corrections that are increasingly unimportant as N grows.

In this work we will consider only the pure gauge theory and then we expect that the leading corrections are suppressed with $1/N^2$.

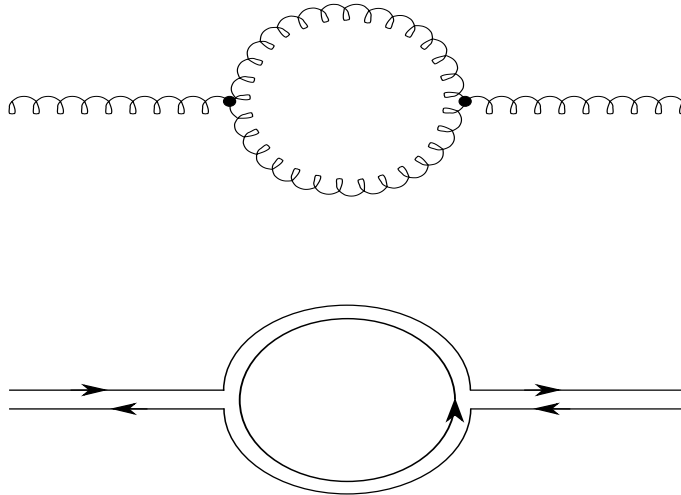


Figure 2.3: The pictorial representation of the one-loop contribution to the gluon propagator. Associated with the closed index line in the double-line notation, there is a factor of N . If we count the g_0 factors of each interaction vertex, we find that the contribution of the diagram is $\sim g_0^2 N \sim 1$.

2.3 The gauge/gravity correspondence

The topological expansion of double-line diagrams has a striking similarity to the string coupling constant expansion in string theories. It is indeed conjectured that a connection between large- N QCD and string theories may exist.

The aim of this section is to provide the necessary information to understand one possible motivation for this work; here we don't want to give a formal description of the subject which, on the other hand, can be found in the literature [20, 21]. We will follow [22] for a review

relevant for our study: the final result of this section will be to show that our study can be used to compare the emerging non-perturbative picture of a large- N four dimensional gauge theory with predictions obtained from a perturbative calculations in string theories.

Let us begin with the conjecture which relates string theories on suitably chosen AdS manifolds with conformally invariant field theories whose symmetries depend on the internal manifold. This is the Maldacena conjecture [4], further investigated in the work of Witten [5]. The conjecture relates the M theory in the $AdS_{d+1} \times \mathbf{X}$ background to the large- N limit of a d dimensional conformal field theory. Different field theory can be described by a careful choice of the internal Einstein manifold \mathbf{X} ; for example it is possible to induce the presence, on the field theoretic side of the correspondence, of supersymmetry, or of a $SU(N)$ gauge symmetry. It is important to stress that this AdS/CFT correspondence is formally only a conjecture. Let us discuss the conjecture in the most studied example of type IIB string in the $AdS_5 \times \mathbf{S}^5$ background. We can recognize three different levels of using the conjecture:

1. the "weak" level statement is that the correspondence only holds between supergravity on $AdS_5 \times \mathbf{S}^5$ and the *strong coupling limit* of large- N $SU(N)$ $\mathcal{N} = 4$ supersymmetric gauge theory in 4 dimensions. Many results that confirm the same behaviour of some observables on both sides have been obtain so far (see for instance [20] for a thorough discussion of all these checks); this level of the Maldacena conjecture is now commonly accepted as a firmly established result;
2. The "normal" level of the conjecture extends the relation from the supergravity limit to the whole type IIB super-string theory in the $AdS_5 \times \mathbf{S}^5$ background. that theory is then related with the large- N limit of $SU(N)$ $\mathcal{N} = 4$, also beyond the region of strong coupling. If we want to obtain from the AdS/CFT correspondence a QCD-like theory in the weak coupling limit, we should work at this level of the conjecture, but essentially no check exists of the Maldacena conjecture at this level;
3. the "strong" level assumes that the conjecture holds also for the string theory at an arbitrary order in the loop expansion (in term of the string coupling constant which is proportional to $1/N$). This would imply that, given the string theory result at a given order, we have, on the field theory side, information about an arbitrary order in the $1/N$ expansion discussed in Sec. 2.2. We have by now a rather good control of the large- N limit on the lattice side and a step in this direction has been made with our present work: knowing the corrections to the $N = \infty$ theory on both side of the correspondence will help in checking the conjecture even at this "strong" level.

It is worthwhile to stress that (independently from the possible applications to QCD) the AdS/CFT correspondence is of great theoretical interest in itself.

If we aim to reach a description of real QCD-like theories by using the gauge/gravity correspondence, it is mandatory to break the conformal invariance which characterizes the resulting field theory independently of the choice of the gravity background. At the same time (if needed) we must somehow break the supersymmetry of the theory.

There are several possible ways to reach the aforementioned results, but we shall briefly expose the proposal suggested by Witten in [6]. The idea, whose main appealing feature is its simplicity, is that we can break the conformal invariance of the theory by compactifying the theory in one (or more) direction(s). Conformal invariance is then explicitly broken by the scale of the compactification radius R_0 . If we then choose appropriate boundary conditions for the particles of the theory in (one of) the compactified directions we can also break supersymmetry. The important point in all these steps is that the Maldacena conjecture can be extended also to the compactified version of the theory and that the theory obtained in this way can be a good candidate for a pure Yang Mills theory.

Let us state the simplest example of a type IIB super-string theory in the $AdS_5 \times S^5$ background. As already mentioned, the Maldacena conjecture allows us to relate this theory with the large- N limit of the $SU(N)$ $\mathcal{N} = 4$ supersymmetric gauge theory in 4 dimensions. Following Witten's proposal, we can break the $\mathcal{N} = 4$ supersymmetry and the conformal invariance by compactifying only one direction, in this case. A nice physical interpretation of this recipe is that, if we choose to compactify the manifold in the time direction we are equivalently studying the original system at a non-zero temperature T : indeed the temperature is proportional to the inverse of the compactification radius R_0 . For this reason, the original SYM theories are referred to as $T = 0$ theories and the non-supersymmetric compactified ones as $T > 0$ theories. In the $R_0 \rightarrow 0$ (hence $T \rightarrow \infty$) limit we then obtain a three dimensional effective theory which has several features in common with large- N 3d YM and could hopefully be identified (at least in some limit) with it.

Many of the attempts which have been made up to now to compare the results obtained in the framework of the finite temperature version of AdS/CFT correspondence with YM theories dealt with the glueball spectrum. In principle the calculation of the glueball spectrum, at least for the 0^{++} state, is rather simple. In the supergravity limit, the 0^{++} glueball is mapped by the Maldacena conjecture into the dilaton field of the corresponding supergravity description. Its mass is then obtained by solving the wave equation corresponding to that field (see [23] for the first performed calculations).

Even if there is no quantitative agreement with the lattice estimates, the pattern of the glueball masses (at least in $d = 3$ [24]) is correctly reproduced. Our study can provide new data from the lattice side of the AdS/CFT correspondence, and supergravity calculations can compare their results. We should first give our results in the continuum limit of the lattice theory before any

comparison can be made.

3. *Setting the physical scale*

In this chapter we are going to explain how we fix the energy scale of $SU(N)$ lattice gauge theories. Since we want to compare observables coming from theories with different gauge groups, we need to be sure that for all the theories we are extracting physical results at the *same* scale. This is done by using the energy scale of the deconfinement transition, which occur for all non-abelian lattice gauge theories.

3.1 *Fixing the lattice spacing*

To extract information about the glueball spectrum in the $N \rightarrow \infty$, we want to be able to compare lattice results for different theories. Perturbatively, we know that a smooth non-trivial $N \rightarrow \infty$ limit is possible only if the 't Hooft coupling $\lambda \equiv g_0^2 N$ is held fixed, as we have already shown in Sec. 2.2. On the lattice, the inverse of λ , can be written in term of the lattice coupling β as

$$\gamma \equiv \frac{1}{\lambda} = \frac{\beta}{2N^2} \quad . \quad (3.1)$$

We should check that, for each N , the spectrum is evaluated at β values such that γ is fixed. However, in the non-perturbative lattice formulation, we can obtain physical results only if we set the scale of our calculations: a physical quantity must be measured. Having in mind our final purpose, we should try to fix the scale such that, for every N , we are describing the same physics: every $SU(N)$ theory on the lattice must be regularized at the same cutoff a .

We decided to fix the lattice spacing using the physical scale characteristic of the deconfinement phase transition: the deconfinement temperature T_c (cfr. Sec. 3.2). However, we should be careful in the choice of a , because, in the end, we hope to perform a smooth continuum limit of our results: this can be achieved only if calculations are done in the scaling region, that is to say, at small enough lattice spacing (and correspondingly big enough values of β).

Since we are going to study thermal properties of a gauge theory, such as the deconfinement temperature, we use a periodic lattice whose temporal direction has a size much smaller than the spatial one. The temperature, in unit of lattice spacing, of the corresponding thermal theory

is then given by

$$a(\beta)T = \frac{1}{L_t} . \quad (3.2)$$

In (3.2) we wrote explicitly the dependence of the cutoff on the lattice coupling, and we referred to the temporal size, in unit of lattice spacing, as L_t . The same equation can be viewed also as a way to fix the cutoff

$$a = \frac{1}{L_t T} . \quad (3.3)$$

We decide, in this work, to fix the cutoff, for every value of N , at the value of

$$a = \frac{1}{6T_c} , \quad (3.4)$$

where 6 is the fixed number of lattice sites in the temporal direction. Given the implicit dependence $a(\beta)$, we can also write

$$a(\beta_c) = \frac{1}{6T_c} . \quad (3.5)$$

Then we are sure that the spectrum extracted from the lattice, for different gauge groups $SU(N)$, is given at the same physical scale.

The method used to find the critical value β_c , at which the deconfinement transition occur in the lattice gauge theory, is explained in the following, after a general discussion about the deconfinement transition in lattice gauge theories.

3.2 The deconfinement transition in LGT

On the basis of asymptotic freedom, one can expect that, at asymptotically large temperatures, the hadronic matter appears as an asymptotically free gas of quarks and gluons (*quark-gluon plasma*). The qualitative differences between this phase at high energy, and the phase of ordinary matter at low energy, imply the existence of a phase transition between the two regimes. This can be proved for instance in the strong coupling limit of lattice QCD [25, 26]. Over the years, many Monte Carlo studies have investigated this transition. A recent review is given in [27]. We shall now describe some aspects of of this phase transition relevant for our work.

Let us consider only pure $SU(N)$ YM theories, which can be seen as a generalization of QCD when the masses of all quarks go to infinity as described in Sec. 2.1; in this case it is easier to find a criterion to distinguish between the two phases of matter. The low temperature (and density) regime of a pure $SU(N)$ gauge theory is characterized by confinement, whereas the high temperature phase is deconfined (this behaviour is confirmed by lattice simulations on the low energy side, and by perturbation theory on the high energy side). As a first step to characterize the phase transition, one can try to describe the behaviour of the deconfined phase using perturbation theory; in fact, the short distance behaviour of matter is dominated by asymptotic

freedom for these theories. Nevertheless, serious infrared divergences appear and the predictive power of this expansion is limited; moreover, long distance properties, like confinement, are prevented from being investigated by the perturbative approach.

Using the purely non-perturbative lattice formulation, we can find a good order parameter to study the phase transition. Because of the periodic structure of the lattice, we can construct gauge-invariant quantities by taking the trace of the product of link variables along topologically non-trivial loops winding around the time direction. Let us consider the following expression, constructed from the temporal link variables starting from a given point \vec{x} :

$$l_p(\vec{x}) = \text{Tr} \prod_{t=0}^{L_t-1} U_{x, x+t\hat{0}} \quad , \quad (3.6)$$

where $\hat{0}$ represents a unit vector in the temporal direction. This expression is invariant under periodic gauge transformations, and it is referred to in the literature as the *Polyakov loop*.

The expectation value of the Polyakov loop has a simple physical interpretation. It is related to the free energy $F_q(\vec{x})$ of the system with a static quark in \vec{x} , measured relative to that in the absence of the quark [28]:

$$\langle l_p(\vec{x}) \rangle = e^{-F_q(\vec{x})/T} \quad . \quad (3.7)$$

Then, it probes the screening properties of a static non-singlet test charge in the surrounding gluonic medium. In the confined phase, a gauge charge in the fundamental representation cannot be screened by gluons, therefore the free energy (minus that of the vacuum) is infinite; on the contrary, in the deconfined phase, the free energy of a static quark is finite. This led to the Polyakov criterion of confinement at finite temperature:

$$\langle l_p(\vec{x}) \rangle \begin{cases} =0 & \text{confinement} \\ \neq 0 & \text{deconfinement} \end{cases} \quad . \quad (3.8)$$

3.2.1 Center symmetry and the order parameter

It can be seen that this criterion is intimately connected with the spontaneous breakdown of a global exact symmetry of the pure $SU(N)$ gauge action on the lattice: the *center symmetry*. We recall that the center of a group refers to that set of group elements which commute with all other elements of the group. For a general $SU(N)$ group, the center is the abelian group \mathbb{Z}_N : its elements are diagonal $N \times N$ unitary matrices proportional to the identity with coefficients

$$z_n = e^{\frac{2\pi i n}{N}} \quad (n = 0, 1, 2, \dots, N-1) \quad . \quad (3.9)$$

Let us call z_n also the matrix of \mathbb{Z}_N which has the elements z_n on the diagonal. The lattice action is then invariant under a global \mathbb{Z}_N transformation of all the time oriented link variables

between two neighbouring spatial slices

$$U_{x,0} \rightarrow U'_{x,0} = z_n U_{x,0} \quad , \quad (3.10)$$

where the z_n is the same for all spatial lattice points. Clearly, the Polyakov loop transform non trivially under this transformation, because only one of the link in the product (3.6) changes. Hence we have

$$l_p(x) \rightarrow z_n l_p(x) \quad . \quad (3.11)$$

Now, if we measure the expectation value of the Polyakov loop as a sum over link configurations distributed according to the exponential of the lattice action, we expect the following picture. Since lattice gauge field configurations related by center symmetry occur with the same probability (because they correspond to the same action), the sum over configurations yields zero for l_p because $\sum_n z_n = 0$. However, this is true only if the symmetry of the action is valid for the ground state as well: if not, then the symmetry is spontaneously broken and the configurations will cluster around any one of the z_n elements. Hence, we can conclude that the center symmetry is realized in the low temperature confining phase of the lattice gauge theory where $\langle l_p \rangle = 0$, whereas the symmetry is spontaneously broken in the deconfined phase and $\langle l_p \rangle \neq 0$. In the study of phase transitions, the spontaneous breakdown of a global symmetry is the first signal one should look for and in the case of lattice pure gauge theories, we have just shown that the Polyakov loop is a good order parameter.

3.2.2 Description of the phase transition

As we said, a pure gauge theory is characterized by a physical phase transition as the temperature is increased. At the critical temperature T_c , both a phase with confined gluons, and a phase which can be described as composed by a gluon plasma, coexist. For gauge group $SU(N)$ with $N \geq 3$ this is a first order phase transition of the lattice theory [29, 30, 31] and it is conjectured to be so also in the continuum [32].

In a first order phase transition, we can describe the two phases as the two vacua of an effective finite- T potential. However, for gauge group $SU(N)$, the deconfining vacua is indeed a set of N degenerate vacua (with the same free energy). On a finite volume, there will be a finite range of temperature T around T_c in which the system has a significant probability to be in both confining and deconfined vacua, occasionally tunnelling between them. Out of the range of temperature where this occurs, the degeneracy lifts and one phase becomes more probable as the free energies of the vacua split by some ΔE : the relative probabilities of the two vacua are then given by $e^{-\beta \Delta E}$. Since the free energy grows with volume $\Delta E \propto V$, we see that the finite volume transition region is typically $\delta\beta \sim O(1/V)$. We will make use of this in the following.

The thermodynamic limit of the phase transition temperature will be extrapolated from a finite

size study; this is a typical study for a second order transition, but it has been shown [33] that, even for first order transitions, it gives the correct values of (pseudo)–critical exponents and can be used to study the properties of the transition region in the thermodynamic limit.

When a physical phase transition is under investigation, it is always necessary to identify an order parameter that help distinguishing the different phases of the system. The order parameter is the Polyakov loop (see Sec. 3.2.1): its expectation value $\langle l_p \rangle$ is zero in the confining phase, but suddenly grows to a non-zero value when the transition temperature is passed. On a finite volume, however, tunnelling occurs between the N different vacua of the deconfined phase because the energy barrier between them is finite (this is related to the fact that a symmetry can be spontaneously broken only if there are an infinite number of degrees of freedom). As a consequence of this, $\langle l_p \rangle = 0 \quad \forall T$, because every N degenerate vacuum corresponds to an element of the center of $SU(N)$, and the Polyakov loops acquire that element as a phase factor when measured in that vacuum: the expectation value, being the average of l_p , sums up all the phase factors which gives always zero.

For finding β_c , we follow a well-known procedure e.g. [29]. We replace the Polyakov loop l_p with its average over a field configuration \bar{l}_p and take its modulus $|\bar{l}_p|$:

$$\bar{l}_p = \frac{1}{L_s^3} \sum_x \text{Tr} \prod_{t=0}^{L_t-1} U_{x, x+ta\hat{0}} \quad , \quad (3.12)$$

where the summation is only on spatial sites, and $\hat{0}$ represents a unit vector in the temporal direction. Since \bar{l}_p is a complex number, its modulus is defined as usual.

Though this is a good order parameter on a finite volume lattice, it is now not true that, in the confined phase, $|\bar{l}_p| = 0$: indeed $|\bar{l}_p| \neq 0 \quad \forall T$, but we should be able to distinguish the two separated phases by looking at the distribution of $|\bar{l}_p|$ as we will explain in the following. One sign of a first order phase transition is a double-peak shape of this distribution. In this case, the peak near zero (the distance from zero is $O(1/V)$ because it is a finite volume effect) is the one associated to the confined phase and it is well separated (in large enough volumes) from the peak corresponding to the deconfined phase. On the other hand, the value of \bar{l}_p itself can be in $N + 1$ different regions of the complex plane in the deconfined phase: a region around the axis origin and N regions distributed at angles corresponding to the N roots of unity. It is straightforward to associate the N regions different from zero, to elements of the broken centre group. In Fig. 3.1, we show the scatter plot of \bar{l}_p in the complex plane and, in Fig. 3.2, we show the histogram of $|\bar{l}_p|$: the features described above are clearly visible.

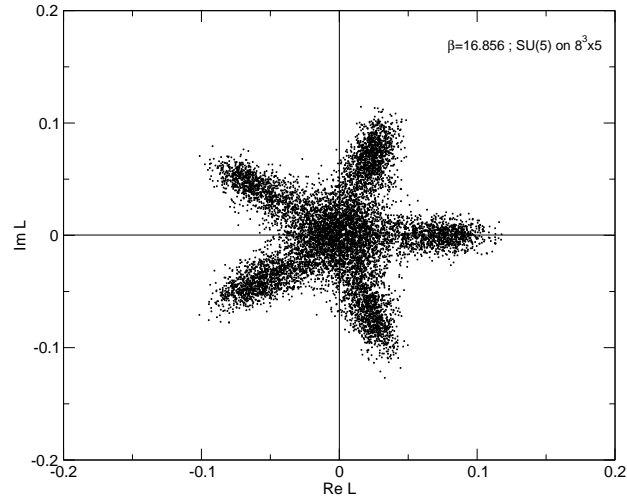


Figure 3.1: Scatter plot, on the complex plane, of the expectation value of \bar{l}_p for SU(5) in the critical region. The 5 regions out of the centre of the plane, correspond to transformations of \bar{l}_p under the 5 elements of the group \mathbb{Z}_5 .

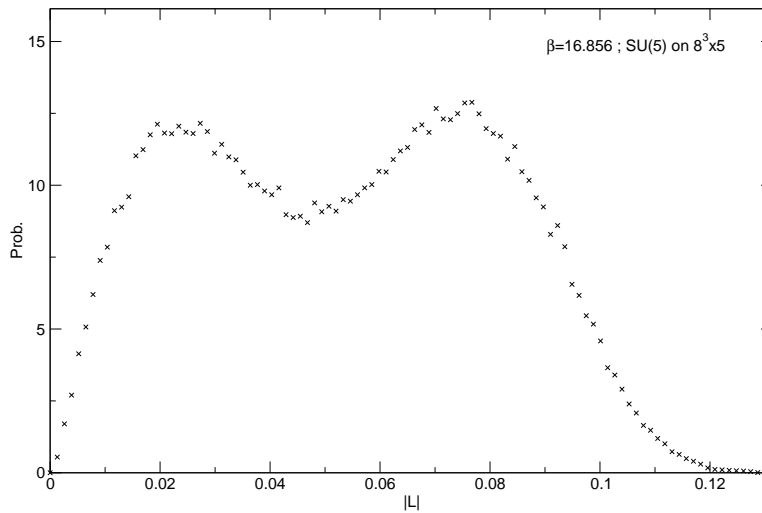


Figure 3.2: Histogram of the expectation value of $|\bar{l}_p|$ for SU(5) in the critical region. The double peak of this distribution is clearly visible even if the volume is only 8^3 .

3.3 Locating the phase transition

As we said at the beginning of this chapter, we look for the deconfinement transition temperature keeping the lattice volume fixed and varying the lattice parameter β . Then the transition has to be found at a certain value β_c . Clearly, we are interested in the infinite volume value, corresponding to the thermodynamic limit of the system. In general, for a first order phase transition, we already said that we expect the following finite- V correction for the (pseudo)-critical β :

$$\beta_c(V) = \beta_c(\infty) + O\left(\frac{1}{V}\right) . \quad (3.13)$$

In an infinite volume, the internal energy of the system will jump across the transition, with an infinite derivative in that point: the location of this jump defines the value β_c and the corresponding critical temperature $a(\beta_c)T_c = 1/L_t$. However, in a finite volume, the change will be continuous but rapid (if V is not too small) and we can define the specific heat $C(\beta)$ measuring this behaviour. The specific heat change is then related to the latent heat which characterizes the transition in the thermodynamic limit and a sensible definition of $\beta_c(V)$ can be the one where the maximum of $C(\beta)$ occurs. Another quantity can be used to locate the (pseudo)-critical $\beta_c(V)$ in a finite volume: it is the Polyakov loop susceptibility χ_L , which is known to diverge in the thermodynamic limit:

$$\chi_L = L_s^3 \cdot (\langle |\bar{l}_p|^2 \rangle - \langle |\bar{l}_p| \rangle^2) . \quad (3.14)$$

In particular, $\beta_c(V)$ is the value at which χ_L has its maximum. If we call the point of the maximum of χ_L , β_c^X , and the point where the specific heat has a maximum, β_c^C , these two definitions will differ by $O(1/V)$ terms, but will be equivalent in the thermodynamic limit. In the following we will use β_c^X because the signal of the Polyakov loop in our numerical simulations is better and χ_L can be measured with good precision (we will use, from now on, β_c referring to β_c^X).

As we remarked above, when the volume is large enough, our estimate for $\beta_c \equiv \beta_c(\infty)$ is given by

$$\beta_c(V) = \beta_c(\infty) - h \frac{L_t^3}{L_s^3} , \quad (3.15)$$

where the volume V of (3.13) is expressed here in physical units. The physical volume where the above formula starts to be valid has to be determined for every N we are going to investigate. In general, one determines T_c for a first order phase transition, as lying in the range of T where the system undergoes back-and-forth tunnelling between the two phases. Roughly locating this region, is the first step required before starting the study of the susceptibility. Unfortunately, the tunnelling probability decreases exponentially with the volume (remember the relative probability between the vacua as a decreasing exponential of the energy splitting ΔE), that is, in

the infinite volume limit, there would be an infinite energy barrier between the two phases, and the tunnelling does not happen. Hence, the first problem we face is to find a small interval of T (or β) where we can see tunnelling and, at the same time, we are at volumes where (3.15) can be used.

In the following, we are going to describe the finite size study we have performed using Monte Carlo numerical simulations to evaluate expectation values. A section of this thesis is dedicated to the explanation of Monte Carlo methods for lattice gauge theories (see Sec. 5.1).

3.3.1 Finite size study

We performed the finite volume study on lattices with $L_t = 5$ for SU(5) and SU(7). The values of β_c for $N = 3, 4, 6, 8$ are obtained in previous works by Lucini, Teper and Wenger [29, 30, 31]. Our work can, on one side, be used to fill the gap and, on the other side, more important, is fundamental to carry on our glueball study on the lattice: we need to fix the physical scale for all values of N we are going to investigate.

In the following, we would like to explain in details the procedure used, which is mostly similar to the one used in the above cited works.

Let us explain first, why this finite- V study was done at precisely the value of $L_t = 5$. This choice is crucial because for $L_t = 4$, the region of T where the phase transition occurs, is known to suffer from the effects of the bulk transition (the transition occurring between the strong and weak coupling regions of a lattice theory). The studies at $L_t = 4$, which means $a = 1/4T$, are on lattices where the bulk transition occurs in the same region of β characteristic of the physical phase transition between confined and deconfined phase. Of course, even at $a = 1/5T$ we can find the bulk transition, but this occurs at smaller β than the physical phase transition, as shown in Fig. 3.3. Moreover, if we were to choose $L_t = 6$, we would have spent too much time doing simulations due to the larger size of the lattice. We want to remark that the choice, we made clear at the beginning of this chapter, was to choose a lattice spacing of $a = 1/6T_c$, but we performed simulations at $a = 1/5T$. The procedure used to calculate β_c at lattice spacing $a = 1/6T$ is the following:

1. perform Monte Carlo (MC) runs in a wide interval of β and look at the expectation value of the plaquette: the bulk transition is in fact characterized by a sudden change of the plaquette average $\langle u_p \rangle$, $\Delta \sim 0.13$;
2. at the same time, measure the order parameter $|\bar{l}_p|$ and find a region in β where it jump from a value close to zero, to a value much greater (on finite volume, this jump is smoothed);

3. scan the region of β where the transition occurs and measure the Polyakov loop susceptibility (3.14). This point has to be done on different volumes. It is important that, on the smallest volume considered, the transition is clearly visible as a double peak in the histogram of $|\bar{l}_p|$;
4. for every volume V , determine $\beta_c(V)$ using a multi-histogram reweighting [34, 35] on the susceptibility: the position of its maximum is then measured with high precision;
5. perform a long simulation on a large volume (in physical units) for $L_t = 6$ and determine $\beta_c(V)$ in the same way described above;
6. use (3.15) to extract $\beta_c(\infty)$ for $L_t = 6$, where the parameter h is fitted using data obtained by the finite size study on $L_t = 5$.

This last point is known to be a weakness of this procedure, because h suffers of correction $O(a^2)$ and of possible violations of asymptotic scaling ($a = 1/5T$ can, for example, be out of the scaling region). However, in a very recent paper [36], the authors measured β_c for SU(4) and SU(6), directly on lattices with $a = 1/6T$ using intensive MC simulations. The results the authors have obtained, using a reweighting analysis similar to ours, are compatible, within the errors, with the results of [30]. The conclusion is that we can then rely on our finite size study for SU(5) and SU(7).

3.4 Results for SU(5) and SU(7)

The study of the finite- V dependence of the critical value β_c for $L_t = 5$ was done on the volumes presented in Tab. 3.1. In the same table, we show the number of configurations used to measure the average spatial and temporal plaquette $\langle u_s \rangle$, $\langle u_t \rangle$, and the average Polyakov loop $\langle \bar{l}_p \rangle$.

A wide range of β is scanned for the smallest volume and the average plaquette plot in Fig. 3.4 clearly indicates the region of the bulk transition. This transition is a lattice artifact; hence it is not physical and there is no scaling with the volume, i.e. it will be in the same region for larger volumes as well.

A scatter plot of $\langle \bar{l}_p \rangle$ shows, in Fig. 3.5 and Fig. 3.6, the presence of one phase when $\beta < \beta_c$ and of N different regions when $\beta > \beta_c$, monitoring the breaking of \mathbb{Z}_N centre symmetry. In general, to see how close we are to the critical value, we plot the MC history of $\langle |\bar{l}_p| \rangle$ for different values of β : the tunnelling is clearly visible in Fig. 3.7. Indeed, we are interested in the distribution of $\langle |\bar{l}_p| \rangle$; we expect a double peak, showing that the system spent part of the simulation time in one phase, and part in the other. That is exactly what we see in Fig. 3.8. We should make sure that a statistical sufficient number of tunnelling events is present, even at the largest volume.

Only if the system has spent enough time in both phases, we can rely on the reweighting method we used: a large part of the phase space (or configurations space) needs to be visited by the system during the simulation, if we want our data to be a good sample for statistical purposes. The tunnelling events on the largest volume investigated are shown in Fig. 3.9 for β values very close to β_c .

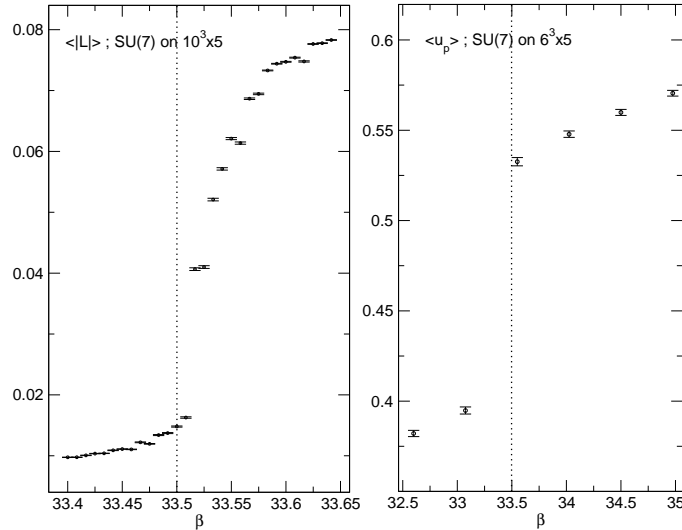


Figure 3.3: Expectation value of the order parameter $\langle |\bar{l}_p| \rangle$ and of the plaquette u_p for SU(7). The plot on the left shows the physical deconfinement transition; the plot on the right shows the bulk transition. The data of the two plots come from different volumes, but same lattice spacing: since the bulk transition is not physical, it occurs always at the same value of β for every volume. We determined it on a small volume.

| | SU(5) | | SU(7) | |
|-------|-------|------------------------|-------|------------------------|
| L_t | L_s | configs. $\times 10^3$ | L_s | configs. $\times 10^3$ |
| 5 | 8 | 100 | 6 | 100 |
| | 10 | 100 | 8 | 100 |
| | 12 | 200 | 10 | 150 |
| | 14 | 200 | 11 | 200 |
| | 16 | 300 | 12 | 250 |
| 6 | 14 | 200 | 12 | 250 |

Table 3.1: Spatial size of the lattices used in the finite volume study, and number of lattice gauge field configurations used to measure the expectation values $\langle u_p \rangle$ and $\langle |\bar{l}_p| \rangle$.

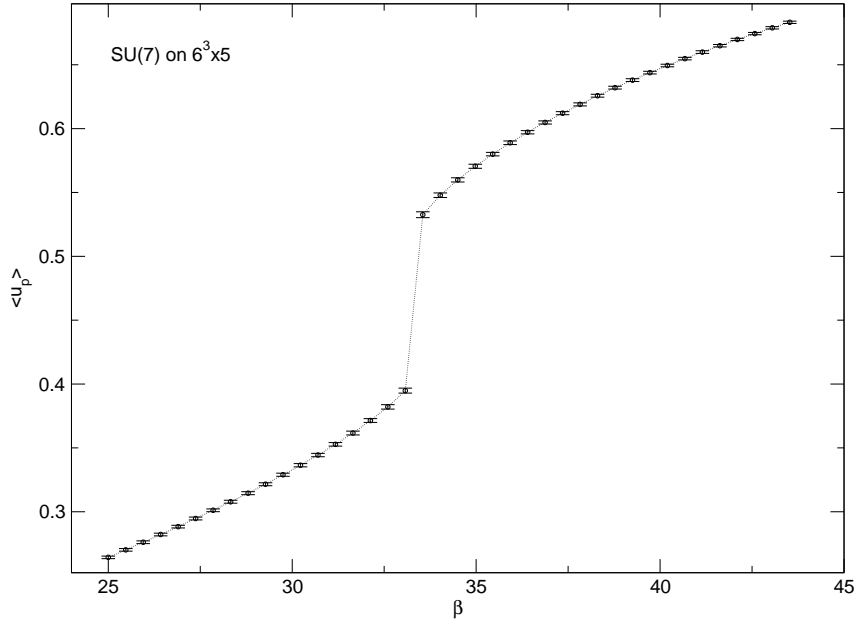


Figure 3.4: Bulk transition for $a = 1/5T$ in SU(7) determined on a lattice of spatial size $L_s = 6$. The average plaquette is not a smooth function of β : the small β behaviour is determined by a strong coupling expansion but it is not a good approximation near to the phase transition.

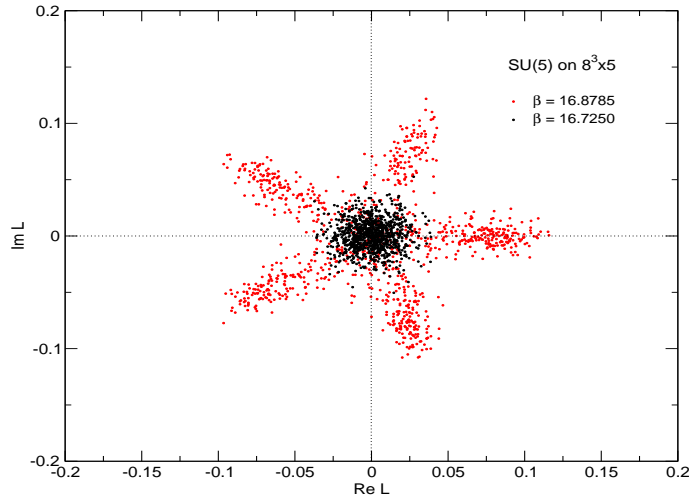


Figure 3.5: Scatter plot, on the complex plane, of the expectation value of \bar{l}_p for SU(5). The 5 regions out of the centre of the plane, correspond to transformations of \bar{l}_p under the 5 elements of the group \mathbb{Z}_5 . The smaller value of β is in the confined phase, the other in the deconfined phase where the centre symmetry is broken. Only points every 1000 measurements are plotted.

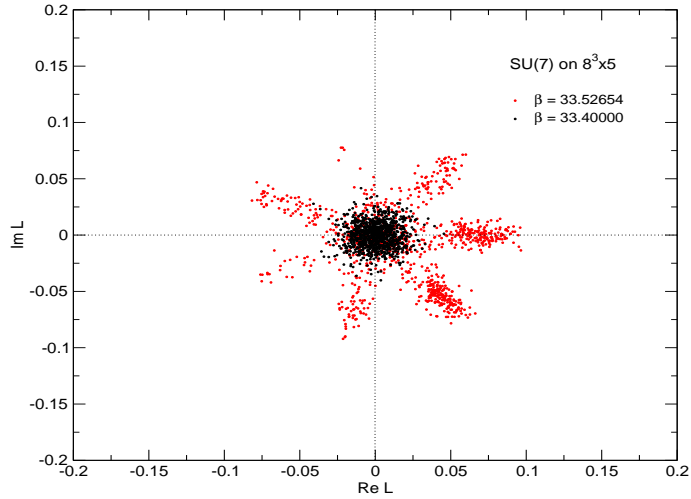


Figure 3.6: Scatter plot, on the complex plane, of the expectation value of \bar{l}_p for SU(7). The 7 regions out of the centre of the plane, correspond to transformations of \bar{l}_p under the 7 elements of the group \mathbb{Z}_7 . The smaller value of β is in the confined phase, the other in the deconfined phase where the centre symmetry is broken. Only points every 1000 measurements are plotted.

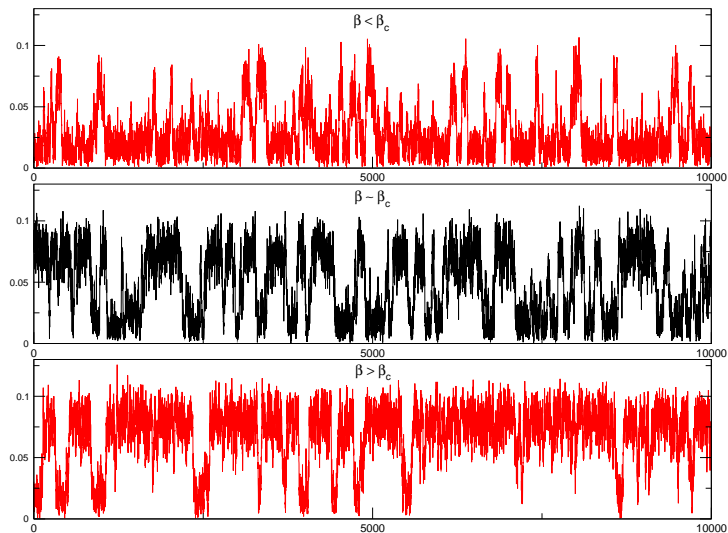


Figure 3.7: History of $|\bar{l}_p|$ for SU(5) at $L_s = 10$. The points are plotted every 10 MC steps. From top to bottom: $\beta = 16.840 < \beta_c$; $\beta = 16.86125 \approx \beta_c$; $\beta = 16.88875 > \beta_c$.

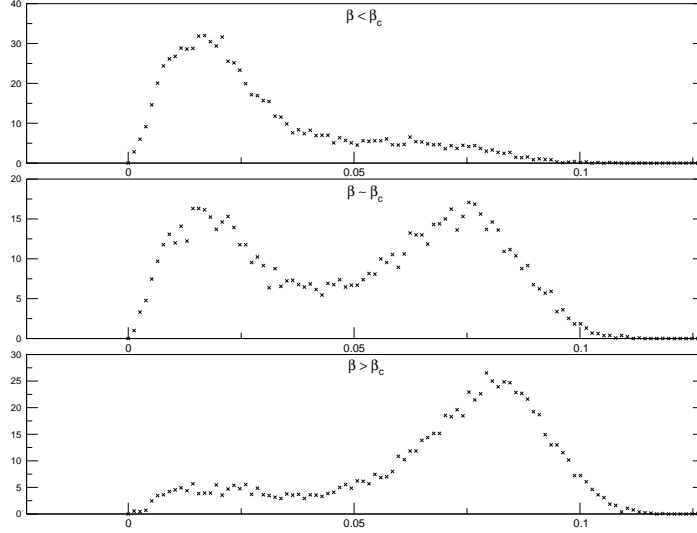


Figure 3.8: Normalized distribution of $|\bar{l}_p|$ for SU(5) at $L_s = 10$. Each of the two peaks present, is centered around the most probable value of $|\bar{l}_p|$ of each phase. From top to bottom: $\beta = 16.840 < \beta_c$; $\beta = 16.86125 \approx \beta_c$; $\beta = 16.88875 > \beta_c$.

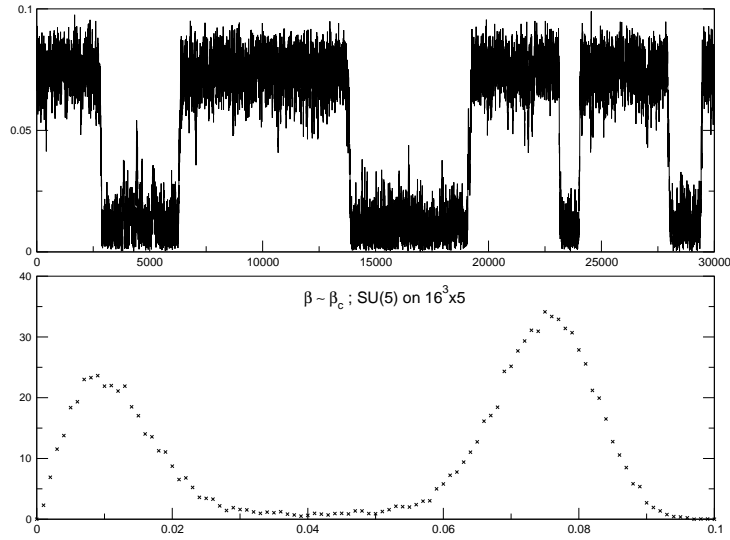


Figure 3.9: History and distribution of $|\bar{l}_p|$ for SU(5) on the largest volume investigated $L_s = 16$. The points of the top plot are taken every 10 MC steps. The simulation is made at $\beta = 16.87500$, which is very close to β_c . As can be seen from the distribution in the bottom plot, on larger volumes the two peaks are well separated.

3.4.1 Reweighting and error estimation

For all the simulation summarized in Tab. 3.2, we measured the susceptibility χ_L . The position in β where it has its maximum is then determined with an uncertainty given at least by the distance between the scanned β 's. The scan in β is already quite fine, but we want to reach a higher precision. To reach our goal, we used a reweighting technique: starting from the probability distribution of $\langle \bar{l}_p \rangle$ at a given value of β , this technique allows us to extract the susceptibility at other values of β . From only one simulation, which gives the starting distribution, say at $\bar{\beta}$, it is possible then to obtain χ_L in a small range of β near $\bar{\beta}$. However, the method works properly only if the reweighted points come from a distribution not very different from the starting one. To have a more robust statistical analysis, we used a multi-histogram reweighting, where different distributions coming from different simulations are taken into account. We examined the stability of this analysis through the comparison of the multi-histogram method with different numbers of histograms in input. As shown in Fig. 3.10, the choice of the histograms is important: as we have already remarked, the points need to be properly sampled. We did this stability analysis especially in situations where a small number of tunnelling was visible. The reweighted points are summarized in Tab. 3.3 for every volume.

In a reweighting procedure, the output points (in this case for the susceptibility) are statistically correlated and a usual procedure to deal with this is given by the bootstrapping [37, 38]. The bootstrap method consists in a resampling, with uniform probability, of the starting distribution; in general, the number of different resamplings, is equal to the number of points of the input distribution, but it can be smaller. By construction, the different bootstrap samples are independent and the distribution of their average values can be used to better estimate the variance of the input distribution. We obtain, from the bootstrap analysis, not only one value of χ_L for each β reweighted, but n_b of these values. n_b is the number of bootstrap samples. In order to give the right estimate for β_c , we analyzed the position of the maximum of χ_L using two different strategies. We note that the errors on $\beta_c(V)$ we obtain from the two strategies, are quite different.

1. The first strategy amounts in fitting the susceptibility points; each of these points is given with an error and it comes from the analysis of the bootstrap samples at each value of β . A typical plot is shown in Fig. 3.11. The fitting formula is parabolic and the fit with lowest reduced χ^2 is chosen. We made fit in various ranges of β because the parabolic form is a correct approximation only in a small neighbourhood of the maximum. An example is given in Fig. 3.12. Information about the value of $\beta_c(V)$ obtained, and about the fits, are given in Tab. 3.4.
2. The second strategy considers each bootstrap sample separately. The points of χ_L in each

sample are without errors. Hence, if we find the β value of the maximum in each sample, it is natural to consider, as $\beta_c(V)$ and as its error, the mean and standard deviation over the samples. In other words, since each bootstrap sample is an independent set, the critical β values coming from them are normally distributed and the usual gaussian analysis can be used. We also perform an analysis varying the number n_b of bootstrap samples: we can conclude that, choosing $n_b = 100$ is sufficient, in general, to have a stable statistical error. A typical distribution of β_c is the one in Fig. 3.13. In the end, we summarize the estimated values of $\beta_c(V)$ from this strategy, in Tab. 3.5.

| $L_t = 5$ | L_s | β range | points |
|-----------------|-------|-----------------|--------|
| SU(5) | 8 | 16.820 – 16.880 | 40 |
| | 10 | 16.840 – 16.890 | 40 |
| | 12 | 16.86 – 16.87 | 18 |
| | | 16.862 – 16.876 | 8 |
| | 14 | 16.860 – 16.872 | 8 |
| | 16 | 16.855 – 16.880 | 24 |
| 16.865 – 16.885 | | 8 | |
| SU(7) | 8 | 33.4 – 33.6 | 30 |
| | 10 | 33.40 – 33.65 | 30 |
| | | 33.50 – 33.55 | 8 |
| | 11 | 33.45 – 33.58 | 20 |
| | 12 | 33.50 – 33.60 | 16 |
| 33.53 – 33.55 | | 8 | |
| $L_t = 6$ | L_s | β range | points |
| SU(5) | 14 | 16.87 – 17.29 | 20 |
| SU(7) | 12 | 33.55 – 34.35 | 37 |

Table 3.2: Summary of the simulations done. In the β range, the points scanned are at fixed distances. Where two ranges are present, the first one is a preliminary study, usually with less configurations, to roughly locate the region of the transition. From the values of β in the smallest region and for every volume, we take the simulations to reweight. Both the values for $a = 1/5T$ and for $a = 1/6T$ are shown.

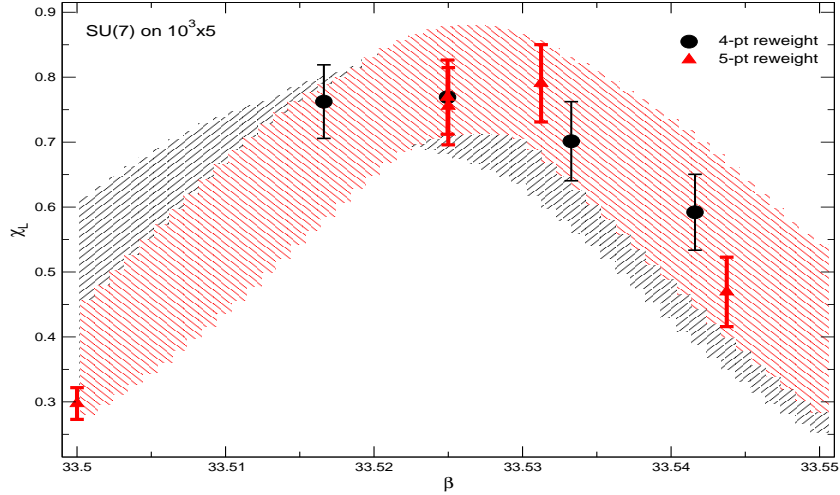


Figure 3.10: Different number of input points for the reweighting technique. We found that choosing 5 points spread in the whole region of β reweighted, was, when possible, the best choice. The lines highlight the region of reweighted points coming from $n_b = 100$ bootstrap samples. This gives a qualitative idea of the statistical distribution of the reweighted points.

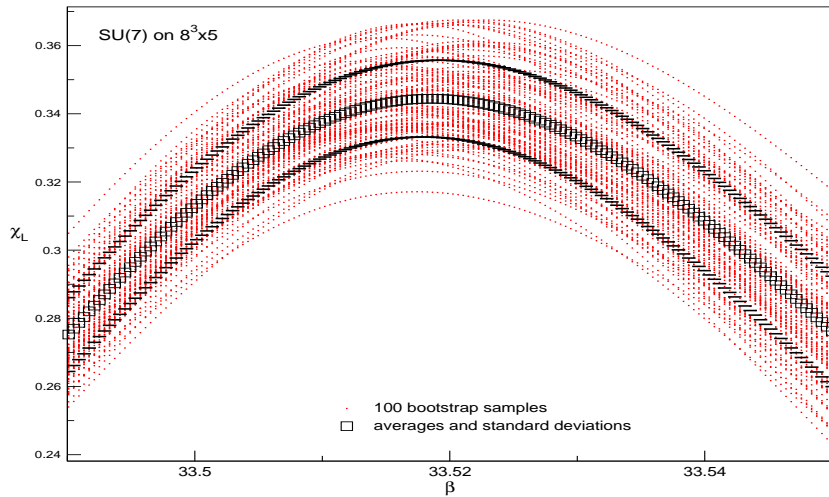


Figure 3.11: Bootstrap samples and average values from the reweight of 5 input histograms done for SU(7) at $L_s = 8$. The number of samples is $n_b = 100$, and the points reweighted are 200. The average values of χ_L are then fitted following the first strategy explained.

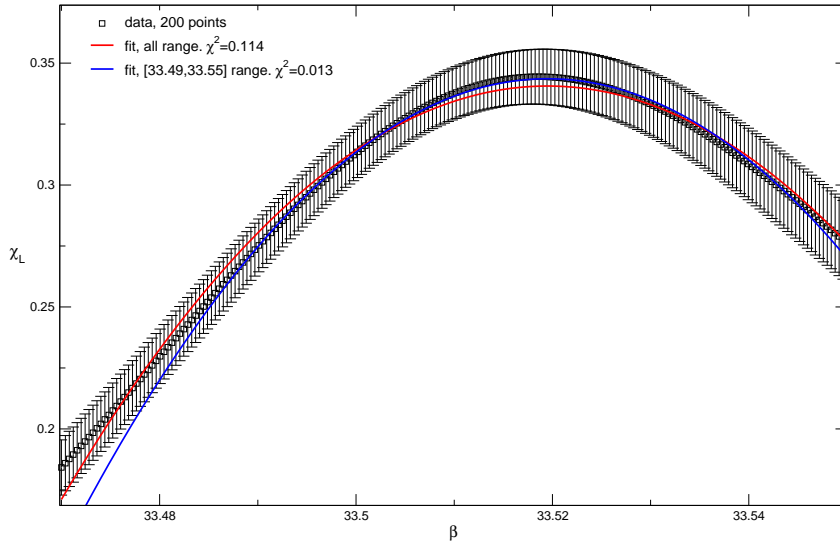


Figure 3.12: Fit of the reweighted susceptibility χ_L using different β ranges. The parabolic approximation is clearly better in the small range around the maximum. The χ^2 values are small because we know that the error are underestimated: a simple fit can not count for correlation error.

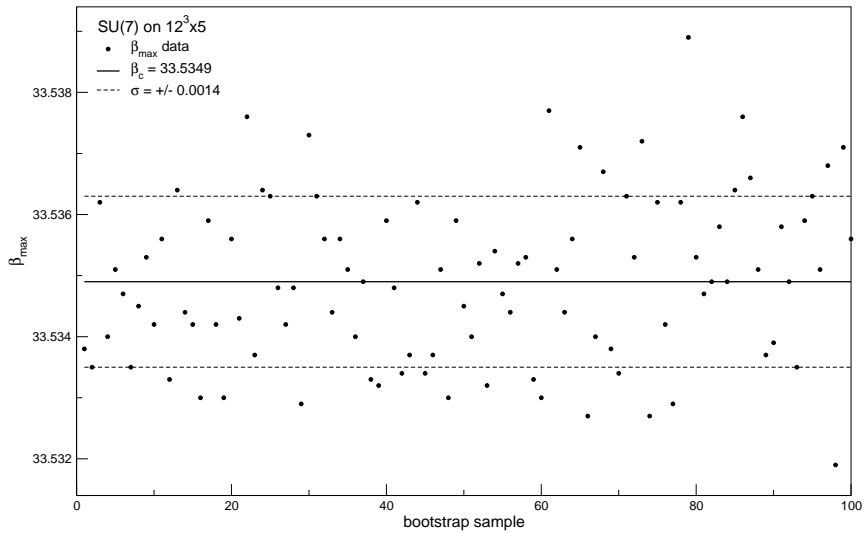


Figure 3.13: The β value corresponding to the maximum of χ_L are plotted for each bootstrap sample. The average value and its standard deviation are taken as the $\beta_c(V)$ and its error.

| $L_t = 5$ | L_s | β values in input |
|-----------|-------|--|
| SU(5) | 8 | 16.8335, 16.8500, 16.8560, 16.8590, 16.8785 |
| | 10 | 16.840, 16.85875, 16.86125, 16.86375, 16.87625 |
| | 12 | 16.86375, 16.86550, 16.86725, 16.86900, 16.87075 |
| | 14 | 16.8615, 16.8645, 16.8660, 16.8690 |
| SU(7) | 8 | 33.473260, 33.508560, 33.513220, 33.519880, 33.54652 |
| | 10 | 33.500, 33.52500, 33.53125, 33.54375, 33.52495 |
| | 11 | 33.5150, 33.5280, 33.5345, 33.5410, 33.5475 |
| | 12 | 33.5300, 33.5350, 33.5375, 33.5425, 33.5475 |
| $L_t = 6$ | L_s | β values in input |
| SU(5) | 14 | 17.0635, 17.0850, 17.1065, 17.1280 |
| SU(7) | 12 | 33.93, 33.97, 33.99, 34.03, 33.98 |

Table 3.3: Summary of the simulations used to reweight the susceptibility. The β points are chosen to have a good sampling of all the configurations space. Both the values for $a = 1/5T$ and for $a = 1/6T$ are shown.

| $L_t = 5$ | SU(5) | | | SU(7) | | |
|-----------|-----------------|--------------|------------------|-----------------|-------------|------------------|
| L_s | range | β_c | $\tilde{\chi}^2$ | range | β_c | $\tilde{\chi}^2$ |
| 8 | [16.84,16.88] | 16.85980(4) | 0.0067 | [33.50,33.53] | 33.51670(1) | 0.0002 |
| 10 | [16.850,16.875] | 16.86261(1) | 0.0055 | [33.51,33.54] | 33.52653(2) | 0.006 |
| 11 | | | | [33.525,33.540] | 33.53190(1) | 0.0025 |
| 12 | [16.860,16.875] | 16.867141(1) | 0.004 | [33.525,33.545] | 33.53497(2) | 0.014 |
| 14 | [16.864,16.874] | 16.869693(8) | 0.0037 | | | |
| 16 | [16.868,16.878] | 16.8726(8) | 0.02 | | | |
| $L_t = 6$ | SU(5) | | | SU(7) | | |
| L_s | range | β_c | $\tilde{\chi}^2$ | range | β_c | $\tilde{\chi}^2$ |
| 12 | | | | [33.95,34.01] | 33.9798(1) | 0.02 |
| 14 | [17.08,17.11] | 17.09640(3) | 0.005 | | | |

Table 3.4: Finite volume value of the deconfinement temperature β_c for SU(5) and SU(7) at lattice spacing $a = 1/5T$ and $a = 1/6T$. The analysis was done fitting the reweighted susceptibility χ_L in the range shown. All fits have more than 100 points and $\tilde{\chi}^2$ is defined as usual equal to χ^2/dof . Only best fits are shown.

| $L_t = 5$ | SU(5) | SU(7) |
|-----------|--------------|--------------|
| L_s | β_c | β_c |
| 8 | 16.859(2) | 33.5165(36) |
| 10 | 16.8623(10) | 33.5265(20) |
| 11 | | 33.53184(88) |
| 12 | 16.86699(74) | 33.5349(14) |
| 14 | 16.86969(81) | |
| 16 | 16.87258(80) | |
| $L_t = 6$ | SU(5) | SU(7) |
| L_s | β_c | β_c |
| 12 | | 33.9798(34) |
| 14 | 17.0966(24) | |

Table 3.5: Finite volume value of the deconfinement temperature β_c for SU(5) and SU(7) at lattice spacing $a = 1/5T$ and $a = 1/6T$. The analysis was done on $n_b = 100$ bootstrap samples for all volumes.

3.4.2 The thermodynamic limit

To extrapolate the infinite volume value $\beta_c(\infty)$, we fit the data of Tab. 3.5 with (3.15). We choose to use the data from the bootstrap analysis of the previous section, because they better account for the statistical auto-correlations coming from the reweighting technique.

The resulting values for $\beta_c(\infty)$, the critical value in the thermodynamic limit, are summarized in Tab. 3.6. Usually the small volume points do not follow (3.15) very well, because that behaviour is only asymptotically valid. We try to find the region of validity of (3.15) doing the fit using various number of volumes and choosing the best χ^2 fit as shown in Fig. 3.14 and Fig. 3.15. To obtain the corresponding $\beta_c(\infty)$ at the cutoff $a = 1/6T$, following the previously described strategy, we perform simulations on a single volume (see bottom of Tab. 3.2) for $L_t = 6$, and, with the same reweighting technique, we obtain the value of $\beta_c(V)$ shown at the bottom of Tab. 3.5. Then, using (3.15), where the value of h comes from the finite size study at $L_t = 5$, we obtain

$$\beta_c(\infty)_{\text{SU}(5)} = 17.1068(30) \quad \beta_c(\infty)_{\text{SU}(7)} = 33.9995(37) \quad . \quad (3.16)$$

We only calculate these values for SU(N), $N = 5, 7$, because the corresponding values for $N = 3, 4, 6, 8$ were present in the literature, as we have already mentioned. Let us summarize in Tab. 3.7 all the β_c we used in our simulations of the glueball spectrum. Now, if we want to measure a mass in lattice unit $\hat{m} = ma$, we can write a as $1/6T_c$ and then $m/6T_c$ will be our physical result for every N .

Now we should go back to the beginning of this chapter and remind two important points:

- we would like to extract the glueball spectrum at zero temperature, that is, on symmetric lattices. We used the deconfinement transition to fix the scale of all our lattice calculations. One of the things we are interested in, is the continuum limit, then we want to assure that the cutoff is in the scaling region. This was recently shown in [36]; $a = 1/6T_c$ is sufficiently small that can be used to extract continuum physics using renormalization group equations;
- another thing we are interested in, is the large- N limit. At this point we have fixed the lattice spacing for all our lattice calculations, in such a way to have the same energy scale for every N . We want to be sure that, in the large- N limit, the spectrum we get is non trivial and, following the 't Hooft limit, we should require perturbatively that β_c/N^2 is constant in N . We verify that this is the case, with small corrections $O(1/N^2)$. This scaling checks shows that for our cutoff $a = 1/6T_c$, we have a large- N theory which is non-trivial.

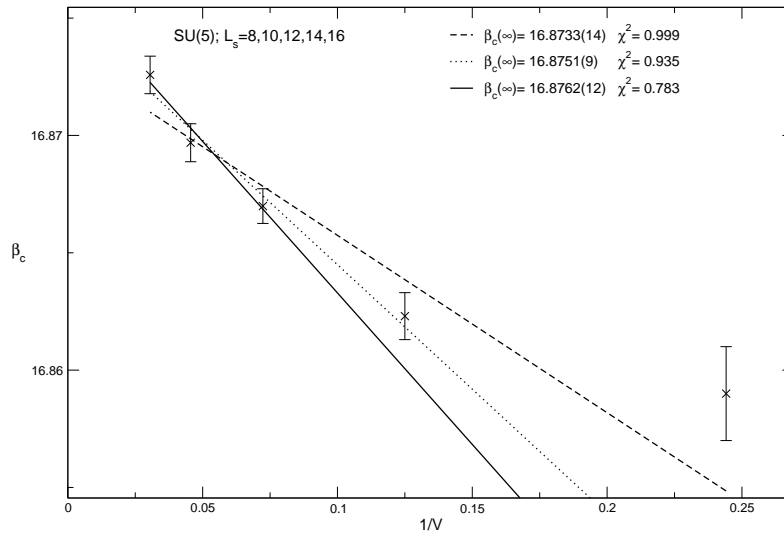


Figure 3.14: Finite volume fit with various ranges of the lattice spatial size for SU(5). The points are taken from Tab. 3.5.

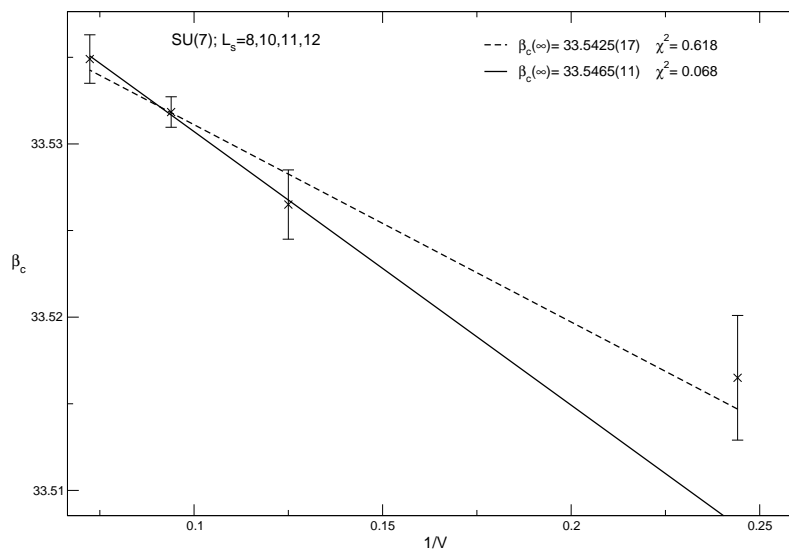


Figure 3.15: Finite volume fit with various ranges of the lattice spatial size for SU(7). The points are taken from Tab. 3.5.

| | $\beta_c(\infty)$ | h | L_s fitted | $\tilde{\chi}^2$ |
|-------|-------------------|-----------|--------------|------------------|
| SU(5) | 16.8762(12) | 0.129(23) | 12, 14, 16 | 0.783 |
| SU(7) | 33.5465(11) | 0.158(12) | 10, 11, 12 | 0.068 |

Table 3.6: Critical values, in the thermodynamic limit, of the deconfinement transition on lattices with $a = 1/5T$. All the values are obtained from fits (best $\tilde{\chi}^2$ shown) to the range of volumes shown.

| SU(N) \rightarrow | 3 | 4 | 5 | 6 | 7 | 8 |
|-------------------------|------------|-------------|-------------|-------------|-------------|-----------|
| $\beta_c(\infty)$ | 5.8941(12) | 10.7893(23) | 17.1068(30) | 24.8458(33) | 33.9995(37) | 44.496(3) |

Table 3.7: β_c values used in the simulations of the glueball spectrum: the lattice spacing is fixed at $a = 1/6T_c$. For $N = 3, 4, 6, 8$, we used the values in [30].

4. *Glueballs operators methodology*

4.1 *Glueballs masses on the lattice*

We are going to discuss now the central topic of the work. From lattice calculations we can infer the mass of particles in the theory under investigation; how this is done in practice for a pure lattice gauge theory is the topic of the following discussion. Briefly, we can say that, by constructing suitable operators as products of lattice gauge fields, it is possible to obtain information about the spectrum looking at their correlators (which are the propagators in the Euclidean space–time).

4.1.1 *Euclidean correlators: effective masses*

Our present purpose is to extract the mass of propagating particles of a pure gauge theory. In the continuum Minkowskian space–time, we would look at the poles in the propagator of the gauge fields; in the Euclidean lattice regularized theory, the spectrum can be otherwise extracted from the large–time decay rate of the two point functions of the lattice gauge field (i.e. the link variable). The mass gap, that is the mass of the lowest state of the spectrum (the ground state) above the vacuum, can be viewed as the largest correlation length of the statistical system corresponding to the lattice gauge theory.

Following the statistical mechanics correspondence, we can interpret the two point correlation function in a physical appealing way by using the transfer matrix formalism [39]. The lattice 4–d gauge theory can be viewed as a 3–d quantum mechanical system with a Hilbert space \mathcal{H} of physical states, a Hamilton operator \hat{H} and linear operators $\hat{\Phi}$ corresponding to the Euclidean functionals Φ (see Sec. 1.1.3). The transfer matrix \hat{T} can be defined explicitly as an operator acting on \mathcal{H} , and it is related to the partition function by

$$\mathcal{Z} = \text{Tr } \hat{T}^{L_t} \quad . \quad (4.1)$$

In the previous formula, L_t is the size of the temporal direction of the lattice, and the trace is over all the states of \mathcal{H} . From the above relation, the Hamiltonian is defined through

$$\hat{T} = e^{-a\hat{H}} \quad . \quad (4.2)$$

The transfer matrix evolves the states defined on one time slice of the lattice to states on a different time slice. Thus the two point function of an operator $\hat{\Phi}(t)$ localised on a time slice t , reads

$$C_{\Phi\Phi}(t) \equiv \langle \hat{\Phi}^\dagger(t) \hat{\Phi}(0) \rangle = \langle 0 | \hat{\Phi}^\dagger(0) \hat{T}^t \hat{\Phi}(0) | 0 \rangle = \langle 0 | \hat{\Phi}^\dagger(0) e^{-t\hat{H}} \hat{\Phi}(0) | 0 \rangle \quad . \quad (4.3)$$

Inserting a complete set of energy eigenstates $\hat{H} |n\rangle = E_n |n\rangle$, we get

$$C_{\Phi\Phi}(t) = \sum_n \langle 0 | \hat{\Phi}^\dagger(0) |n\rangle \langle n | \hat{\Phi}(0) | 0 \rangle e^{-E_n t} = \sum_n |\langle n | \hat{\Phi} | 0 \rangle|^2 e^{-E_n t} \quad . \quad (4.4)$$

The interpretation is particularly simple: the operator $\hat{\Phi}(0)$ "creates", from the vacuum $|0\rangle$, states which can have a projection $c_n = \langle n | \hat{\Phi} | 0 \rangle$ on $|n\rangle$ at time $t = 0$, and $\hat{\Phi}^\dagger(t)$ "annihilates" them at time t .

The basic principle of lattice spectroscopy measurements is that the sum on the right hand side of (4.4) is dominated by the state with the smallest energy when t is large (if the "overlap" coefficient $|c_n|^2$ of that state does not vanish). Then, the eigenvalues of the Hamiltonian of the system can be calculated from the $t \rightarrow \infty$ limit of suitable correlators $C_{\Phi\Phi}(t)$ (let us call this correlators simply $C(t)$ in the following).

To extract the mass spectrum, we decide to restrict ourselves to consider only zero-momentum operators $\hat{\Phi}_{\vec{p}=0}$; this is done for simplicity and because operators of this kind give the best measured signal in numerical simulations. Since the lattice is chosen with periodic boundary conditions, the system described has translational invariance, and the operators can always be chosen to have definite momentum : in Fourier transform, $\hat{\Phi}_{\vec{p}=0}(t) = \sum_x \hat{\Phi}_x(t)$. Moreover, we can think that, near the continuum limit, the continuum relativistic dispersion relation $E^2 = m^2 + |\vec{p}|^2$ is approximated on the lattice and the zero-momentum correlators give us the mass spectrum from (4.4).

So far, we have talked only of the mass of the lowest state of the theory (i.e. the mass gap). However, the pure gauge theory has a very rich spectrum composed by states (particles) called *glueballs*. Glueballs are colour singlet bound states of gluons and are the states in the spectrum arising in a continuum pure gauge theory (we will see that on a finite lattice we can find other states which vanish in the infinite space-time limit). In general, physical states are characterized by quantum numbers dictated by the symmetry group of the theory; for example, in the continuum, glueballs are classified as irreducible representations of the Lorentz symmetry group and, moreover, they are also eigenstates of discrete symmetry transformations such as parity and charge conjugation. Zero-momentum glueball states are then labelled with spin J , parity P and charge conjugation C . Therefore, the mass m of a J^{PC} state can be calculated from the correlation function of operators capable of creating from the vacuum a state with the right quantum numbers.

In our lattice approach, however, the pure gauge theory defined by (1.73) has a different symmetry group which is a restriction of the continuum one. For example, the continuum rotation invariance is only approximated: we can have rotations only in unit of $\pi/2$. Moreover, only discrete translations are allowed, so momentum is conserved, but in discrete steps $p = 2\pi L/n$, where L is the spatial extent of the cubic lattice and n is an integer.

This implies that zero-momentum glueball states on a simple cubic lattice are characterized by irreducible representations of the cubic group O combined with parity P and charge conjugation C : we label these states with R^{PC} , or simply R . We will go further into details of lattice glueball states in the following.

Now, provided that we can write operators with the right symmetry properties, and that we can measure the asymptotic behaviour of the correlators, it is possible to extract the mass spectrum. The first mass estimate is given by the *effective mass* (we set the lattice spacing to unity in the following):

$$m_{eff} = -\ln \frac{\langle \hat{\Phi}^\dagger(1)\hat{\Phi}(0) \rangle}{\langle \hat{\Phi}^\dagger(0)\hat{\Phi}(0) \rangle} . \quad (4.5)$$

Since it involves the correlator $C(1)$ at such a short temporal distance, this effective mass overestimate the real mass; it can be a good estimate only if, even at $t = 1$, $\langle \hat{\Phi}^\dagger(t)\hat{\Phi}(0) \rangle$ can be written as a single exponential. This assertion is certainly false because more massive state usually propagate as well in such a short distance.

We can do better considering effective masses at different temporal distance, to see whether or not, from a certain time t_{min} , $C(t)$ starts to behave like a single exponential. Using the definition

$$m_{eff}(t) = -\ln \frac{C(t)}{C(t-1)} , \quad (4.6)$$

we try to identify a plateau $t \geq t_{min}$ where the effective mass $m_{eff}(t)$ is the same as $m_{eff}(t_{min})$ within the errors: if this effective mass does not change, then the exponential decay of the correlators is governed by a single scale, which is the plateau mass $m_{eff}(t_{min})$.

We use numerical Monte Carlo simulation (see Sec. 5.1) to evaluate the correlators $C(t) = \langle \hat{\Phi}^\dagger(t)\hat{\Phi}(0) \rangle$ as vacuum expectation values of product of Euclidean functionals at different times. This numerical approach implies that, for every time separation t , $C(t)$ is measured with a statistical error. The error is mainly independent of t , however, the correlator decreases with increasing time: the ratio between signal and statistical noise decreases and the small t points of the correlator have the smallest relative errors. Hence, the effective mass is best determined at small times. On the other hand, from (4.4) it is easy to see that, far away from the asymptotic $t \rightarrow \infty$ regime, the correlator is a sum of exponentials; the effective mass then is not a good definition for the mass of the state of interest and excited states contribute as well in the

exponential decay. The conclusion is that, at small t the relative statistical error on the correlator is small, but the effective mass has large systematic errors.

The simple solution to this impasse is to make $C(t)$ behave like a single exponential even at small times. In general, we could have a single exponential decay if the sum on the energy eigenstate is dominated by only one energy eigenstate; this happens, for example, if the normalized overlap coefficient of one state is of order 1. Let us say that we are interested in the mass of the state $|1\rangle$; then, if

$$|c_1|^2 = |\langle 1 | \hat{\Phi} | 0 \rangle|^2 \approx O(1) \quad , \quad (4.7)$$

and we have normalized the coefficients such that

$$\sum_n |c_n|^2 = 1 \quad , \quad (4.8)$$

the correlator reads

$$C(t) = \sum_n |c_n|^2 e^{-m_n t} \approx |c_1|^2 e^{-m_1 t} \quad \forall t \quad . \quad (4.9)$$

The systematic error in the effective masses is drastically reduced.

There are several ways to improve the overlap on the state of interest and then find a good estimate of its mass. We are going to describe two methods in the following: the first is related to the construction of operators which are "good" approximations of the physical wave-function of the desired state; the second is a variational method which tries to minimize the effective mass over a all range of operators and it is also capable of extracting the mass of excited states of the spectrum above the lowest one.

4.1.2 Operators with a physical size

We want to study the correlator of two "glueball" operators; since we are exploring the pure lattice gauge theory, these operators $\hat{\Phi}$ are gauge invariant combinations of link variables $U_{x,\mu}$ (glueballs are colour singlet). Such operators can be constructed starting from products of link variables around closed spatial paths, traced over the gauge group. Making use only of spatial links supports the transfer matrix interpretation of the two point function.

We said that we want operators that are good approximations of glueball states wave-functions, in order to enhance the coefficient $|\langle n | \hat{\Phi} | 0 \rangle|^2$. If we construct $\hat{\Phi}$ using the plaquette, for example, we are using a highly local operator (the plaquette is the smallest closed loop on a cubic lattice), whereas the physical glueball wave-functional has a typical scale: if the lattice spacing is too small, the plaquette operator is dominated by ultra-violet fluctuations and overlaps more or less equally on all the physical states.

To better approximate glueball wave-functions, even at small lattice spacing, we need operators

that are smooth, not only in the ultra-violet, but also at the physical scale of glueball states. In other words, we want to construct operators having the extended structure of physical states (see Fig. 4.1). There are two well-developed procedures to obtain such operators on the lattice: *smearing* [40] and *blocking* [41]. Let us briefly review how these iterative techniques work. Since we are going to use only spatial paths, the indices in the following link variables run from 1 to 3.

The usual smearing algorithm replaces the links in the path, used to construct an operator, with the sum over the five shortest paths connecting the sites of the original link. This substitution allows to "fatten" the links extending the physical size of the resulting operator. The first step of the algorithm consists in evaluating the "staples" and then summing them to the original link : this produces a $N \times N$ matrix which is no more unitary (it is proportional to a unitary matrix only in the SU(2) case). The second step consists in assigning this matrix to the original link, after having projected it to SU(N). This "smearing" procedure produces SU(N) matrices on the links of the lattice. We also introduce a parameter p_a to weight the sum of the staples relatively to the original link; this parameter determines how rapidly the lattice gauge field spreads outwards as the procedure is iterated. If p_a is small with respect to 1, operators constructed using the smeared links will extend, with a fine resolution, over all important length scales.

The first smearing step can be further improved in order to make it more symmetric about the axis of the basic link. To the four staples we can also add 16 "diagonal" staples, each one including links parallel to the original one, but at a distance $\sqrt{2}a$ away. A new parameter p_d is introduced to weight these diagonal staples in the smearing sum. The parameters p_a and p_d are chosen such that the operator constructed using smeared links is a good approximation of the glueball wave-function. The whole procedure can be iterated as follows. Define $\tilde{U}_i^s(x)$ to be the $N \times N$ matrix after s iteration smearing iteration. Each iteration can be written as

$$\begin{aligned}
\tilde{U}_i^{s+1}(x) = & U_i^s(x) + p_a \sum_{j \neq i} U_j^s(x) U_i^s(x + \hat{j}) U_j^{s\dagger}(x + \hat{i}) \\
& + p_a \sum_{j \neq i} U_j^{s\dagger}(x - \hat{j}) U_i^s(x - \hat{j}) U_j^s(x - \hat{j} + \hat{i}) \\
& + p_d \sum_{j \neq i} \sum_{k \neq i, j} U_j^s(x) U_k^s(x + \hat{j}) U_i^s(x + \hat{j} + \hat{k}) \sum_{j' \neq i} \sum_{k' \neq i, j'} U_{j'}^{s\dagger}(x + \hat{i} + \hat{k}) U_{k'}^{s\dagger}(x + \hat{i}) \\
& + p_d [\text{rotated terms}] \quad ,
\end{aligned} \tag{4.10}$$

starting from

$$\tilde{U}_i^{s=0}(x) = U_i(x) \quad . \tag{4.11}$$

The new $SU(N)$ link matrix $U_i^{s+1}(x)$ is then obtained with a unitarization procedure represented by

$$U_i^{s+1}(x) = \mathcal{U}\left\{\tilde{U}_i^{s+1}(x)\right\} . \quad (4.12)$$

In (4.10), the "rotated terms" refers to three further terms similar to the previous one representing the diagonal staples, but rotated around the i -axis of the original link by multiples of $\pi/2$. In Fig. 4.2 we show a pictorial representation of (4.10).

The blocking algorithm is different because the resulting matrices live on "super-links" joining sites that are 2^b lattice spacing apart, where b is the number of blocking iterations. After each iteration, the original link length is doubled and elongated staples are added: this implies that blocking is faster than smearing in increasing the size of an operator, but the resolution of the scale probed is rather crude. This can be a problem, because "blocked" operators (by this we mean operators constructed using "super-links") can just be too large or too small with respect to the typical size of the physical glueball state of interest: we will solve this problem improving the blocking algorithm as we will explain in a moment.

The iterative blocking procedure as follows:

$$\begin{aligned} \tilde{U}_i^{b+1}(x) &= U_i^b(x)U_i^b(x + 2^b\hat{1}) \\ &+ p_b \sum_{j \neq i} U_j^b(x)U_i^b(x + 2^bj)U_i^b(x + 2^bj + 2^b\hat{1})U_j^{b\dagger}(x + 2^{b+1}\hat{1}) \\ &+ p_b \sum_{j \neq i} U_j^{b\dagger}(x - 2^bj)U_i^b(x - 2^bj)U_i^b(x - 2^bj + 2^b\hat{1})U_j^b(x - 2^bj + 2^{b+1}\hat{1}) \quad , \end{aligned} \quad (4.13)$$

where we set

$$\tilde{U}_i^{b=0}(x) = U_i(x) \quad . \quad (4.14)$$

The blocked "super-link" matrices are then projected back to $SU(N)$ following (4.12). The new parameter p_b which weight the sum of elongated staples is typically chosen to be $O(1)$ so that the width of the blocked link grows together with its length. The paths added in the blocking algorithm are shown in Fig. 4.3.

As we said before, we define an improved blocking algorithm following [11]. The improved blocking has both the rapid increasing rate of the blocking above and the fine resolution of the smearing; it consists in multiplying together two smeared links at smearing level s creating a super-smeared-link:

$$\begin{aligned} U_i^{b+1}(x) &= U_i^{b,s}(x)U_i^{b,s}(x + 2^b\hat{1}) \\ U_i^{b,s}(x) &= \text{Smear}^s\left\{U_i^b(x)\right\} \quad . \end{aligned} \quad (4.15)$$

Here Smear^s denotes the smearing procedure iterated at level s and generalized to apply to blocked links $U_i^b(x)$. The difference between (4.15) and the original blocking in (4.13) is that

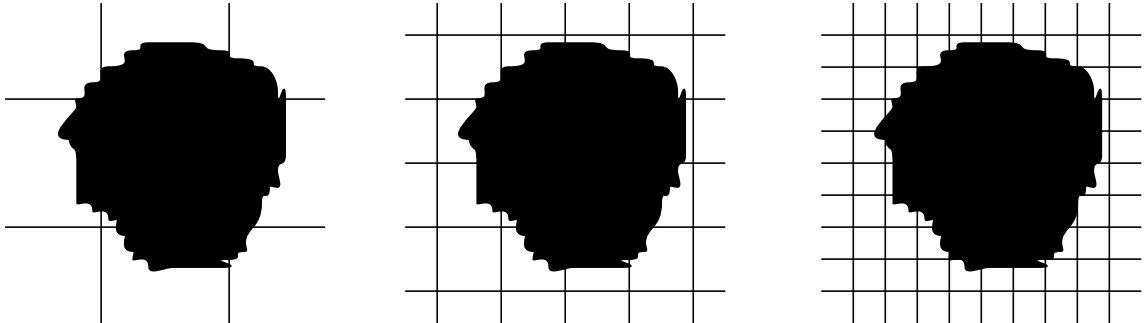


Figure 4.1: When the lattice spacing shrinks, operators constructed only from local path shrink as well and they are no more a good approximation of the glueball wave-functional, which always remains of the same physical extension.

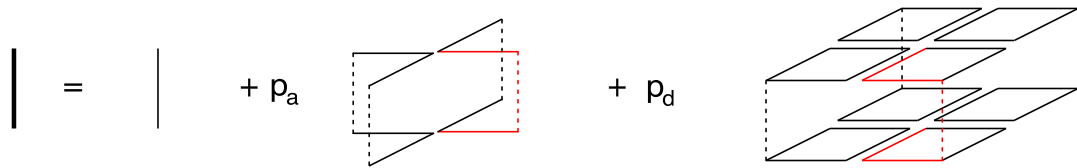


Figure 4.2: In the smearing algorithm, a smeared lattice link (on the left) is obtained adding to the original link the parallel transported nearest neighbour links weighted by the parameter p_a , and the next-to-nearest neighbour links parallel transported along all possible paths on the elementary cube weighted by another parameter p_d . In red we highlight a normal staple and a particular "diagonal" staple; all other diagonal staples are constructed following the lines in the picture.

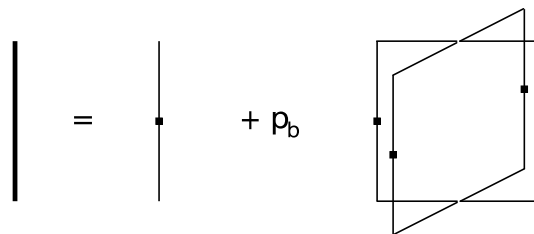


Figure 4.3: Pictorial representation of a blocked super-link as a sum of elongated staples. These staples are parallel transported nearest neighbour links which go from the site x to the site $x + 2^{b+1}\hat{i}$

in the former we use more paths at intermediate length scales and the probability to obtain a good overlap is greater.

The above procedure has two parameters, p_a and p_d , which have to be tuned in order to optimize the overlap. In our simulations, we fix $s = 1$, $b = 0, 1, 2, 3$ and $p_a = 0.40$, $p_d = 0.16$; this choice is dictated by the results in [11], showing that a normalized overlap greater than 0.90 is reached for almost every glueball state investigated. It should be clear that the links resulting from the previous procedure are used to create the operator $\hat{\Phi}$, which now is "dense" and smooth on physical scales.

4.1.3 Effective mass minimization

Another way to find good overlaps for physical glueball states is to choose, not just an operator $\hat{\Phi}$, but a whole set $\{\hat{\Phi}_i\}_{i=1,\dots,N_o}$, and to find the one that minimize the effective mass. To use this method, we simultaneously measure correlators between $\hat{\Phi}_i$ coming from differently shaped closed loops \mathcal{C} ; moreover, we insert in the variational basis, operators with different blocking levels b . The variational method will find the operator which best approximate the wave-function of the state we are interested in. By using this method, it is also possible to extract the mass of excited states as we will explain later.

Let us concentrate on the procedure itself, leaving details of the construction of the variational basis for later discussions. We choose a certain number N_o of operators. These are of different shapes and sizes, but they all have the same symmetry quantum numbers of the glueball state we want to study. Call these operators, forming our variational basis, ϕ_i^R , where i labels the kind of operator and R the quantum numbers (like the irreducible representation of the cubic group, the parity and the charge); since R is the same for all operators, we will omit it in the following.

At this point, we measure the $N_o \times N_o$ correlation matrix for every time separation t

$$\tilde{C}_{ij}(t) = \sum_{\tau} \langle 0 | \phi_i^\dagger(t + \tau) \phi_j(\tau) | 0 \rangle \quad . \quad (4.16)$$

When it is possible that some operators can couple to the vacuum state $|0\rangle$, that is when these operators have the same symmetry of the vacuum, we correlate the corresponding vacuum subtracted operators:

$$\phi_i(t) - \langle \phi_i(t) \rangle \quad . \quad (4.17)$$

This subtraction is done, in practice, only for one value of R , the one corresponding to the vacuum, but in the following we refer for simplicity always to vacuum subtracted operators and their corresponding correlators.

From the basic operators, we want to find an appropriate linear combination

$$\hat{\Phi}(t) = \sum_i v_i \phi_i(t) \quad , \quad (4.18)$$

such that its correlator gives us the best estimation of the mass of the lowest lying state with quantum numbers R . Of course, between different estimates of the mass, the best one in a variational sense, is the lowest one. The coefficients v_i are chosen to minimize the effective mass

$$m_{eff}(\bar{t}) = -\frac{1}{\bar{t}} \ln \frac{\sum_{ij} v_i v_j \tilde{C}_{ij}(\bar{t})}{\sum_{ij} v_i v_j \tilde{C}_{ij}(0)} \quad , \quad (4.19)$$

where we usually choose $\bar{t} = 1$ in lattice units because it gives the best statistical "signal". It is easy to show that the effective mass above is exactly the effective mass we would obtain from $\langle \hat{\Phi}^\dagger(t) \hat{\Phi}(0) \rangle$; then we try to find the optimal coefficients v_i .

This minimization is usually turned into a *generalized eigenvalue problem*. If we denote as \vec{v} a column vector whose elements are the coefficients v_i , then the optimal values for v_i are obtained when \vec{v} is an eigenvector of $\tilde{C}(\bar{t})$. The problem is to numerically solve the following eigenvalue equation

$$\tilde{C}(\bar{t}) \cdot \vec{v} = \lambda(\bar{t}) \vec{v} \quad , \quad (4.20)$$

where the eigenvalues are

$$\lambda(\bar{t}) = e^{-m_{eff}(\bar{t})\bar{t}} \tilde{C}(0) \quad . \quad (4.21)$$

One way to proceed is to diagonalize the matrix $\tilde{C}^{-1}(0)\tilde{C}(\bar{t})$ for $\bar{t} = 1$; we will see how numerical issues can make this task quite hard.

Form (4.20) we see that to each eigenvector \vec{v} corresponds an effective mass. The eigenvector corresponding to the lowest effective mass m_{0eff} yields the coefficients v_{0i} for the operator $\hat{\Phi}_0$ which best overlaps on the lowest-lying glueball state with quantum numbers R . Higher-mass eigenvectors can be used to construct operators with good overlap onto excited states.

To evaluate the mass of the desired states, we then decide to consider only the 4 lowest effective masses (or equivalently the 4 eigenvectors corresponding to the 4 highest eigenvalues); the operators constructed using the components of these eigenvectors are then correlated in the matrix

$$C_{ij}(t) = \langle 0 | \hat{\Phi}_i^\dagger(t) \hat{\Phi}_j(0) | 0 \rangle \quad , \quad (4.22)$$

with the implicit vacuum subtraction when needed. The diagonal correlators $C_{ii}(t)$ contain the information about the mass of the state i , where i (from 1 to 4 in our case) can be the ground state or even some excited state. Fitting this correlators with a single exponential gives us the mass of the state (see (4.4)). Usually, what happens is that we obtain the mass of the lowest state from more than one operator; in other words, since we are dealing with a statistical set of

data, we obtain two masses compatible within errors from correlators of two different operators. In such a situation we choose to consider the operator with the best overlap on the lowest state, which means that the mass has a lower systematic error from the fitting procedure.

At this point we want to make a little remark: on a finite lattice with periodic boundary conditions, the correlator has also contributions from propagation backward in time. When the correlation distance (in time) is large, these contributions cannot be neglected. The functional form of the correlator with time, is not that of a single exponential alone, but that of two exponential; we fit the correlator with

$$C_{ii}(t) = A[e^{-mt} + e^{-m(L_t-t)}] \quad , \quad (4.23)$$

where various regions $[t_{min}, \dots, t_{max}]$ are fitted and the best χ^2 fit is chosen. Clearly, the multiplicative constant A is also fitted and is what we have called the overlap $|c_n|^2$ (see (4.7) and (4.9)).

4.2 Constructing glueballs operators

We have shown how to extract the spectrum of a lattice gauge theory for correlators of certain operators. Now we are going to explain how this operators are chosen and what properties they should have in order to create glueball states from the vacuum of the theory. We begin reviewing the symmetry group of a simple cubic lattice and then we show how to explicitly construct glueball operators.

4.2.1 Cubic group rotations

We want to discuss here the properties of the symmetry group of the cube. As we have already said, zero-momentum glueball states on a simple cubic lattice fall into the irreducible representations of the rotations of the cube combined with parity transformations and charge conjugation. Therefore, if we take an operator, which is a gauge invariant product of link variables around a closed contour, we can say that it creates a glueball state with the same symmetry of the closed contour. We will make this point clearer in the following section, describing how to create closed paths that transform under the irreducible representations of the cubic group, but first we need to show briefly what are this representations and what is the relations between them and the representations of the continuum rotation group.

The cubic group O is the group of symmetry of a cubic polyhedron and it is also called the *octahedral point group*. It contains only pure rotations, that is each element can be written as a rotation around a uniquely defined axis. The rotations are, of course, discrete; if we see that the cube is brought into coincidence with itself after a rotation through an angle $\varphi = 2\pi/n$ (n

integer), we say that the rotation axis is a n -fold axis. If $n = 1$, we have coincidence after rotations through 2π , which is the identity transformation denoted by E . All other rotation through $2\pi/n$ are denoted by C_n , and successive rotations by C_n^2, C_n^3 , etc...

Going back to the cubic group O , we see that it has four 3-fold axis (space diagonals), three 4-fold axis (joining centers of opposite faces), and six 2-fold axis (joining midpoints of opposite edges, see Fig. 4.4). We have in total 24 elements which are further divided in 5 different equivalence classes. Two elements a and b of a group G are equivalent if $b = gaa^{-1}$ for a $g \in G$, and are in the same equivalence class also called *conjugacy class*. We can write O divided into

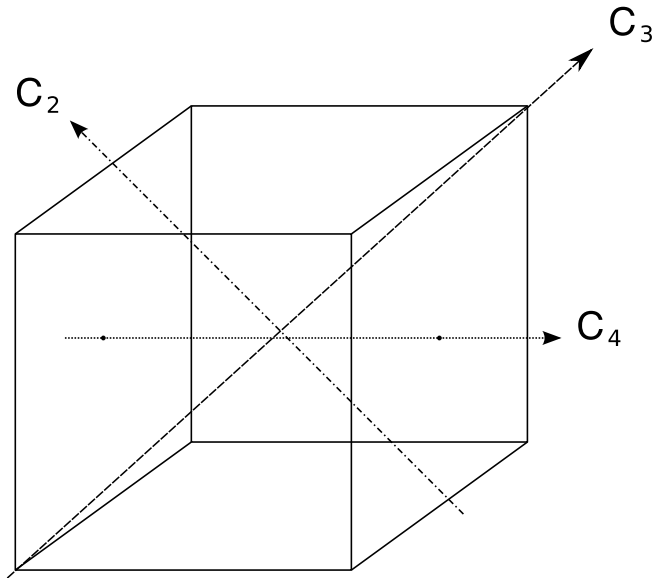


Figure 4.4: Symmetry axis of the cube.

conjugacy classes as

$$O: \quad E; \quad C_2(6); \quad C_3, C_3^2(8); \quad C_4, C_4^3(6); \quad C_4^2(3); \quad (4.24)$$

where in brackets we show the number of element in each class.

In group theory there are theorems about irreducible representations of finite groups which help identifying them. The first theorem we are going to use, tells us that the number of conjugacy classes is equal to the number of irreducible representations: then the cubic group O has 5 irreducible representations that we call A_1, A_2, E, T_1 and T_2 . A second theorem states that the dimension of these representations satisfies the following relation

$$\sum_{\mu} n_{\mu}^2 = \dim(G) \quad , \quad (4.25)$$

where $\dim(G)$ is the order of the finite group G and n_{μ} is the dimension of each irreducible representation μ (the sum runs over all μ 's). In our case, we have only one possibility to satisfy the

relation above, and this gives us the dimensions of the irreducible representations: 1, 1, 2, 3, 3 respectively for A_1 , A_2 , E , T_1 and T_2 .

The usual way to represent the relation between the conjugacy classes and the irreducible representations is the table of characters; for the group O this table is shown in Tab. 4.1.

Now we want to consider the group O as a subgroup of the continuum rotation group $SO(3)$;

| | E | $C_2(6)$ | $C_3(8)$ | $C_4(6)$ | $C_4^2(3)$ |
|-------|-----|----------|----------|----------|------------|
| A_1 | 1 | 1 | 1 | 1 | 1 |
| A_2 | 1 | -1 | 1 | -1 | 1 |
| E | 2 | 0 | -1 | 0 | 2 |
| T_1 | 3 | -1 | 0 | 1 | -1 |
| T_2 | 3 | 1 | 0 | -1 | -1 |

Table 4.1: Character table of the cubic group O . The character of a conjugacy class is invariant inside the class because it is the trace of the matrix associated to the class elements in each representation.

glueball states on the lattice transform under irreducible representations of O , but continuum glueball states must be in irreducible representations of $SO(3)$. The aim is to obtain the continuum spectrum making the continuum limit of the discrete one. Therefore we need to know how the irreducible representations of $SO(3)$ are decomposed in terms of those of O . We are interested only in single-valued representations of the continuum rotation group, identified by an integer number J , the spin of the particle (glueballs are made of gluons, hence they are bosons). Each representation J has a degeneracy of $2J + 1$ (its dimension), but on the lattice this degeneracy is splitted into terms belonging to irreducible representations of O : for example, the spin 2 representation has 5 polarizations in the continuum which split into the E and T_2 (respectively 2 and 3 dimensional). The irreducible representations of spin J of $SO(3)$ restricted to O are called *subduced representations* $J \downarrow O$ and are reducible in O . The decomposition of the subduced representations $J \downarrow O$ is shown in Tab. 4.2.

It is then possible to reconstruct the continuum spectrum from the masses extracted on the lattice by matching the patterns of degeneracies observed in each level; by this we mean, for example, that if the same mass (within the errors) is present in the irreducible representations A_2 , T_1 and T_2 , then it corresponds, in the continuum limit, to the mass of a spin $J = 3$ particle. So far, we have neglected parity and charge conjugation transformations. However it is easy to include them in the discussion above. Including parity means adding reflections in the cubic point group; this is easily done by taking the direct product of O with \mathcal{C}_i , the group of order 2 containing the identity and the inversion with respect to the origin of the axis. The full group is then $O_h = O \times \mathcal{C}_i$: it contains 48 elements, which are combinations of pure rotations and

| J | A_1 | A_2 | E | T_1 | T_2 |
|-----|-------|-------|-----|-------|-------|
| 0 | 1 | 0 | 0 | 0 | 0 |
| 1 | 0 | 0 | 0 | 1 | 0 |
| 2 | 0 | 0 | 1 | 0 | 1 |
| 3 | 0 | 1 | 0 | 1 | 1 |
| 4 | 1 | 0 | 1 | 1 | 1 |

Table 4.2: Subduced representations $J \downarrow O$ of the cubic group up to $J = 4$. In the table we give the multiplicities with which the irreducible representations of O can be found in the subduced representation for each J .

reflections, divided in 10 classes. The group \mathcal{C}_i has 2 irreducible representations which we can identify with the parity eigenvalues $P = \pm 1$; then the irreducible representations of O_h are obtained directly from those of O using the character table in Tab. 4.1: we get 10 irreducible representations, labelled by A_1^\pm , A_2^\pm , E^\pm , T_1^\pm and T_2^\pm .

Adding also the charge conjugation brings us to a total of 20 irreducible representations of the group O_h^C (or O^{PC}). In each of these "channels" we can extract the mass of the lowest-lying state, usually denoted as R^{PC} , where $R \in \{A_1, A_2, E, T_1, T_2\}$, $P \in \{+1, -1\}$ and $C \in \{+1, -1\}$. Moreover, excited states in a particular symmetry channel will be denoted by the representation label R^{PC*} with one or more asterisks.

4.2.2 Operators for glueball states

Now we want to describe how we can, in practice, obtain lattice glueball states with the desired symmetries. As explained in Sec. 4.1.1, we can extract the mass of the ground state of glueballs in every R^{PC} channel, but for this purpose, we need operators capable of projecting on the desired states, that is with the same symmetry. On the lattice, this symmetry will be that of the closed path around which we multiply the link variables to create the operator.

In general we can write a lattice glueball operator as

$$\phi^R = \sum_{c \in \mathcal{C}} \text{Tr} \prod_{l \in c} U(l) \quad , \quad (4.26)$$

where \mathcal{C} is a collection of spatial loops and depends on the quantum numbers $R \equiv R^{PC}$.

In the following, we will denote our operators ϕ^R simply as paths \mathcal{P} because that is the only structure important in order to understand their symmetry properties. Let us follow the notation in [9], where a path \mathcal{P} of length L is represented by a L -tuple

$$(\hat{f}_1, \hat{f}_2, \dots, \hat{f}_L) \quad , \quad (4.27)$$

with the constraint given by the fact that the path is closed $\sum_{i=1}^L \hat{f}_i = 0$. The vectors \hat{f}_i are $\pm \hat{e}_j$, the unit vectors corresponding to the spacelike coordinates of the lattice. Given a path \mathcal{P} , it is independent of the point where it starts, as long as the orientation is preserved; hence we can construct equivalence classes in which paths are equivalent if we make a cyclic permutation of the \hat{f}_i . The equivalence class of $(\hat{f}_1, \hat{f}_2, \dots, \hat{f}_L)$ is denoted by $[\hat{f}_1, \hat{f}_2, \dots, \hat{f}_L]$.

Obtaining the operator with the desired charge conjugation C symmetry is easy in this case, because on link variables, the conjugation operation is equivalent to reverse the orientation of the link :

$$C[\hat{f}_1, \hat{f}_2, \dots, \hat{f}_L] = [-\hat{f}_L, -\hat{f}_{L-1}, \dots, -\hat{f}_1] \quad . \quad (4.28)$$

A path with defined charge $C = \pm 1$ is defined as the combination

$$[\hat{f}_1, \hat{f}_2, \dots, \hat{f}_L]_{\pm} = \frac{[\hat{f}_1, \hat{f}_2, \dots, \hat{f}_L] \pm [-\hat{f}_L, -\hat{f}_{L-1}, \dots, -\hat{f}_1]}{2} \quad . \quad (4.29)$$

This amounts in taking only the real part of the trace in (4.26) for a $C = +1$ operator and only the imaginary part for a $C = -1$ operator. Therefore, we just need to find oriented paths which transforms under the 10 irreducible representations of O_h .

The parity operation applied on a path, simply reverts every link \hat{f}_i , because it is equivalent to an inversion with respect to the starting point of the path. Thus we can write

$$P[\hat{f}_1, \hat{f}_2, \dots, \hat{f}_L] = [-\hat{f}_1, -\hat{f}_2, \dots, -\hat{f}_L] \quad , \quad (4.30)$$

and paths with defined parity $P = \pm 1$ are

$$[\hat{f}_1, \hat{f}_2, \dots, \hat{f}_L]_{\pm} = \frac{[\hat{f}_1, \hat{f}_2, \dots, \hat{f}_L] \pm [-\hat{f}_1, -\hat{f}_2, \dots, -\hat{f}_L]}{2} \quad . \quad (4.31)$$

Our aim is then to find paths which transforms in the 5 irreducible representations of O (A_1, A_2, E, T_1, T_2); after that, from each of them, we can construct every combination of parity and charge R^{PC} following (4.29) and (4.31) (even if in practice the charge conjugation is done calculating real and imaginary part of the trace).

We now define how a given element of the symmetry group O , i.e. a rotation \mathcal{R} , acts on a given path. Since the path is a collection of elementary space-like unit vectors, the operation of rotation on the path is defined by what that rotation does to each of the vectors:

$$M_{\mathcal{R}}(\mathcal{P}) = [\mathcal{R}(\hat{f}_1), \mathcal{R}(\hat{f}_2), \dots, \mathcal{R}(\hat{f}_L)] \quad , \quad (4.32)$$

where \mathcal{R} on the right hand side of the equation stands for an operator in a 3 dimensional vector representation (we use the same symbol for the operator and for its representation), whereas on the left hand side we have it in an arbitrary representation M . The standard way to construct a representation of a group, is to choose any function on which the elements of the group can act

as operators, and then apply to this function all the operators of the group. The transformed functions can be linearly independent or not; if they are, they form a basis for a representation with dimension equal to the order of the group. In our case, the function is replaced by a path, and the transformed paths are given by (4.32) for each rotation; if we want $M_{\mathcal{R}}(\mathcal{P})$ to be linearly independent we should choose a path \mathcal{P} with no symmetry at all under the cubic group. This is the point where we start to construct all the irreducible representations of the cubic group; after that we will be able to construct an orthonormal basis of each representation starting from any path \mathcal{P} (which has a projection on that representation, as we will show later).

Let us start with the path

$$\mathcal{P}_{base} = [\hat{e}_1, \hat{e}_2, \hat{e}_3] \quad , \quad (4.33)$$

which is not left invariant by any rotation \mathcal{R} . The 24 rotated paths $\mathcal{P}_{\mathcal{R}} = M_{\mathcal{R}}(\mathcal{P}_{base})$ are an orthonormal basis for a 24 dimensional representation M_{base} . This representation is fully decomposable and we want to find its irreducible content, which consists, as we already know, of 5 irreducible representations. This means that $\mathcal{P}_{\mathcal{R}}$ can be expressed as linear combinations of $n \leq 24$ other paths, the basis of a new representation of smaller dimension. The result is that there exists a unitary matrix A which change my initial basis into the new one, and transforms the original representation in a new representation which has a $n \times n$ diagonal block in its matrix form (this block corresponds to the new basis of n paths):

$$M' = A^{-1}M_{base}A \quad . \quad (4.34)$$

There is a general method used to decompose a representation of finite dimension and it is based on the Schur lemmas (which is related to the existence of the matrix A): it consists in turning the original 24×24 matrix representation M_{base} into its Jordan form, with blocks on the main diagonal, using matrices that commutes with M_{base} . In practice we construct matrices C which commute with M_{base} using sum of matrices in the conjugacy classes of M_{base} , then we try to find a matrix A which diagonalizes them, or better, that turns them into their Jordan form $C_{Jord} = A^{-1}CA$; as a result, M_{base} gets decomposed using (4.34). We need to stress that with this method we are able to Jordanize matrices of all conjugacy classes at the same time. To find the fully reduced form of M_{base} , we need to iterate this procedure: after 3 iterations using matrices C_i coming from 3 different conjugacy classes, we get a M''' matrix with 5 blocks on its diagonal, corresponding to the invariant subspaces of the 5 irreducible representations of O :

$$M''' = A_3^{-1}A_2^{-1}A_1^{-1}M_{base}A_1A_2A_3 \quad , \quad (4.35)$$

where the A_i comes from the 3 Jordanization of matrices C_i .

Using the matrix $\bar{A} = A_1A_2A_3$ we can change the original 24-dimensional basis made of \mathcal{P}_{base} ,

in a new set of paths which is subdivided into 5 more subsets forming the basis of each of the invariant subspaces of the irreducible representations; if we take the vectors

$$\mathcal{P}_{irr} = \bar{A} \cdot \mathcal{P}_{base} \quad , \quad (4.36)$$

they are the base paths of the 5 irreducible representations of the cubic group O . Following our method just discussed we are able to reproduce the table given in [42], which prescribes how to create an orthonormal basis of each irreducible representation R starting from an arbitrary path: the table is given by the 24 \mathcal{P}_{irr} vectors, taken as a 24×24 matrix (remember that \mathcal{P}_{base} are 24 vectors in a 24 dimensional space): they form the projection table $Pr(R, \mathcal{R})$.

To conclude this section we show how we can find a set of basic operators in each R^{PC} channel to be used in the variational method described in Sec. 4.1.3. We start from a set of prototypical paths \mathcal{P}^i of different shapes with length varying from 4 lattice spacings up to 8 lattice spacings; they are shown in Fig. 4.5. From each of them, we define a basis for the irreducible representation R using the projection table $Pr(R, \mathcal{R})$ by means of

$$\mathcal{P}_R^i = \sum_{\mathcal{R}} Pr(R, \mathcal{R}) M_{\mathcal{R}}(\mathcal{P}^i) \quad , \quad (4.37)$$

where we \mathcal{P}_R^i are linear combinations of rotated paths ($M_{\mathcal{R}}(\mathcal{P}^i)$ is defined in (4.32)), weighted by coefficients in the projection table. However, the \mathcal{P}_R^i obtained are not linearly independent in general because, for every R , we have in $Pr(R, \mathcal{R})$ a number of \mathcal{R} equal to the square of the dimension of the representation; we then try to identify only a subset of \mathcal{P}_R^i which are actually different from one another and we perform the parity and charge conjugation operations as defined in (4.31) and (4.29): this leaves us with a full range of combinations of paths \mathcal{P}_{RPC}^i in each of the R^{PC} channels, from which we can construct operators

$$\phi^{RPC} = \sum_{c \in \mathcal{P}_{RPC}^i} \text{Tr} \prod_{l \in c} U(l) \quad . \quad (4.38)$$

The sum in the previous expression means that an operator ϕ^{RPC} is created from a single combination in \mathcal{P}_{RPC}^i , but, since this combination is made up summing paths c with appropriate coefficients, we should sum the traces around the paths c using exactly those coefficients. Moreover, we don't perform the charge conjugation operation on the paths because, as we already said, it is sufficient to take the real or imaginary part of the trace above; this saves us time in the computation of the operators. In Tab. 4.3 we summarize the number of operators in each symmetry channel R^{PC} . Recall that each operator is also "blocked" following the algorithm described at the end of Sec. 4.1.2; hence in our variational basis, for each R^{PC} , the number of operators measured is equal to the number written in Tab. 4.3 multiplied by the number of

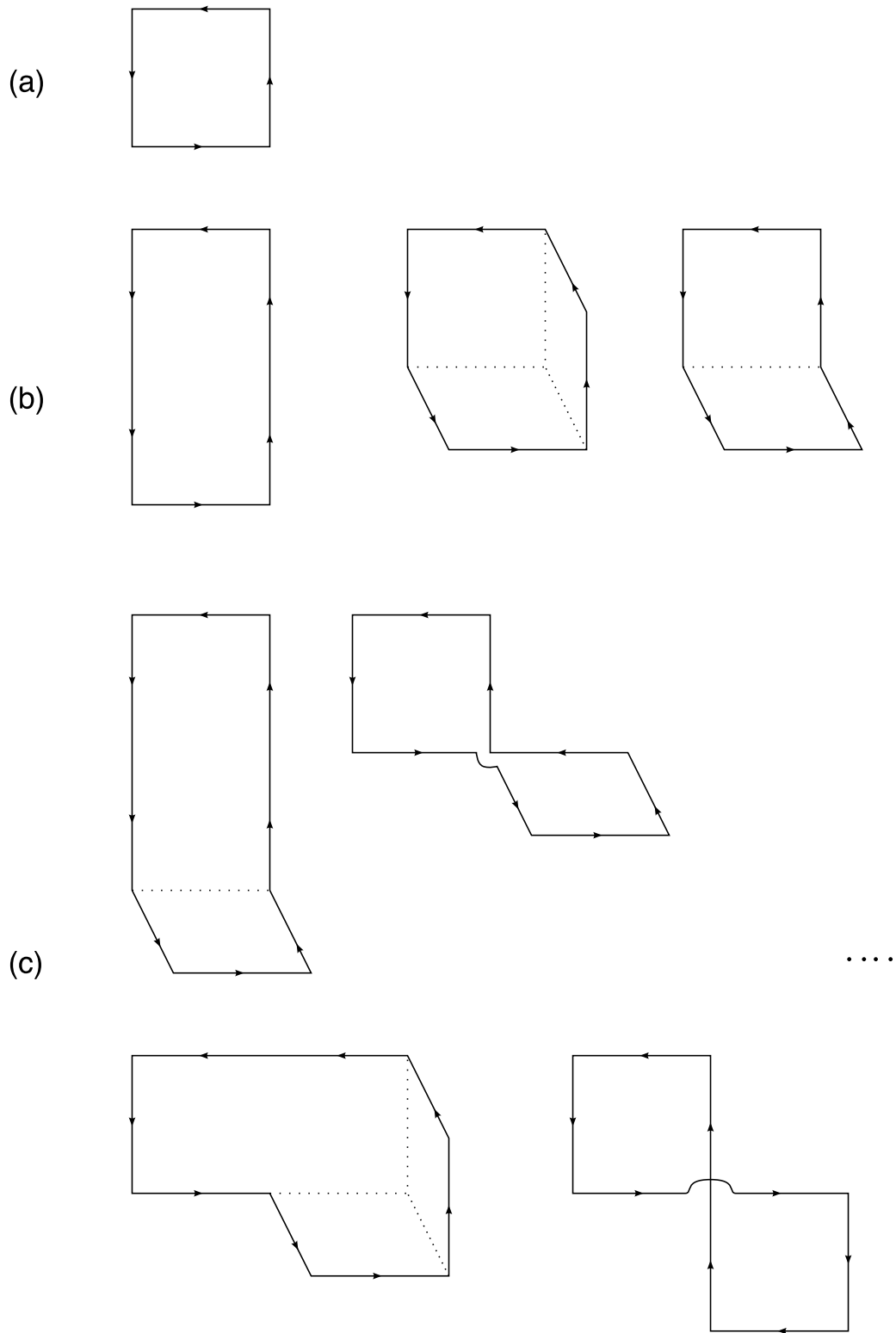


Figure 4.5: Set of basic prototypical path used to construct operators in all the $20 R^{PC}$ symmetry channels. The path in (a) is the only possible one of length $4a$; in (b) there are the 3 possible paths of length $6a$; in (c) we show 4 of the 21 paths of length $8a$. Their projections on each symmetry channel is used to construct basis operators for the variational method.

blocking iterations.

The code we have written to create and transform these paths and to write the operators as products of link matrices on the lattice around those closed paths is entirely new and it is a first original contribution given by this thesis work. Moreover, it gives total freedom in the choice of the operators one would like to use (the only constraint is the amount of available memory for the computation of the operators).

4.3 *Mixing with other states*

After we have obtained a set of operators that we can correlate to extract the mass of the glueball states, we want to be sure that these operators are really projecting only onto one-particle states. It is indeed possible that some of them have non-vanishing overlaps onto two-particle scattering states. However, two-particle states are clearly heavier than a one-particle state and they do not enter in the calculation of the low-lying spectrum: we want to look at them to avoid their presence when we look for excitations in the spectrum.

Moreover, since we are on a finite lattice with periodic boundary conditions, it is possible to get a gluon excitation which wraps around the toroidal lattice, called *torelon state*. If a torelon state has a lower mass than the lightest glueball in a given symmetry channel, than the possibility exists that the mass we extract from the asymptotic decay of the correlator will be that of the torelon state. Due to their symmetry properties under the center group, torelon states cannot be created by the operators we constructed in the previous section; however, as we will show later, pairs of torelons in opposite directions can couple to our operators and we want to identify their contribution in the spectrum.

4.3.1 *Two glueballs scattering states*

Multi-glueball states have an energy that can be approximately determined. In our case we restrict only to two-glueball states having zero total momentum. We expect their mass to be greater than or equal to double the mass of the one-glueball states in each symmetry channel (if we neglect all interactions): this gives us a threshold near and above which we are not sure to obtain the spectrum of only one-particle states. However, we can do better by including in our variational basis (see Sec. 4.1.3) operators that are expected to overlap significantly on two-glueball states. Adding these new operators in the variational procedure results in a set of optimized coefficients v_i (see (4.19) and following) encoding the mixing of the two-particle states with the low-lying eigenstate of interest.

Let us take two operators $\phi_A(x)$ and $\phi_B(x)$ which are supposed to create one-particle states;

the Fourier representation of an operator which projects on a two-particle state with relative momentum p is then given by

$$\phi_2(p) = \sum_{x,y} e^{ip \cdot (x-y)} \phi_A(x) \phi_B(y) \quad . \quad (4.39)$$

Hence, the zero-momentum operator we are searching for is

$$\phi_2(p=0) = \sum_x \phi_A(x) \sum_y \phi_B(y) = \phi_A(p=0) \phi_B(p=0) \quad , \quad (4.40)$$

that is the product of 2 zero-momentum operators. Therefore, there is no need to create other paths, but we simply need to correlate products of 2 operators, coming from paths that we already had, with other operators (which can in principle project on both one and two-globes states).

It is possible to choose $\phi_A(x)$ and $\phi_B(x)$ in different way to obtain $\phi_2(x)$, and we decide to choose $\phi_A(x) = \phi_B(x)$ because, in this case, we expect that their correlators decay more slowly and then project more on the lowest part of the spectrum that we are interested in (recall that slow decay implies a lower mass). Moreover, we want to be able to decide from which kind of prototypical paths ϕ_A comes from: this will allow us to understand, after the variational procedure, which shape better project onto glueball scattering states.

Following the naive argument that at $N = \infty$ direct products of two operators factorize, we expect that they create states which are good approximation of two non-interacting glueballs. However, there is *a priori* no reason to say that they do not mix at all with single glueball states, since selection rules allow this type of overlap. We are aware of only another study of this kind in the literature (see [43]) restricted to the SU(3) case and very preliminary (only 2 operators in the $A1^{++}$ were considered).

Our code, on the contrary, is written in a way that one has complete freedom in the choice of the operators and in our simulations we chose "scattering" operators coming from path (a), (b) and (c) in Fig. 4.5: in total we get operators that can project onto two-globes states in every symmetry channel.

When an eigenstate \vec{v} is extracted from (4.20), it can contain, between his coefficients v_i , those coming from two-globes operators ϕ_2 : if the relative weight of coefficients v_i , with the index i related to operators ϕ_2 , is significant (more than 20%), than there is the possibility that this state has an important contamination from scattering states. However, we can repeat the analysis without the "scattering" operators; comparing the resulting spectrum of eigenvectors, in the two distinct cases, gives us a measure of the influence of such operators.

4.3.2 Torelon pairs mixing

Whereas multi-glueball states can only affect the mass of excited states, torelon state can be lighter than one-particle glueballs in every symmetry channel. Hence, identifying their presence in the spectrum is mandatory. However, their contribution vanish in the infinite-volume limit, because, as we will see, their energy is proportional to the size of the lattice box.

A torelon state, being an excitation winding around the spatial toroidal lattice, can be classified by its transformation under the discrete center group \mathbb{Z}_N of $SU(N)$: if we apply an element $z_n \in \mathbb{Z}_N$, to the state, it acquires a phase factor $exp(\frac{2\pi i n}{N})$ ($n = 0, 1, 2, \dots, N-1$). More generally, representations of $SU(N)$ can be divided in classes of same N -ality with respect to \mathbb{Z}_N : for each representation of N -ality k , a transformation by $z_n \in \mathbb{Z}_N$ corresponds to multiplication by a factor $exp(\frac{2\pi i k n}{N})$. Simple torelon state have 1 N -ality and operators that project on them can be constructed using Polyakov loops l_p wrapping around the spatial dimensions. For large lattice size L , the Polyakov loop represents a flux tube with energy given by σL , then it increases with the volume of the lattice: it decouples from the glueball spectrum in the infinite-volume limit. To be precise, our operators constructed from spatial closed loops can not have a non-vanishing overlap onto torelon state, because they have 0 N -ality; if we combine two torelon states with opposite center charge, that is Polyakov loops winding around the same dimension in opposite directions, then we obtain a state with 0 N -ality that mix with glueballs. This state is usually called a *bi-torelon state*.

A method that can be used to find these states in the spectrum used the finite-volume nature of them and study the dependence of the volume of every level in the spectrum. We do not try this attempt, but we follow what we have done with two-particle states, and we insert in the variational basis operators that strongly project on bi-torelon states. The mass of the eigenstates coming from the variational procedure is referred to a bi-torelon state if, again, the coefficients of the eigenstates contains those of the new operators added.

We construct zero-momentum operators coupling to bi-torelon states by multiplying together two spatial Polyakov loops at different lattice points winding in opposite directions

$$\phi_{tor}(p=0) = \sum_{x,y} l_p(x) l_p^*(y) \quad , \quad (4.41)$$

where the sum is intended only on spatial coordinate x and y in the plane orthogonal to the Polyakov loop direction, due to its translational invariance along that. Using (4.41), we can only obtain operators in two symmetry channels (A_1^{++} and E^{++}) by summing l_p 's rotated in different ways. However, if we use a "wiggly" path to construct the Polyakov loop, we find that there exists a basis of ϕ_{tor} operators in almost each irreducible representation of O_h^C .

In practice we can use the same method of Sec. 4.2.2 and the projection table $Pr(R, \mathcal{R})$, but for that the paths to be rotated have to be closed: a path closed around a direction, such as

a Polyakov loop, is too much symmetric because it is rotationally invariant around the axis, and this invalid the whole procedure. The simplest solution is to consider in (4.41) one straight Polyakov loop l_p multiplied by a "decorated" Polyakov loop \tilde{l}_p as they were a single path closed at the edges of the spatial lattice slice: this procedure identifies a plane for the operator, which is thus no more rotational invariant. It is, however, important to note that the links used to close the path are not evaluated when calculating the operators, because they do not enter (4.41). In Fig. 4.6 we show the prototypical paths used to construct the operators in all the symmetry channels. We expect that adding decorations to the straight Polyakov loop will increase its energy resulting in operators coupling to higher glueball states in the spectrum; that's way we choose only the two shortest (in lattice units) paths which allow us to obtain a projection on all the irreducible representations of O_h^C . In Tab. 4.4 we show the number of "bi-torelon" operators we calculate in each symmetry channel R^{PC} .

If we apply the improved blocking procedure, we see that different length regions are automatically spanned even if the "decorations" are originally only one lattice spacing wide and if the two opposite Polyakov loops are one lattice spacing apart. Using blocked super-links results in having operators with "decorations" of all sizes. However, a careful treatment of the blocking iterations is needed when we deal with Polyakov loops with "decorations", due to their non-trivial topological structure: this structure remains the same under the blocking procedure only if a "decoration" does not start to wrap around the direction of the loop axis when using blocked super-links instead of the original links. Another way to say this is that the "decorated" Polyakov loop has a maximum size in the direction of his symmetry axis.

We then decide to iterate the blocking procedure in different ways for the direction of the loop axis and for the orthogonal directions: the number of steps in the axis direction is limited by the number of "decorations" of the loop, whereas there is no limit for the number of iterations in the orthogonal directions. The result is that the physical size of the operator is increased in the right way on all the directions: when the maximum size is reached in one direction, the blocking stops in that direction, but can continue in the others. Moreover, when the blocked super-links cannot fit a given lattice size, we blocked them at different "levels" (which means different lengths) in order to fill the winding direction completely. A pictorial representation of this procedure is shown in Fig. 4.7.

| | | | | | |
|----------|------------|------------|----------|------------|------------|
| R^{++} | A_1^{++} | A_2^{++} | E^{++} | T_1^{++} | T_2^{++} |
| # op. | 8 | 3 | 22 | 19 | 44 |
| R^{-+} | A_1^{-+} | A_2^{-+} | E^{-+} | T_1^{-+} | T_2^{-+} |
| # op. | 2 | 1 | 7 | 24 | 33 |
| R^{+-} | A_1^{+-} | A_2^{+-} | E^{+-} | T_1^{+-} | T_2^{+-} |
| # op. | 1 | 3 | 7 | 48 | 33 |
| R^{--} | A_1^{--} | A_2^{--} | E^{--} | T_1^{--} | T_2^{--} |
| # op. | 3 | 3 | 14 | 27 | 29 |

Table 4.3: Different operators calculated in each of the 20 symmetry channels. All these operators are used in the variational basis and to each of them we apply the improved blocking procedure of Sec. 4.1.2.

| | | | | | |
|----------|------------|------------|----------|------------|------------|
| R^{++} | A_1^{++} | A_2^{++} | E^{++} | T_1^{++} | T_2^{++} |
| # op. | 2 | 1 | 7 | 3 | 9 |
| R^{-+} | A_1^{-+} | A_2^{-+} | E^{-+} | T_1^{-+} | T_2^{-+} |
| # op. | 1 | 0 | 3 | 3 | 9 |
| R^{+-} | A_1^{+-} | A_2^{+-} | E^{+-} | T_1^{+-} | T_2^{+-} |
| # op. | 0 | 1 | 3 | 14 | 8 |
| R^{--} | A_1^{--} | A_2^{--} | E^{--} | T_1^{--} | T_2^{--} |
| # op. | 0 | 1 | 3 | 9 | 3 |

Table 4.4: Different "bi-torelon" operators calculated in each of the 20 symmetry channels. All these operators are used in the variational basis and to each of them we apply the improved blocking procedure of Sec. 4.1.2.

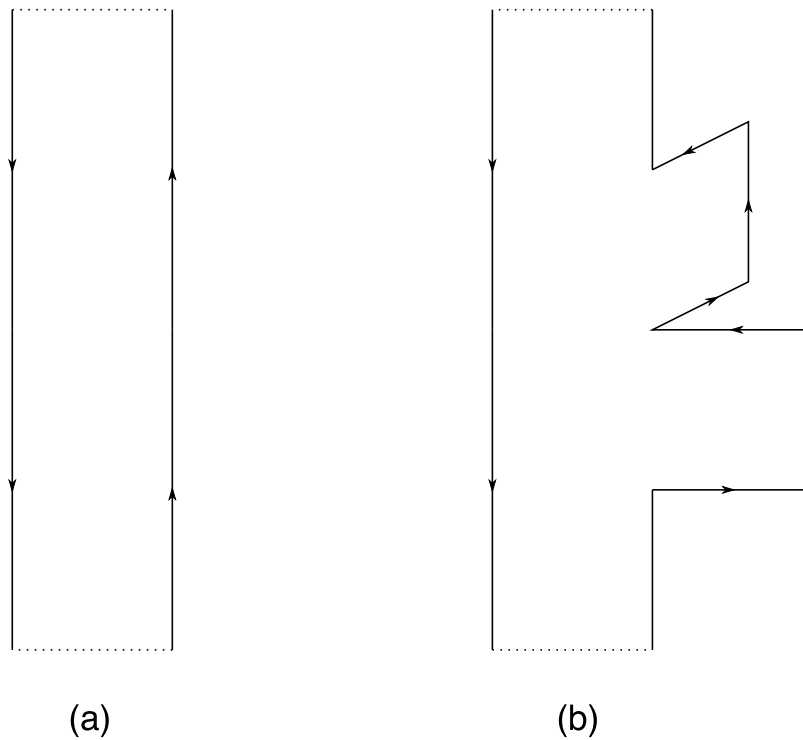


Figure 4.6: Paths used for the construction of operators coupling with bi-torelon states. Both these paths extend over the entire lattice in one direction, whereas the distance between the Polyakov loops composing them is chosen to be one lattice spacing. (a) is the simplest (and shortest) path made of two simple Polyakov loops in opposite directions; (b) is made of one straight Polyakov loop and one Polyakov loop with 2 "decorations" one lattice spacing wide.

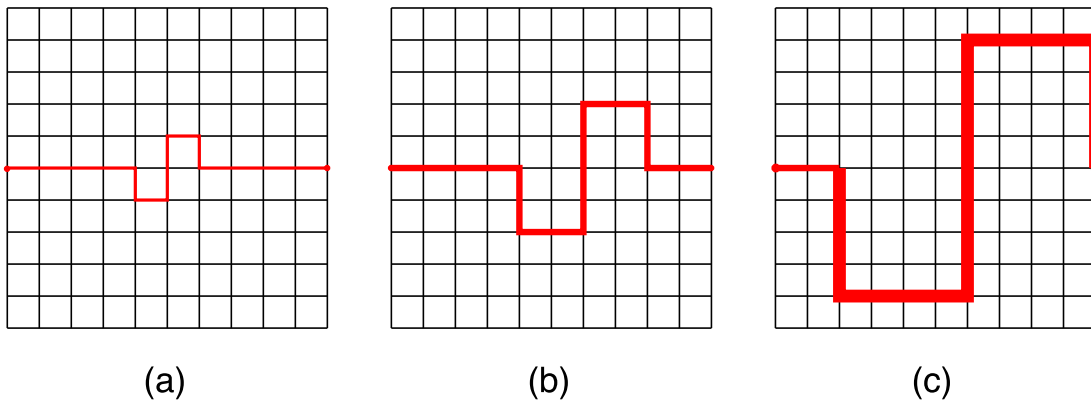


Figure 4.7: A Polyakov loop with two "decorations" on a plane lattice of dimension $L = 10$ in the winding direction of the loop. (a) shows the original loop, then at blocking level $b = 0$: each "decoration" is one lattice spacing wide; (b) shows the blocked loop at $b = 1$ where the links are thicker meaning that they are super-links (and also smeared, as described in (4.15)): each decoration is 2 lattice spacing wide and all links are blocked at the same level; (c) shows the same path at blocking level $b = 2$ where the super-links of the "decorations" have length $2^b = 4$, but the loops fill the whole length of the lattice only if we choose the first link of length 2, that is at blocking level $b = 1$.

5. Numerical simulations and data analysis

5.1 Monte–Carlo simulations

One of the mainly used tools in the non–perturbative lattice approach to quantum field theories is numerical computer simulations. As we showed in Sec. 1.1.3, the structure of the Euclidean path integral, allows us to obtain expectation values of field operators as averages over an ensemble of variables distributed according to the weight given by the exponential of the action

$$\langle \mathcal{O} \rangle = \frac{\int \mathcal{D}\phi \mathcal{O}[\phi] e^{-\mathcal{S}_E[\phi]}}{\int \mathcal{D}\phi e^{-\mathcal{S}_E[\phi]}} . \quad (5.1)$$

On the lattice, the above integration is finite dimensional and can be afforded using well–known statistical methods due to the large number of stochastic variables and the fact that, being the Euclidean action \mathcal{S}_E real and lower bounded, the exponential weight can be interpreted as the Boltzmann factor of a statistical mechanics system. A first estimate of $\langle \mathcal{O} \rangle$ is given by the ensemble average

$$\langle \mathcal{O} \rangle \approx \frac{\sum_{conf} \mathcal{O}[\phi_i]}{N_{conf}} , \quad (5.2)$$

where ϕ_i are field configurations that appear in the statistical system with probability $e^{-\mathcal{S}_E[\phi]}$; this estimate has an error which goes as $1/\sqrt{N_{conf}}$ if the ϕ_i configurations are statistically independent. This way of choosing the configurations is often referred to in the literature as *important sampling*.

In numerical simulation the main problem is to generate an ensemble of configurations ϕ_i with a distribution which is the Boltzmann one (the equilibrium distribution); in Monte–Carlo simulations, this is achieved by generating a sequence of configurations starting from an initial one ϕ_0 and following an *update algorithm*: after every application of the update step on ϕ_i , we obtain a new configuration ϕ_{i+1} . The entire set of configurations for a given algorithm is called a Markov chain. General mathematical theorems on Markov chains (for an introductory review see [44]) ensure that the correct distribution is reached asymptotically if the update satisfies the detailed

balance

$$e^{-S[C]}\text{Prob.}(C \rightarrow C') = e^{-S[C']}\text{Prob.}(C' \rightarrow C) \quad , \quad (5.3)$$

where C and C' are two configurations of the Markov chain. It is then possible to measure the operator \mathcal{O} on the configurations ϕ_i and obtain its expectation value following (5.2). In order to ensure the detailed balance relation, we should require that the configurations on which we measure have lost every memory of the initial configuration ϕ_0 ; this happens if we evolve the system of configurations until it has reached its equilibrium state. From that point onward, we say that the system is *thermalized*. The thermalization time depends on the type of update algorithm, the observable \mathcal{O} and on the bare parameters in the action $\mathcal{S}_E[\phi]$: general experience gives rules to establish a safe bound for the thermalization time (our choice is shown in Tab. 5.1). A good update algorithm should be able to generate configurations from all the regions of the configuration space, and, in order to ensure their statistical independence, successive configurations must have the lowest possible auto-correlation. There are several update algorithms and in our Monte-Carlo simulations we use a *heat-bath* update to generate lattice gauge field configurations weighted by the exponential of the lattice action (1.73). The particular heat-bath update we use is the version of Kennedy and Pendleton [45]: it updates each of the four real parameters of a generic SU(2) matrix according to the distribution given by the lattice action. Since every link variable is a $N \times N$ matrix of the SU(N) group, we actually update elements of a group different from SU(2): this is done by updating the maximal covering set of $N(N - 1)/2$ SU(2) subgroups through the Cabibbo-Marinari algorithm [46]. These choices are the most widely used in the pure gauge lattice simulations. The update algorithm acts on a single link per time and must be used to update all the links of the lattice to have an updated configuration: the update of a configuration is called *sweep*.

To reduced correlations of a sequence of configurations obtained by local changes of link variables, it has been proved that the use of an intermediate update step called *over-relaxation* step [47] can help. Such an update simply changes a link variable in the maximal way compatible with the invariance of the action. The fact that the action does not change implies that only a subset of zero measure of the configuration space is explored and we can use this step only in conjunction with a heat-bath update. However, an over-relaxation step spans the configuration space faster than a heat-bath update generating less auto-correlated configurations; we use it in a ratio 1:4 between the number of heat-bath and over-relaxation sweeps: such a sequence of 4 over-relaxation sweeps followed by 1 heat-bath sweep is called *compound sweep*. We can choose to measure our observables/operators after each compound sweep or after a certain number of them, in order to further reduce correlations between subsequent measures.

Even when we apply the above setup in a simulation, we need to keep in mind that our measures are not strictly independent and a careful analysis of correlation time is always mandatory to

estimate the right variance. We have already described in Sec. 3.4.1 the bootstrap method used to deal with correlations in a given set of measures; in the analysis of our simulations we use another technique called *jackknife* [38] to estimate the right variance of observables without having to rely on a particular statistical distribution. The jackknife method is supposed to work on statistically independent data and to ensure this condition we bin measures in groups larger than the auto-correlation time. We usually make bins of 20 measures and we have a total number of bins of order 500.

A summary of the parameters of all the simulations performed is shown in Tab. 5.1.

5.2 Diagonalization and numerical issues

In every simulation we measure the correlators between operators in a given set $\{\phi_i^R\}_{i=1}^{N_0}$ constructed following the method described in the previous chapter. The correlators are measured as expectation values of product of operators on different temporal lattice slices

$$\tilde{C}_{ij}(t) = \sum_{\tau} \langle \phi_i^{\dagger}(t + \tau) \phi_j(\tau) \rangle \quad , \quad (5.4)$$

on background gauge field configurations generated by the Monte-Carlo procedure described in the previous section; for every set $\{i, j, t\}$ we make ~ 10000 measures further grouped in ~ 500 bins: all these measures are then analyzed with the jackknife method to obtain an average value of $\tilde{C}_{ij}(t)$ together with its statistical error for each $\{i, j, t\}$.

Recall from Sec. 4.1.3, that we need to perform the diagonalization of the matrix $\tilde{C}^{-1}(0)\tilde{C}(1)$ and before this, the inversion of $\tilde{C}(0)$; this is done by means of numerical routines [48]. Clearly, the inversion of a square matrix is possible only if the matrix is non singular, or, in other words, if its rows (columns) are linearly independent and different from zero. The main issue related to the singularity of the correlator matrix is that we should not allow two equal operators to enter the variational basis, because this will result in two equal rows (columns) and in the impossibility of performing the inversion of $\tilde{C}(0)$; moreover we should avoid linear combinations of operators to appear, because they bring to the same consequences. In constructing the operators for the variational basis we check, in each symmetry channel, if there are "formally" equal operators or "zero" operators and discard them immediately. By "formally" equal operators, we mean operators constructed using exactly the same set of link variables whereas, with "zero" operators, we refer to operators constructed summing rotated paths which exactly cancel due to the coefficients of the projection table. The former can appear in our construction, because parity and charge conjugation transformations, as defined in Sec. 4.2.2, can sometimes send an operator in a given R irreducible representation of the cubic group into another in the same representation; this can be seen only if we directly perform the charge conjugation operation on

the underlying paths instead of taking the real or the imaginary part of the trace of the related operator.

On the other hand, the check just presented is not enough to ensure that $\tilde{C}_{ij}(0)$ is invertible, because we can not check all the linear combination of operators. Since the number of operators that can be created on a finite lattice is finite, it is always possible that in our basis we are using operators that can be written as linear combinations of other operators already included. This sort of problem can not be avoided and it can totally spoil our diagonalization procedure and the possibility of getting any mass of the spectrum; this is exactly what we found when we tried for the first time to invert the correlation matrix using all the operators (blocked and unblocked) in a given symmetry channel.

The natural approach to circumvent this issue, is to start from a small basis of operators, and consequently a small correlator matrix, and then add operators (considering each blocked operator separately, even when they come from the same original operator): whenever the diagonalization is possible, we proceed by adding more and more operators, but, if an added operator forbid the diagonalization process, we discard it and we go on with the following one. Since the inversion is only approximated (because it is numerical) we need to fix a minimum tolerance value of 10^{-10} on the off-diagonal elements of the matrix $\tilde{C}^{-1}(0)\tilde{C}(0)$: if adding an operator gives an off-diagonal minimum value greater than our tolerance, that operator is also discarded. The result is the widest possible variational basis (starting from our original set of operators) compatible with the best diagonalization of the correlator matrix.

In Tab. 5.2 we compare the number of total operators (including "scattering" and "bi-torelons" operators) in the variational basis before and after the "cutting" of the correlators in each symmetry channel for SU(3); moreover, we note that to different gauge groups SU(N), it corresponds, in general, a slightly different number of operators in the cut basis even if of the same order of magnitude.

5.3 The glueball spectrum

When the diagonalization in the variational procedure goes right, we can obtain the optimized eigenvectors, and in their basis, the diagonal correlators give us the spectrum from their exponential decay. For every gauge group SU(N), with $N = 3, 4, 5, 6, 7, 8$, and in each symmetry channel, we apply the procedure described in Sec. 4.1.3 and the cutting method described above, to obtain the low-lying spectrum and some of the excitations of glueballs. In this section we want to show the main features of each spectrum (such as excited states, scattering and bi-torelon mixing) and in the next section we will perform the large- N limit of the spectrum (when possible).

| N | β | L | N_τ | N_{MC} | $N_{compound}$ | N_{width} | N_{bins} | runs |
|-----|---------|----|----------|----------|----------------|-------------|------------|------|
| 3 | 5.8945 | 12 | 10k | 100k | 200 | 20 | 25 | 20 |
| 4 | 10.789 | 12 | 10k | 100k | 200 | 20 | 25 | 20 |
| 5 | 17.107 | 12 | 10k | 100k | 200 | 20 | 25 | 20 |
| 6 | 24.845 | 12 | 10k | 100k | 200 | 20 | 25 | 20 |
| 7 | 33.995 | 12 | 10k | 65k | 250 | 20 | 13 | 40 |
| 8 | 44.496 | 12 | 10k | 100k | 250 | 16 | 25 | 20 |

Table 5.1: The table summarize the parameters used for the simulations. A typical run has N_τ thermalization sweeps after which we start measuring. The thermalization starts with 200 heat-bath updates followed by compound sweeps, which are sequence of 1 heat-bath update followed by 4 over-relaxation sweeps. After the thermalization process we start N_{MC} sweeps. We then decide to measure every $N_{compound}$ sweeps to reduce autocorrelation between the measures. The $N_{measures}$ measure sweeps are further divided in N_{bins} bins where each one is an average over N_{width} measures. This is the relation that has to be satisfied between the parameters: $N_{width} \times N_{bins} \times N_{compound} = N_{MC}$ The total set of measures to be analyzed is then $N_{bins} \times runs$, where each run starts with a different random seed and is indeed independent of all the others.

| SU(3) variational basis before \rightarrow after the cut | | | | | |
|--|---------------------|---------------------|-----------------------|-----------------------|-----------------------|
| R^{++} | A_1^{++} | A_2^{++} | E^{++} | T_1^{++} | T_2^{++} |
| # op. | 72 \rightarrow 45 | 28 \rightarrow 28 | 204 \rightarrow 192 | 164 \rightarrow 144 | 388 \rightarrow 281 |
| R^{-+} | A_1^{-+} | A_2^{-+} | E^{-+} | T_1^{-+} | T_2^{-+} |
| # op. | 20 \rightarrow 20 | 8 \rightarrow 8 | 68 \rightarrow 60 | 204 \rightarrow 192 | 300 \rightarrow 245 |
| R^{+-} | A_1^{+-} | A_2^{+-} | E^{+-} | T_1^{+-} | T_2^{+-} |
| # op. | 8 \rightarrow 8 | 28 \rightarrow 28 | 68 \rightarrow 60 | 440 \rightarrow 337 | 296 \rightarrow 244 |
| R^{--} | A_1^{--} | A_2^{--} | E^{--} | T_1^{--} | T_2^{--} |
| # op. | 24 \rightarrow 24 | 28 \rightarrow 28 | 124 \rightarrow 112 | 252 \rightarrow 209 | 244 \rightarrow 204 |

Table 5.2: Number of operators in each symmetry channel of the variational basis used to extract the spectrum of SU(3). The number of operators on the left of the arrow refers to the original basis with blocked and unblocked operators of every kind; on the right of the arrow there is the number of the operators with which the correlator matrix is invertible and the diagonalization is possible.

5.3.1 A general overview

The pure gauge spectrum of SU(3) has already been largely studied with lattice simulations, even in the continuum limit [14, 43]. In our present work we have data for only a single lattice spacing and a single volume, but previous works at the same value of β and L [49, 11] suggest that we are already in the scaling region and in the infinite volume limit; notwithstanding this, we performed a test run on a bigger lattice and confirmed the observation previously done.

We have in this case the possibility of comparing some of our results with previous ones in the literature, but, in addition, we try a first attempt of including, in our variational calculations, a very large number of operators coupling with bi-torelon states and multi-gluon states. For SU(3), a study of the mixing with scattering states on the lattice was done in [43] using the same kind of operators that we use (the direct product of two single trace operators), but only for 2 operators in the A_1^{++} ; we extend the survey for scattering states including, in the variational basis, the same number of "scattering" operators as of single-gluon operators. However, we note that, after the cut of the correlator, in order to obtain an invertible matrix in the variational procedure, many of these "scattering" states were discarded (though leaving us with a number of them between 4 and 180 depending on the symmetry channel).

It is important to remark that we explicitly include also operators winding around the spatial toroidal lattice coupling to bi-torelon states for each set of R^{PC} quantum numbers, whereas previous works could deal only with the simplest combinations of them, projecting only onto the A_1^{++} and E^{++} (and onto the T_1^{--} considering the imaginary part of some particular combinations [50]).

Our aim is to better identify the one-particle states of the glueball spectrum and to extend the above strategy to a quite large number of gauge groups. Previous large- N studies of the glueball spectrum, perform the $N \rightarrow \infty$ extrapolation using 3 or 4 points of $N \in [3, 8]$. What we have done is a full analysis of all the symmetry sectors for every value of N in the above interval.

In Tab. 5.3 we present the SU(3) spectrum coming from our simulations. First of all, let us explain what kind of information we are showing for each symmetry channel:

- the first column contains the information about the mass in unit of lattice spacing am and its statistical error σ , for the channel indicated on the left of the column;
- in the second column we show the overlap of the operator for the given mass; as we already said, the overlap $|c_n|^2 = |\langle n|\hat{\Phi}|0\rangle|^2$ measures how good is the operator in approximating the wave-function of the glueball state. As a consequence, a good overlap implies a reliable extrapolation of the mass from the single-exponential decay of the correlator (higher mass

states do not contribute even at small time). Since the overlap is fitted from the correlator decay (it is the multiplicative constant in front of the exponential) it comes with an error which we estimate to be 0.05; we decide to consider "reliable" operators with $|c_n|^2 \geq 0.90$ and we also consider overlaps $|c_n|^2 \geq 1.00$ as long as they remain ≤ 1.10 : then we are choosing a conservative $2\sigma = 0.10$ wide interval around the best overlap possible, which is unity. In the following tables, overlaps outside this reliability range are bold-face;

- the third column shows the reduced χ^2 of the exponential fit (see (4.23)) which is the best possible fit coming from different ranges of the temporal distance; the best fitted range is usually made up by 3 points starting from $t = a$ to $t = 3a$. We choose to consider good fits the ones with $\chi^2 \leq 1.20$ and values greater than this bound are highlighted in the following tables;
- the last three columns, labelled by mix_G , mix_S and mix_T , contain the information about the mixing of the operator $\hat{\Phi}$, whose correlator is used to extract the mass, and the original basis operators ϕ_i , where the index i can label a single-glueball operator (G), a "scattering" operator (S) or a "bi-torelon" operator (T) for a total of N_0 operators. Using (4.18), and recalling that v_i are the components of the eigenvector \vec{v} corresponding to the operator $\hat{\Phi}$, we define the normalized mixing of a particular state with each of the subsets of basic operators G , S and T by

$$\text{mix}_A = \frac{\sum_{i \in A} v_i^2}{\sum_{i=1}^{N_0} v_i^2} \quad , \quad A = G, S, T \quad . \quad (5.5)$$

We decide to consider as single-glueball states, those with a mixing with the operators in the group G greater than 80%; those states with mix_G below that threshold have the mark "(?)" next to the name of the representation, as long as mix_G is still the dominant contribution (but we cannot be sure of their interpretation as one-particle states). When the contribution to the state splits almost equally between operators in G and in T we use the mark "(2T?)" and if the contribution of mix_T is greater than 50% we decide to discard that state from the one-particle states we are interested in and we use the mark "(2T)" (even we are still not sure that it is a bi-torelon state). States with an appreciable mixing with the "scattering" operators do not appear apart from the A_1^{++} channel, on which we want to comment in a separate section for all the gauge groups;

In the next paragraphs we want to discuss the main features of the $SU(3)$ spectrum, which is summarized in Tab. 5.3. All the important aspects are checked in the same way for the other gauge groups as well.

In the A_1^{++} representation we clearly see the ground state and 3 excitations, two of which are above the energy threshold where scattering states can appear (using a free relativistic dispersion relation for such states). All the overlaps are very good ($\geq 93\%$) and the χ^2 values indicate that the masses are reliable, which is a consequence of our big variational basis and of the improved blocking method. The high mixing coefficients with the "scattering" operators are a completely new feature revealed by our work and we will go a bit into the details of this issue in Sec. 5.3.2; however, by comparing our A_1^{++} spectrum with previous works, we can say that, at least for the two lightest states, the one-particle interpretation is the most probable.

In the A_1 representation we find only another state, in the $-+$ sector, which comes from one-particle operators for the 99% of its composition.

In the E^{++} we have two operators that, after the variational procedure, give the same mass (within a 1σ interval) and we can interpret them as the same state or as the 2 degenerate magnetic polarizations of a continuum spin 2 glueball; however one of them has a χ^2 out of our reliability range and in the extrapolation of the large- N spectrum we will use only the reliable state. The continuum spin 2 glueball, with 5 polarizations, gain contributions from the lattice state in the E and T_2 representation (see Tab. 4.2), hence we expect to find state in the T_2^{++} channel corresponding to that in the E^{++} . From the table it is clear that we find such a state, and indeed we see it from 3 different operators which can therefore corresponds to 3 of the 5 polarizations of the spin 2 continuum state. In the large- N extrapolation we will use in this case the operator with the lowest χ^2 , as it gives the most reliable mass estimate. The splitting of a continuum state into degenerate multiplets in the lattice representations is seen also for the $-+$ sector of the E and T_2 representations: 2 operators in the E^{-+} give a mass compatible, within 1σ , with the states coming from 3 different operators in the T_2^{-+} channel.

The other interesting feature of our $SU(3)$ spectrum is the presence of 2 bi-torelon states, one in the A_2^{++} and one in the E^{++} ; although their χ^2 are not reliable, the mixing with operators winding around the spatial lattice is more than 80% for both of them. The E^{++} bi-torelon we see here, is probably the one seen in the same position by the author of [43].

The state in the T_1^{--} channel is another interesting state because it comes from an operator whose components are half from single-glueball operators and half from "bi-torelon" operators. The bi-torelon contribution is less and less manifest at higher N except for $N = 8$ and this behaviour is still to be understood.

As we increase N , we note, from Tab. 5.4 to Tab. 5.8, really small differences in the glueball spectrum and the variation of the mass of each state with the number of colours will be investigated deeply in Sec. 5.4.

| SU(3) at $\beta = 5.8945$ and $L = 12, T = 12$ | | | | | | |
|--|--------------|-------------|-------------|----------------|----------------|----------------|
| R^{PC} | $am(\sigma)$ | $ c_n ^2$ | χ^2 | mix_G | mix_S | mix_T |
| A_1^{++} | 0.798(14) | 0.98 | 0.10 | 0.5391 | 0.4609 | 0.0000 |
| A_1^{++*} | 1.320(44) | 0.95 | 0.13 | 0.5535 | 0.4465 | 0.0000 |
| A_1^{+++} | 1.624(89) | 0.93 | 0.54 | 0.5041 | 0.4959 | 0.0000 |
| A_1^{++++} | 2.02(17) | 1.03 | 0.11 | 0.4924 | 0.5076 | 0.0000 |
| A_1^{-+} | 1.429(59) | 0.91 | 0.49 | 0.9927 | 0.0056 | 0.0017 |
| $A_2^{++}(2T)$ | 1.82(12) | 0.91 | 2.31 | 0.0508 | 0.0108 | 0.9383 |
| E^{++} | 1.260(36) | 0.97 | 1.28 | 0.8552 | 0.0692 | 0.0756 |
| E^{++} | 1.293(40) | 0.98 | 0.06 | 0.8308 | 0.0855 | 0.0837 |
| $E^{++*}(2T)$ | 1.372(63) | 0.91 | 1.50 | 0.1629 | 0.0316 | 0.8055 |
| E^{+-} | 2.59(45) | 1.06 | 0.76 | 0.9269 | 0.0618 | 0.0114 |
| E^{-+} | 1.662(89) | 0.93 | 0.63 | 0.9752 | 0.0229 | 0.0019 |
| E^{-+} | 1.614(81) | 0.87 | 0.31 | 0.9768 | 0.0199 | 0.0033 |
| E^{-+*} | 2.37(33) | 1.01 | 0.54 | 0.9738 | 0.0188 | 0.0074 |
| T_1^{+-} | 1.628(80) | 1.01 | 0.41 | 0.9002 | 0.0814 | 0.0185 |
| $T_1^{--}(2T?)$ | 2.19(25) | 0.93 | 0.13 | 0.4905 | 0.0375 | 0.4721 |
| T_1^{-+} | 2.29(31) | 0.96 | 0.62 | 0.8597 | 0.1309 | 0.0094 |
| T_2^{++} | 1.293(41) | 0.99 | 0.33 | 0.9250 | 0.0520 | 0.0230 |
| T_2^{++} | 1.233(38) | 0.92 | 1.87 | 0.9261 | 0.0512 | 0.0227 |
| T_2^{++} | 1.329(41) | 0.99 | 0.89 | 0.8983 | 0.0858 | 0.0159 |
| T_2^{--} | 1.96(19) | 0.81 | 0.20 | 0.9231 | 0.0689 | 0.0080 |
| T_2^{--} | 2.26(27) | 1.00 | 0.38 | 0.9187 | 0.0784 | 0.0028 |
| T_2^{-+} | 1.571(80) | 0.87 | 0.73 | 0.8888 | 0.0962 | 0.0149 |
| T_2^{-+} | 1.707(90) | 0.99 | 0.01 | 0.8748 | 0.1011 | 0.0241 |
| T_2^{-+} | 1.625(94) | 0.88 | 2.48 | 0.8384 | 0.1327 | 0.0290 |

Table 5.3: The full spectrum of pure SU(3) gauge theory from lattice simulations at the parameters shown in the header. Bold-face values correspond to non-reliable states which will not be used in the large- N extrapolation.

| SU(4) at $\beta = 10.789$ and $L = 12, T = 12$ | | | | | | |
|--|--------------|-------------|-------------|---------|---------|---------|
| R^{PC} | $am(\sigma)$ | $ c_n ^2$ | χ^2 | mix_G | mix_S | mix_T |
| A_1^{++} | 0.821(15) | 0.99 | 0.99 | 0.5733 | 0.4267 | 0.0000 |
| A_1^{++*} | 1.381(46) | 0.94 | 1.67 | 0.5490 | 0.4510 | 0.0000 |
| A_1^{+++} | 1.93(16) | 0.84 | 0.15 | 0.6071 | 0.3929 | 0.0000 |
| A_1^{-+} | 1.424(54) | 0.89 | 0.15 | 0.9908 | 0.0083 | 0.0009 |
| A_1^{-+*} | 2.52(54) | 0.94 | 0.88 | 0.9474 | 0.0441 | 0.0085 |
| $A_2^{++}(2T)$ | 1.82(14) | 0.85 | 1.40 | 0.0260 | 0.0094 | 0.9646 |
| A_2^{++} | 2.06(21) | 0.85 | 0.17 | 0.8638 | 0.0201 | 0.1161 |
| A_2^{+-} | 2.10(19) | 1.02 | 0.29 | 0.9925 | 0.0074 | 0.0002 |
| E^{++} | 1.264(41) | 0.94 | 0.01 | 0.9431 | 0.0334 | 0.0235 |
| E^{++} | 1.346(47) | 1.01 | 0.41 | 0.8872 | 0.0700 | 0.0427 |
| $E^{+++}(2T)$ | 1.635(75) | 1.04 | 0.54 | 0.3102 | 0.1063 | 0.5835 |
| E^{-+} | 1.728(97) | 0.95 | 0.12 | 0.9660 | 0.0262 | 0.0078 |
| E^{-+} | 1.635(90) | 0.83 | 0.85 | 0.9633 | 0.0322 | 0.0045 |
| T_1^{++} | 1.85(16) | 0.75 | 0.28 | 0.9292 | 0.0645 | 0.0063 |
| T_1^{+-} | 1.637(82) | 1.02 | 1.05 | 0.8856 | 0.1014 | 0.0130 |
| T_1^{+-} | 1.669(76) | 1.03 | 0.43 | 0.9103 | 0.0633 | 0.0264 |
| T_1^{+-} | 1.695(82) | 1.03 | 0.17 | 0.8635 | 0.1053 | 0.0312 |
| $T_1^{--}(?)$ | 2.25(27) | 0.99 | 0.08 | 0.6288 | 0.1067 | 0.2645 |
| T_1^{-+} | 2.28(35) | 0.87 | 0.60 | 0.8781 | 0.1039 | 0.0179 |
| T_2^{++} | 1.333(48) | 0.99 | 0.85 | 0.9128 | 0.0754 | 0.0119 |
| $T_2^{+-}(2T?)$ | 1.97(16) | 0.95 | 1.53 | 0.4000 | 0.1435 | 0.4565 |
| T_2^{-+} | 1.636(88) | 0.90 | 0.02 | 0.8485 | 0.1386 | 0.0128 |
| T_2^{-+} | 1.676(91) | 0.90 | 0.40 | 0.8859 | 0.0772 | 0.0369 |

Table 5.4: The full spectrum of pure SU(4) gauge theory from lattice simulations at the parameters shown in the header. Bold-face values correspond to non-reliable states which will not be used in the large- N extrapolation.

| SU(5) at $\beta = 17.107$ and $L = 12, T = 12$ | | | | | | |
|--|--------------|-------------|-------------|----------------|----------------|----------------|
| R^{PC} | $am(\sigma)$ | $ c_n ^2$ | χ^2 | mix_G | mix_S | mix_T |
| A_1^{++} | 0.800(16) | 0.98 | 0.84 | 0.5173 | 0.4826 | 0.0001 |
| A_1^{++*} | 1.386(56) | 0.90 | 0.39 | 0.5224 | 0.4771 | 0.0005 |
| A_1^{+++} | 1.548(79) | 0.86 | 0.45 | 0.4881 | 0.5119 | 0.0000 |
| A_1^{+++} | 1.70(10) | 0.95 | 0.47 | 0.5063 | 0.4901 | 0.0036 |
| A_1^{++++} | 1.84(14) | 0.86 | 0.51 | 0.5323 | 0.4674 | 0.0003 |
| A_1^{-+} | 1.408(57) | 0.88 | 0.09 | 0.9852 | 0.0124 | 0.0024 |
| A_1^{-+*} | 2.32(30) | 0.96 | 0.36 | 0.9764 | 0.0111 | 0.0124 |
| $A_2^{++}(2T)$ | 1.90(16) | 0.86 | 0.05 | 0.0748 | 0.0039 | 0.9213 |
| A_2^{+-} | 2.21(23) | 1.13 | 0.53 | 0.9849 | 0.0132 | 0.0019 |
| A_2^{+-} | 2.48(55) | 0.83 | 2.23 | 0.9970 | 0.0018 | 0.0012 |
| E^{++} | 1.317(43) | 0.97 | 1.57 | 0.9354 | 0.0484 | 0.0161 |
| $E^{+++}(2T)$ | 1.613(84) | 0.94 | 1.44 | 0.2979 | 0.0612 | 0.6409 |
| $E^{+++}(2T?)$ | 1.604(85) | 0.91 | 0.05 | 0.4385 | 0.1560 | 0.4055 |
| E^{--} | 1.99(20) | 0.80 | 0.03 | 0.9174 | 0.0535 | 0.0290 |
| E^{-+} | 1.71(10) | 0.90 | 0.24 | 0.9530 | 0.0372 | 0.0098 |
| E^{-+} | 1.69(10) | 0.86 | 0.09 | 0.9889 | 0.0086 | 0.0024 |
| E^{-+*} | 2.58(46) | 1.10 | 0.02 | 0.9554 | 0.0373 | 0.0073 |
| T_1^{++} | 2.08(20) | 0.93 | 0.12 | 0.9485 | 0.0462 | 0.0053 |
| T_1^{++} | 2.02(21) | 0.82 | 0.15 | 0.9621 | 0.0330 | 0.0049 |
| T_1^{+-} | 1.485(65) | 0.87 | 1.55 | 0.9250 | 0.0595 | 0.0154 |
| T_1^{+-} | 1.500(70) | 0.88 | 0.56 | 0.8359 | 0.1375 | 0.0265 |
| T_1^{+-} | 1.613(74) | 0.97 | 0.94 | 0.8379 | 0.1206 | 0.0416 |
| $T_1^{--}(?)$ | 2.25(29) | 0.92 | 0.40 | 0.7642 | 0.0467 | 0.1891 |
| T_1^{-+} | 2.31(29) | 0.96 | 0.47 | 0.8839 | 0.1091 | 0.0070 |
| T_2^{++} | 1.258(43) | 0.91 | 0.80 | 0.8667 | 0.1175 | 0.0158 |
| T_2^{++} | 1.381(47) | 1.02 | 0.23 | 0.9273 | 0.0649 | 0.0079 |
| T_2^{++} | 1.323(45) | 0.96 | 0.14 | 0.8741 | 0.1043 | 0.0215 |
| T_2^{+++} | 1.77(11) | 0.90 | 0.18 | 0.9413 | 0.0366 | 0.0221 |
| $T_2^{+-}(?)$ | 1.99(16) | 1.02 | 0.70 | 0.7312 | 0.1130 | 0.1558 |
| T_2^{+-} | 1.94(15) | 0.90 | 0.82 | 0.8007 | 0.1156 | 0.0837 |
| T_2^{+-} | 1.95(17) | 0.85 | 0.04 | 0.8582 | 0.1074 | 0.0344 |
| T_2^{--} | 2.00(20) | 0.82 | 0.48 | 0.8843 | 0.1101 | 0.0056 |
| T_2^{-+} | 1.74(11) | 0.96 | 0.53 | 0.9132 | 0.0759 | 0.0109 |

Table 5.5: The full spectrum of pure SU(5) gauge theory from lattice simulations at the parameters shown in the header. Bold-face values correspond to non-reliable states which will not be used in the large- N extrapolation.

| SU(6) at $\beta = 24.845$ and $L = 12, T = 12$ | | | | | | |
|--|--------------|-------------|-------------|----------------|----------------|----------------|
| R^{PC} | $am(\sigma)$ | $ c_n ^2$ | χ^2 | mix_G | mix_S | mix_T |
| A_1^{++} | 0.785(14) | 0.96 | 0.15 | 0.4854 | 0.5144 | 0.0002 |
| A_1^{++*} | 1.508(62) | 1.01 | 2.04 | 0.4969 | 0.5030 | 0.0001 |
| A_1^{++*} | 1.534(87) | 0.84 | 0.03 | 0.4959 | 0.5041 | 0.0000 |
| A_1^{-+} | 1.416(59) | 0.89 | 1.54 | 0.9983 | 0.0013 | 0.0004 |
| A_2^{+-} | 1.84(14) | 0.80 | 0.68 | 0.9923 | 0.0070 | 0.0007 |
| A_2^{+-} | 2.56(48) | 0.97 | 0.02 | 0.9964 | 0.0027 | 0.0009 |
| E^{++} | 1.253(41) | 0.92 | 1.83 | 0.9147 | 0.0396 | 0.0457 |
| E^{++} | 1.247(43) | 0.89 | 0.59 | 0.9437 | 0.0311 | 0.0252 |
| $E^{++*}(2T)$ | 1.620(87) | 0.94 | 0.64 | 0.2264 | 0.0745 | 0.6991 |
| E^{-+} | 1.74(11) | 0.92 | 0.77 | 0.9774 | 0.0159 | 0.0068 |
| E^{-+} | 1.71(11) | 0.85 | 1.03 | 0.9838 | 0.0115 | 0.0047 |
| E^{-+*} | 2.45(40) | 0.97 | 0.01 | 0.9387 | 0.0527 | 0.0086 |
| T_1^{++} | 2.10(22) | 0.85 | 0.41 | 0.9393 | 0.0574 | 0.0033 |
| T_1^{+-} | 1.518(67) | 0.90 | 0.37 | 0.9060 | 0.0820 | 0.0120 |
| T_1^{+-} | 1.640(77) | 0.98 | 0.24 | 0.8386 | 0.1191 | 0.0423 |
| T_1^{+-*} | 1.89(13) | 0.94 | 1.57 | 0.8600 | 0.0858 | 0.0542 |
| T_1^{-+} | 2.45(38) | 1.02 | 0.35 | 0.9056 | 0.0831 | 0.0113 |
| T_1^{-+} | 2.40(37) | 0.96 | 0.02 | 0.8694 | 0.1223 | 0.0082 |
| T_2^{++} | 1.275(39) | 0.92 | 0.60 | 0.9173 | 0.0758 | 0.0069 |
| T_2^{++} | 1.362(44) | 1.00 | 1.71 | 0.9290 | 0.0556 | 0.0154 |
| T_2^{++*} | 1.98(14) | 1.08 | 0.97 | 0.9429 | 0.0473 | 0.0098 |
| $T_2^{+-}(\?)$ | 1.93(15) | 0.91 | 0.03 | 0.7748 | 0.1109 | 0.1144 |
| T_2^{+-} | 2.02(16) | 0.99 | 0.63 | 0.8765 | 0.0883 | 0.0351 |
| T_2^{--} | 2.03(20) | 0.81 | 0.34 | 0.8607 | 0.1330 | 0.0063 |
| T_2^{--} | 2.23(25) | 0.96 | 1.11 | 0.9212 | 0.0757 | 0.0031 |
| T_2^{-+} | 1.85(11) | 1.07 | 0.34 | 0.8408 | 0.1036 | 0.0555 |
| T_2^{-+} | 1.77(11) | 0.95 | 0.34 | 0.8670 | 0.1119 | 0.0211 |
| T_2^{-+} | 1.66(10) | 0.85 | 0.97 | 0.9321 | 0.0458 | 0.0221 |

Table 5.6: The full spectrum of pure SU(6) gauge theory from lattice simulations at the parameters shown in the header. Bold-face values correspond to non-reliable states which will not be used in the large- N extrapolation.

| SU(7) at $\beta = 33.995$ and $L = 12, T = 12$ | | | | | | |
|--|--------------|-------------|-------------|----------------|----------------|----------------|
| R^{PC} | $am(\sigma)$ | $ c_n ^2$ | χ^2 | mix_G | mix_S | mix_T |
| A_1^{++} | 0.820(15) | 0.98 | 0.43 | 0.5586 | 0.4414 | 0.0000 |
| A_1^{++*} | 1.570(61) | 1.09 | 0.90 | 0.4952 | 0.5044 | 0.0005 |
| A_1^{+++} | 1.734(88) | 0.97 | 1.87 | 0.4709 | 0.5050 | 0.0241 |
| A_1^{+++*} | 1.96(15) | 0.95 | 2.22 | 0.5492 | 0.4504 | 0.0004 |
| A_1^{-+} | 1.451(58) | 0.92 | 0.06 | 0.9978 | 0.0016 | 0.0007 |
| $A_2^{++}(2T)$ | 1.84(13) | 0.78 | 1.41 | 0.0386 | 0.0094 | 0.9520 |
| A_2^{++} | 2.19(26) | 0.90 | 0.44 | 0.9002 | 0.0306 | 0.0692 |
| A_2^{+-} | 2.44(45) | 0.85 | 0.58 | 0.9963 | 0.0033 | 0.0004 |
| E^{++} | 1.303(45) | 0.96 | 0.86 | 0.9435 | 0.0406 | 0.0158 |
| E^{++} | 1.307(46) | 0.93 | 1.27 | 0.9338 | 0.0392 | 0.0271 |
| $E^{+++}(2T)$ | 1.670(90) | 0.94 | 0.77 | 0.2598 | 0.0879 | 0.6522 |
| $E^{+++}(2T)$ | 1.71(10) | 0.93 | 1.49 | 0.3531 | 0.0596 | 0.5873 |
| E^{+-} | 2.55(56) | 0.86 | 0.12 | 0.9693 | 0.0257 | 0.0049 |
| E^{+-} | 2.62(64) | 0.87 | 0.31 | 0.9572 | 0.0385 | 0.0043 |
| E^{-+} | 1.80(11) | 0.93 | 0.13 | 0.9701 | 0.0280 | 0.0019 |
| T_1^{+-} | 1.517(69) | 0.88 | 0.03 | 0.8716 | 0.0962 | 0.0322 |
| T_1^{+-} | 1.622(80) | 0.96 | 0.37 | 0.8713 | 0.0838 | 0.0449 |
| T_1^{+-} | 1.612(77) | 0.93 | 0.38 | 0.8651 | 0.1112 | 0.0236 |
| T_1^{+-*} | 1.85(12) | 0.88 | 1.08 | 0.8500 | 0.0754 | 0.0746 |
| T_1^{--} | 2.21(23) | 0.99 | 0.72 | 0.8766 | 0.0612 | 0.0622 |
| T_1^{-+} | 2.30(30) | 0.92 | 0.38 | 0.8915 | 0.0982 | 0.0103 |
| T_1^{-+} | 2.31(34) | 0.89 | 1.17 | 0.8354 | 0.1301 | 0.0345 |
| T_2^{++} | 1.328(44) | 0.97 | 0.22 | 0.8891 | 0.0988 | 0.0121 |
| T_2^{++} | 1.355(49) | 0.97 | 0.67 | 0.9392 | 0.0499 | 0.0109 |
| T_2^{++} | 1.445(50) | 1.05 | 1.84 | 0.8792 | 0.0995 | 0.0213 |
| T_2^{+-} | 2.08(17) | 1.02 | 1.62 | 0.9001 | 0.0737 | 0.0262 |
| $T_2^{+-}(?)$ | 2.05(18) | 0.95 | 0.98 | 0.6316 | 0.0795 | 0.2889 |
| T_2^{--} | 2.28(29) | 0.97 | 0.51 | 0.8500 | 0.1407 | 0.0093 |
| T_2^{-+} | 1.77(10) | 0.98 | 0.50 | 0.8903 | 0.0870 | 0.0227 |
| T_2^{-+} | 1.675(98) | 0.84 | 1.10 | 0.9323 | 0.0539 | 0.0138 |
| T_2^{-+*} | 2.37(32) | 1.05 | 0.92 | 0.9177 | 0.0358 | 0.0465 |

Table 5.7: The full spectrum of pure SU(7) gauge theory from lattice simulations at the parameters shown in the header. Bold-face values correspond to non-reliable states which will not be used in the large- N extrapolation.

| SU(8) at $\beta = 44.496$ and $L = 12, T = 12$ | | | | | | |
|--|--------------|-------------|-------------|----------------|----------------|----------------|
| R^{PC} | $am(\sigma)$ | $ c_n ^2$ | χ^2 | mix_G | mix_S | mix_T |
| A_1^{++} | 0.786(16) | 0.96 | 0.78 | 0.5868 | 0.4131 | 0.0000 |
| A_1^{+++} | 1.406(63) | 0.90 | 0.50 | 0.5052 | 0.4943 | 0.0005 |
| A_1^{-+} | 1.404(62) | 0.83 | 1.44 | 0.9973 | 0.0022 | 0.0005 |
| A_1^{-+*} | 2.39(39) | 1.03 | 0.03 | 0.9720 | 0.0260 | 0.0020 |
| A_2^{+-} | 2.20(26) | 1.08 | 2.73 | 0.9612 | 0.0366 | 0.0021 |
| A_2^{--} | 2.46(61) | 0.79 | 0.07 | 0.9260 | 0.0637 | 0.0103 |
| E^{++} | 1.335(53) | 0.96 | 0.19 | 0.9394 | 0.0532 | 0.0073 |
| E^{++} | 1.231(46) | 0.84 | 1.79 | 0.9376 | 0.0487 | 0.0137 |
| $E^{+++}(2T?)$ | 1.78(12) | 0.96 | 0.45 | 0.5361 | 0.0805 | 0.3834 |
| E^{-+} | 1.88(13) | 1.04 | 0.40 | 0.9745 | 0.0233 | 0.0023 |
| T_1^{++} | 2.19(32) | 0.86 | 0.22 | 0.9257 | 0.0623 | 0.0120 |
| T_1^{+-} | 1.717(98) | 1.05 | 0.10 | 0.8786 | 0.0987 | 0.0228 |
| T_1^{+-} | 1.686(96) | 1.01 | 1.37 | 0.8541 | 0.1220 | 0.0240 |
| T_1^{+-} | 1.567(96) | 0.89 | 0.03 | 0.8664 | 0.0808 | 0.0528 |
| T_1^{+-*} | 1.99(17) | 1.04 | 0.31 | 0.8685 | 0.1131 | 0.0184 |
| $T_1^{--}(?)$ | 2.26(29) | 1.02 | 0.69 | 0.6625 | 0.0825 | 0.2550 |
| T_1^{--} | 2.33(36) | 1.05 | 1.65 | 0.8065 | 0.0347 | 0.1588 |
| T_1^{-+} | 2.32(37) | 0.99 | 0.12 | 0.8516 | 0.1324 | 0.0160 |
| T_1^{-+} | 2.51(42) | 1.10 | 0.10 | 0.8465 | 0.1411 | 0.0124 |
| T_2^{++} | 1.325(51) | 0.95 | 0.01 | 0.9301 | 0.0547 | 0.0151 |
| T_2^{++} | 1.457(56) | 1.06 | 1.11 | 0.9006 | 0.0750 | 0.0244 |
| T_2^{++} | 1.386(56) | 0.98 | 0.19 | 0.8878 | 0.0897 | 0.0225 |
| T_2^{+++} | 1.91(14) | 0.99 | 1.23 | 0.9357 | 0.0565 | 0.0078 |
| $T_2^{+-}(?)$ | 2.06(19) | 1.07 | 0.47 | 0.7608 | 0.1913 | 0.0479 |
| T_2^{+-} | 1.91(17) | 0.85 | 0.02 | 0.8966 | 0.0732 | 0.0303 |
| T_2^{+-} | 2.07(23) | 0.94 | 1.86 | 0.8905 | 0.0951 | 0.0143 |
| T_2^{--} | 2.27(30) | 1.05 | 0.40 | 0.8430 | 0.1435 | 0.0135 |
| T_2^{-+} | 1.84(14) | 1.02 | 0.79 | 0.8885 | 0.0742 | 0.0373 |
| $T_2^{-+}(?)$ | 2.14(27) | 0.87 | 0.08 | 0.7799 | 0.1499 | 0.0702 |

Table 5.8: The full spectrum of pure SU(8) gauge theory from lattice simulations at the parameters shown in the header. Bold-face values correspond to non-reliable states which will not be used in the large- N extrapolation.

5.3.2 Scattering states

Before exploring the $N \rightarrow \infty$ limit, we want to take a closer look to the representation where we see the largest number of states, which is the A_1^{++} . For every value of N , we see in this representation, that every state has a significant mixing with "scattering" operators. Remember that we have started with a variational basis in which there were the same number of operators in the group G and operators in the group S ; however, after the cutting procedure described in Sec. 5.2, the total number of "scattering" operators has changed to values between 1/3 and 1/8 of the initial number. Although the number of these operators is significantly smaller than the number of one-particle operators, we clearly see that they couple equally well with the states in the spectrum. This seems to tell us that a pure multi-glueballs interpretation of the "scattering" operators is not possible, even when N is as big as $N = 8$, and our physical understanding of large- N factorisation suggests that non-interacting glueballs should be created by that kind of operators.

We know that there is the possibility that "scattering" operators couple to every state with their set of quantum numbers, but, at the same time, we expect the contribution of scattering states to the spectrum to become relevant only above the energy threshold of twice the ground state mass; from Tab. 5.3 to Tab. 5.8, there is no clue for a particular state with A_1^{++} quantum numbers to be a scattering state, but we can be sure that the ground state is not, even if excited states remain ambiguous.

In order to clarify the relative importance of a "scattering" operators besides looking at the mixing coefficients, we repeat the variational procedure using different sets of operators: first we use only single-glueball operators G and then we look at the spectrum using only "scattering" operators S . The results for each gauge group are shown in Tab. 5.9 to Tab. 5.14. By looking at those tables is apparent that the low-lying spectrum does not change at all when we change the variational basis as we said above.

There is still not a definite and clear answer to what we are seeing in our spectra for what it concerns the "scattering" operators; they are not acting as we would expect and further studies are required in order to understand this issue.

| SU(3) at $\beta = 5.8945$ and $L = 12, T = 12$ | | | | | | |
|--|--------------|-------------|----------|---------|---------|---------|
| R^{PC} | $am(\sigma)$ | $ c_n ^2$ | χ^2 | mix_G | mix_S | mix_T |
| A_1^{++} | 0.798(15) | 0.98 | 0.11 | 1.0 | 0.0 | 0.0 |
| A_1^{+++} | 1.365(48) | 0.97 | 0.42 | 1.0 | 0.0 | 0.0 |
| A_1^{++++} | 1.66(10) | 0.90 | 0.46 | 1.0 | 0.0 | 0.0 |
| A_1^{++++} | 1.93(14) | 0.97 | 0.36 | 1.0 | 0.0 | 0.0 |
| A_1^{++} | 0.799(15) | 0.97 | 0.12 | 0.0 | 1.0 | 0.0 |
| A_1^{+++} | 1.328(46) | 0.94 | 0.25 | 0.0 | 1.0 | 0.0 |
| A_1^{++++} | 1.72(12) | 0.88 | 0.13 | 0.0 | 1.0 | 0.0 |
| A_1^{++++} | 2.21(23) | 1.10 | 1.09 | 0.0 | 1.0 | 0.0 |

Table 5.9: The A_1^{++} spectrum for SU(3) obtained with a different choice of the variational basis: in the upper panel, we use a total of 32 single-trace operators which are expected to couple with single-gluon states; in the lower panel, we use 13 "scattering" operators alone in the variational basis.

| SU(4) at $\beta = 10.789$ and $L = 12, T = 12$ | | | | | | |
|--|--------------|-----------|-------------|---------|---------|---------|
| R^{PC} | $am(\sigma)$ | $ c_n ^2$ | χ^2 | mix_G | mix_S | mix_T |
| A_1^{++} | 0.821(15) | 0.99 | 1.04 | 1.0 | 0.0 | 0.0 |
| A_1^{+++} | 1.413(47) | 0.96 | 1.52 | 1.0 | 0.0 | 0.0 |
| A_1^{++++} | 1.81(11) | 0.93 | 1.22 | 1.0 | 0.0 | 0.0 |
| A_1^{++} | 0.820(15) | 0.99 | 0.95 | 0.0 | 1.0 | 0.0 |
| A_1^{+++} | 1.386(47) | 0.94 | 1.23 | 0.0 | 1.0 | 0.0 |
| A_1^{++++} | 1.76(11) | 0.90 | 1.51 | 0.0 | 1.0 | 0.0 |

Table 5.10: The A_1^{++} spectrum for SU(4) obtained with a different choice of the variational basis: in the upper panel, we use 32 single-trace operators which are expected to couple with single-gluon states; in the lower panel, we use 32 "scattering" operators as our variational basis.

| SU(5) at $\beta = 17.107$ and $L = 12, T = 12$ | | | | | | |
|--|--------------|-------------|----------|----------------|----------------|----------------|
| R^{PC} | $am(\sigma)$ | $ c_n ^2$ | χ^2 | mix_G | mix_S | mix_T |
| A_1^{++} | 0.797(14) | 0.98 | 0.70 | 1.0 | 0.0 | 0.0 |
| A_1^{+++} | 1.457(58) | 0.94 | 0.02 | 1.0 | 0.0 | 0.0 |
| A_1^{++**} | 1.68(12) | 0.76 | 0.21 | 1.0 | 0.0 | 0.0 |
| A_1^{+++*} | 1.99(19) | 0.85 | 0.88 | 1.0 | 0.0 | 0.0 |
| A_1^{++} | 0.797(15) | 0.98 | 0.40 | 0.0 | 1.0 | 0.0 |
| A_1^{+++} | 1.439(58) | 0.93 | 0.06 | 0.0 | 1.0 | 0.0 |
| A_1^{+++*} | 2.23(28) | 1.02 | 1.03 | 0.0 | 1.0 | 0.0 |

Table 5.11: The A_1^{++} spectrum for SU(5) obtained with a different choice of the variational basis: in the upper panel, we use 32 single-trace operators which are expected to couple with single-gluon states; in the lower panel, we use 32 "scattering" operators as our variational basis.

| SU(6) at $\beta = 24.845$ and $L = 12, T = 12$ | | | | | | |
|--|--------------|-------------|-------------|----------------|----------------|----------------|
| R^{PC} | $am(\sigma)$ | $ c_n ^2$ | χ^2 | mix_G | mix_S | mix_T |
| A_1^{++} | 0.785(14) | 0.96 | 0.21 | 1.0 | 0.0 | 0.0 |
| A_1^{+++} | 1.509(63) | 0.99 | 2.40 | 1.0 | 0.0 | 0.0 |
| A_1^{++**} | 2.03(19) | 0.83 | 0.06 | 1.0 | 0.0 | 0.0 |
| A_1^{++} | 0.785(14) | 0.96 | 0.19 | 0.0 | 1.0 | 0.0 |
| A_1^{+++} | 1.523(64) | 1.02 | 2.30 | 0.0 | 1.0 | 0.0 |

Table 5.12: The A_1^{++} spectrum for SU(6) obtained with a different choice of the variational basis: in the upper panel, we use 32 single-trace operators which are expected to couple with single-gluon states; in the lower panel, we use 32 "scattering" operators as our variational basis.

| SU(7) at $\beta = 33.995$ and $L = 12, T = 12$ | | | | | | |
|--|--------------|-------------|-------------|---------|---------|---------|
| R^{PC} | $am(\sigma)$ | $ c_n ^2$ | χ^2 | mix_G | mix_S | mix_T |
| A_1^{++} | 0.820(15) | 0.98 | 0.44 | 1.0 | 0.0 | 0.0 |
| A_1^{++*} | 1.569(61) | 1.08 | 1.12 | 1.0 | 0.0 | 0.0 |
| A_1^{+++} | 1.87(13) | 0.88 | 2.69 | 1.0 | 0.0 | 0.0 |
| A_1^{+++*} | 2.23(25) | 1.00 | 0.26 | 1.0 | 0.0 | 0.0 |
| A_1^{++} | 0.820(14) | 0.98 | 0.39 | 0.0 | 1.0 | 0.0 |
| A_1^{++*} | 1.575(62) | 1.08 | 1.17 | 0.0 | 1.0 | 0.0 |

Table 5.13: The A_1^{++} spectrum for SU(7) obtained with a different choice of the variational basis: in the upper panel, we use 32 single-trace operators which are expected to couple with single-gluon states; in the lower panel, we use 8 "scattering" operators alone in the variational basis.

| SU(8) at $\beta = 44.496$ and $L = 12, T = 12$ | | | | | | |
|--|--------------|-------------|----------|---------|---------|---------|
| R^{PC} | $am(\sigma)$ | $ c_n ^2$ | χ^2 | mix_G | mix_S | mix_T |
| A_1^{++} | 0.786(16) | 0.96 | 0.76 | 1.0 | 0.0 | 0.0 |
| A_1^{++*} | 1.414(63) | 0.90 | 0.40 | 1.0 | 0.0 | 0.0 |
| A_1^{++} | 0.798(17) | 0.90 | 1.23 | 0.0 | 1.0 | 0.0 |
| A_1^{++*} | 1.499(80) | 0.84 | 0.20 | 0.0 | 1.0 | 0.0 |

Table 5.14: The A_1^{++} spectrum for SU(8) obtained with a different choice of the variational basis: in the upper panel, we use 32 single-trace operators which are expected to couple with single-gluon states; in the lower panel, we use 5 "scattering" operators as our variational basis.

5.4 Large- N extrapolation

The final purpose of this work is to provide some evidence that spectral quantities of pure $SU(N)$ gauge theories, such as glueball masses, can be described by their values for $N = \infty$, plus subleading corrections of order $1/N^2$ in a smooth large- N limit; this is suggested by many arguments, from the continuum perturbation theory in the 't Hooft planar limit to string perturbative calculations. From the continuum limit of lattice measurements, this has been proven by Lucini and Teper from a first attempt in [49] to improved calculations in [11]. Their analysis was carried on only on the 2 channels with lightest masses, the A_1^{++} and the E^{++} , but they found evidences that even the pure gauge spectrum of $SU(3)$ can be described very well by the $N = \infty$ contribution.

We should recall that our present work can only try to describe the $N = \infty$ spectrum at a fixed value of the lattice spacing, but this is not a real obstacle in obtaining the continuum spectrum because it has been shown that the continuum limit and the large- N limit commute. Hence we will be able, in a future work, to reach the continuum limit without affecting this first large- N computation.

As can be seen in Tab. 5.15 to Tab. 5.19, we have a large number of lattice glueballs which can be studied in the large- N limit. In the same tables we show the $SU(\infty)$ value obtained for each state by fitting the masses with

$$am(N) = am(\infty) + \frac{c}{N^2} \quad . \quad (5.6)$$

The details of the fits performed to obtain the $SU(\infty)$ lattice gauge spectrum are summarized in Tab. 5.20.

We usually have small χ^2 values due to the large errors on the masses (which are however, always below 20%) and the results on the fits is a very large uncertainty on the determination of the linear coefficient c . For the A_1^{++} channel the data and the fit is plotted in Fig. 5.1. We also try to fit the points in each symmetry channel with a constant value: we find an agreement, within one standard deviation, with the $am(\infty)$ value from the linear fit except for the quantum numbers T_2^{--} and T_2^{-+} . In those particular representations, the best linear fits come from discarding the smallest N value (which is $N = 3$) (see Fig. 5.10 and Fig. 5.11) and the constant fits performed give a value for the mass which is not compatible in 2σ .

For all the other representations, the conclusion of our analysis is that, given our errors on the fitted masses, it is not possible to discern for certain between a constant value, from $SU(\infty)$ down to $SU(3)$, and a linear behaviour with $1/N^2$ corrections. However, as we already said, the uncertainty on the linear coefficient is large, and more precise measurements of the spectra are needed in order to confirm our just stated conclusion. In this direction, we have already planned future simulations with anisotropic lattices, where a finer resolution in the temporal direction

helps in extracting correlators with lower statistical fluctuations and hence more precise masses (due to the higher stability of the effective mass plateau, cfr. Sec. 4.1.1).

| Masses in the A_1 representation | | | | | |
|------------------------------------|------------|------------------|------------------|------------------|-------------|
| | A_1^{++} | A_1^{++*} | A_1^{+++} | A_1^{-+} | A_1^{-+*} |
| SU(3) | 0.798(14) | 1.320(44) | 1.624(89) | 1.429(59) | – |
| SU(4) | 0.821(15) | 1.381(46) | 1.93(16) | 1.424(54) | 2.52(54) |
| SU(5) | 0.797(15) | 1.386(56) | 1.70(10) | 1.408(57) | 2.32(30) |
| SU(6) | 0.785(14) | 1.534(87) | – | 1.416(59) | – |
| SU(7) | 0.820(15) | 1.570(61) | 1.734(88) | 1.451(58) | – |
| SU(8) | 0.786(16) | 1.406(63) | – | 1.404(62) | 2.39(39) |
| SU(∞) | 0.799(12) | 1.507(51) | 1.774(97) | 1.420(13) | 2.31(17) |

Table 5.15: Values of the masses in unit of the lattice spacing a for each SU(N) gauge group in the A_1 representation. These are the values used in fits and bold-face quantities are included to have a wider overview, but they come from non reliable operators. The SU(∞) values are obtained by fits using (5.6).

| Masses in the A_2 representation | |
|------------------------------------|-----------------|
| | A_2^{+-} |
| SU(3) | – |
| SU(4) | 2.10(19) |
| SU(5) | 2.21(23) |
| SU(6) | 2.56(48) |
| SU(7) | 2.44(45) |
| SU(8) | – |
| SU(∞) | 2.60(15) |

Table 5.16: Values of the masses in unit of the lattice spacing a for each SU(N) gauge group in the A_2 representation. The A_2^{++} is not shown because what we see is probably a bi-torelon state.

| Masses in the E representation | | | |
|----------------------------------|------------------|-----------|-----------|
| | E^{++} | E^{-+} | E^{-+*} |
| SU(3) | 1.293(39) | 1.662(89) | 2.37(33) |
| SU(4) | 1.264(41) | 1.728(97) | – |
| SU(5) | 1.317(43) | 1.71(10) | 2.58(46) |
| SU(6) | 1.247(43) | 1.74(11) | 2.45(40) |
| SU(7) | 1.303(45) | 1.80(11) | – |
| SU(8) | 1.335(53) | 1.88(13) | – |
| SU(∞) | 1.297(25) | 1.818(34) | 2.55(11) |

Table 5.17: Values of the masses in unit of the lattice spacing a for each $SU(N)$ gauge group in the E representation. The $E^{++*}(2T)$ is not shown because what we see is probably a bi-torelon state. The states chosen come from the best possible operators (when this is not true we highlight the corresponding state, which has usually a high χ^2 or a small overlap $|c_n|^2$).

| Masses in the T_1 representation | | | |
|------------------------------------|-----------------|------------|-----------------|
| | T_1^{++} | T_1^{+-} | T_1^{-+} |
| SU(3) | – | 1.628(80) | 2.29(31) |
| SU(4) | 1.85(16) | 1.695(82) | 2.28(35) |
| SU(5) | 2.08(20) | 1.613(74) | 2.31(29) |
| SU(6) | 2.10(22) | 1.640(77) | 2.40(36) |
| SU(7) | – | 1.622(80) | 2.30(30) |
| SU(8) | 2.19(32) | 1.717(98) | 2.51(42) |
| SU(∞) | 2.332(57) | 1.654(32) | 2.382(54) |

Table 5.18: Values of the masses in unit of the lattice spacing a for each $SU(N)$ gauge group in the T_1 representation.

| Masses in the T_2 representation | | | | |
|------------------------------------|------------|-------------|------------|-----------------|
| | T_2^{++} | T_2^{++*} | T_2^{-+} | T_2^{--} |
| SU(3) | 1.293(41) | – | 1.707(90) | 2.26(27) |
| SU(4) | 1.333(48) | – | 1.636(88) | – |
| SU(5) | 1.323(45) | 1.77(11) | 1.74(11) | 2.00(20) |
| SU(6) | 1.275(39) | 1.98(12) | 1.77(11) | 2.23(25) |
| SU(7) | 1.328(44) | – | 1.77(10) | 2.28(30) |
| SU(8) | 1.325(51) | 1.91(14) | 1.84(14) | 2.27(30) |
| SU(∞) | 1.316(19) | 2.07(20) | 1.782(45) | 2.16(11) |
| | | | 1.868(23) | 2.514(84) |

Table 5.19: Values of the masses in unit of the lattice spacing a for each $SU(N)$ gauge group in the T_2 representation. The two $SU(\infty)$ values in T_2^{-+} and T_2^{--} come from different fits: the first value include the $N = 3$ point in the fit, whereas the second doesn't.

| SU(∞) | | | | |
|----------------|--------------|-----------|---------------|----------|
| R^{PC} | $am(\sigma)$ | c | N fitted | χ^2 |
| A_1^{++} | 0.799(12) | 0.05(22) | (3,4,5,6,7,8) | 1.42 |
| A_1^{++*} | 1.507(51) | -1.7(8) | (3,4,5,6,7,8) | 1.43 |
| A_1^{+++} | 1.774(97) | -1.1(1.3) | (3,4,5,7) | 1.10 |
| A_1^{-+} | 1.420(13) | 0.06(23) | (3,4,5,6,7,8) | 0.10 |
| A_1^{-+*} | 2.31(17) | 1.6(4.4) | (4,5,8) | 0.10 |
| A_2^{+-} | 2.60(15) | -8(3) | (4,5,6,7) | 0.12 |
| E^{++} | 1.297(25) | -0.13(41) | (3,4,5,6,7,8) | 0.63 |
| E^{-+} | 1.818(34) | -1.5(5) | (3,4,5,6,7,8) | 0.19 |
| E^{-+*} | 2.55(11) | -1.5(1.5) | (3,5,6) | 0.07 |
| T_1^{++} | 2.332(57) | -7.5(1.2) | (4,5,6,8) | 0.04 |
| T_1^{+-} | 1.654(32) | -0.14(56) | (3,4,5,6,7,8) | 0.30 |
| T_1^{-+} | 2.382(54) | -0.99(91) | (4,5,6,8) | 0.05 |
| T_2^{++} | 1.316(19) | -0.13(32) | (3,4,5,6,7,8) | 0.36 |
| T_2^{++*} | 2.07(20) | -6(6) | (5,6,8) | 0.72 |
| T_2^{-+} | 1.868(23) | -3.6(6) | (4,5,6,7,8) | 0.04 |
| T_2^{--} | 2.514(84) | -12(2) | (5,6,7,8) | 0.04 |

Table 5.20: Spectrum of the SU(∞) lattice gauge theory. The masses, in unit of lattice spacing, are obtained from fits over the range of N shown following (5.6); also the fitted coefficient c of the $1/N^2$ correction is shown. All χ^2 values quoted are best fits.

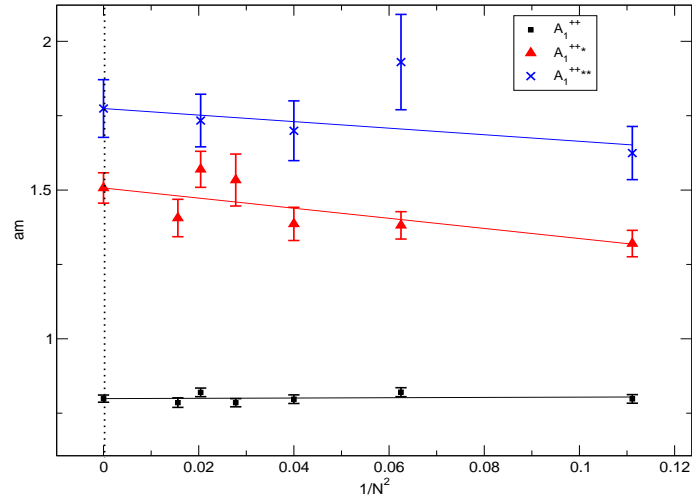


Figure 5.1: Ground state and two excited states in the A_1^{++} representation expressed in unit of the lattice spacing for all N in $[3, 8]$. The points in zero are the $N = \infty$ extrapolations done using the linear fits shown.

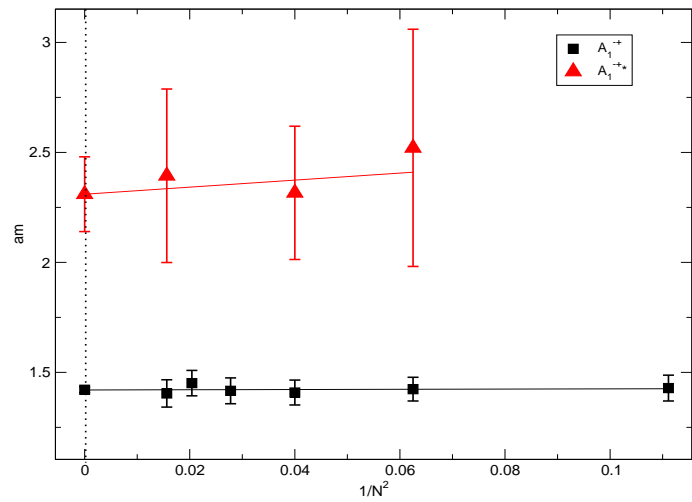


Figure 5.2: Ground state and first excited state in the A_1^{-+} representation expressed in unit of the lattice spacing for all N in $[3, 8]$. The points in zero are the $N = \infty$ extrapolations done using the linear fits shown.

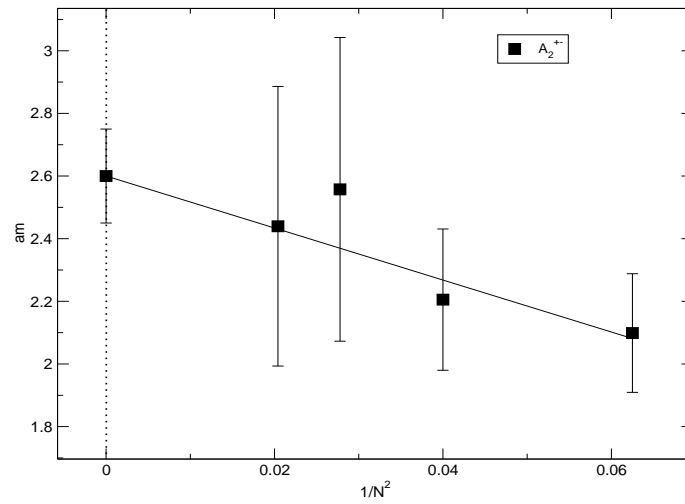


Figure 5.3: Ground state in the A_2^{+-} representation expressed in unit of the lattice spacing for all N in $[3, 8]$. The point in zero is the $N = \infty$ extrapolation done using the linear fits shown.

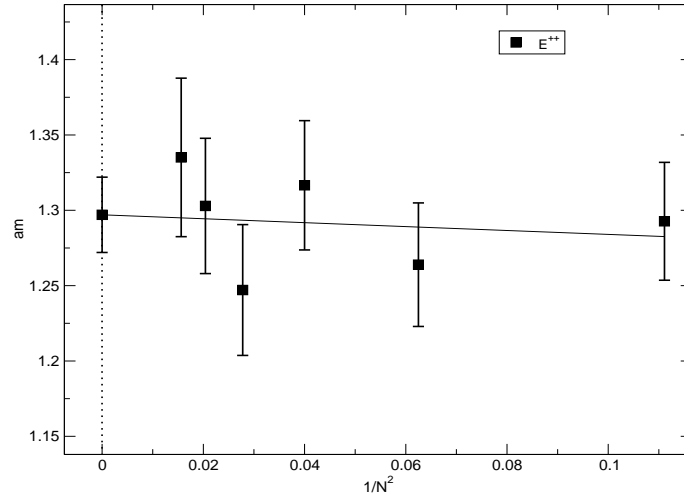


Figure 5.4: Ground state in the E^{++} representation expressed in unit of the lattice spacing for all N in [3, 8]. The point in zero is the $N = \infty$ extrapolation done using the linear fit shown.

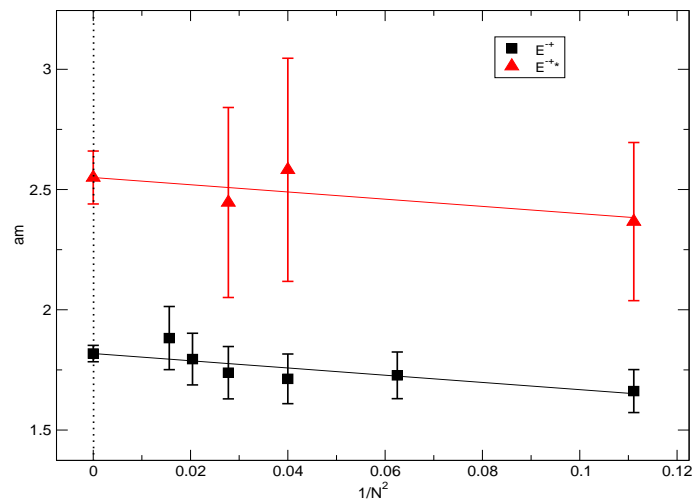


Figure 5.5: Ground state and first excited state in the E^{-+} representation expressed in unit of the lattice spacing for all N in [3, 8]. The points in zero are the $N = \infty$ extrapolations done using the linear fits shown.

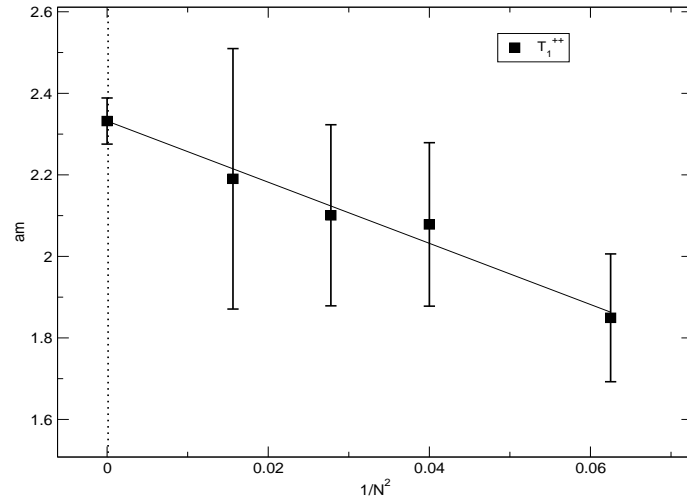


Figure 5.6: Ground state in the T_1^{++} representation expressed in unit of the lattice spacing for all N in [3, 8]. The point in zero is the $N = \infty$ extrapolation done using the linear fit shown.

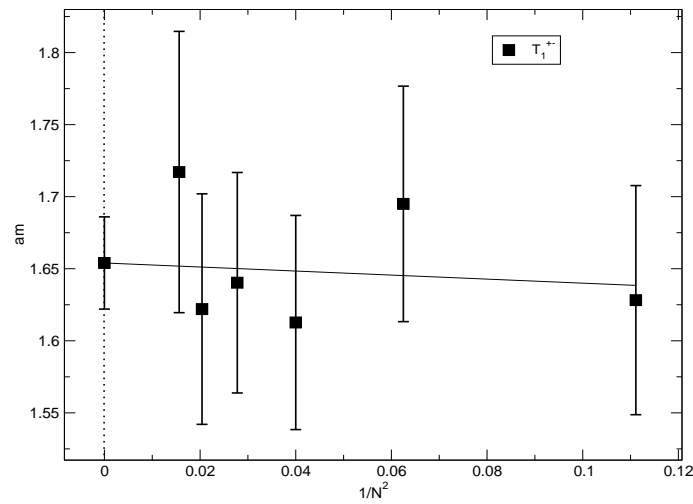


Figure 5.7: Ground state in the T_1^{+-} representation expressed in unit of the lattice spacing for all N in [3, 8]. The point in zero is the $N = \infty$ extrapolation done using the linear fit shown.

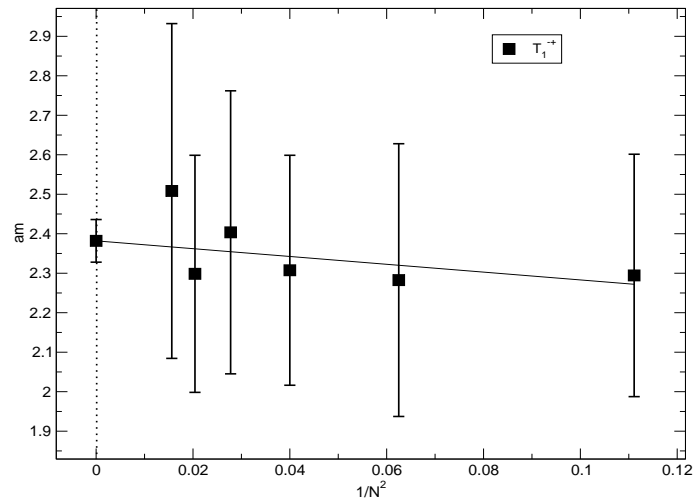


Figure 5.8: Ground state in the T_1^{-+} representation expressed in unit of the lattice spacing for all N in $[3, 8]$. The point in zero is the $N = \infty$ extrapolation done using the linear fit shown.

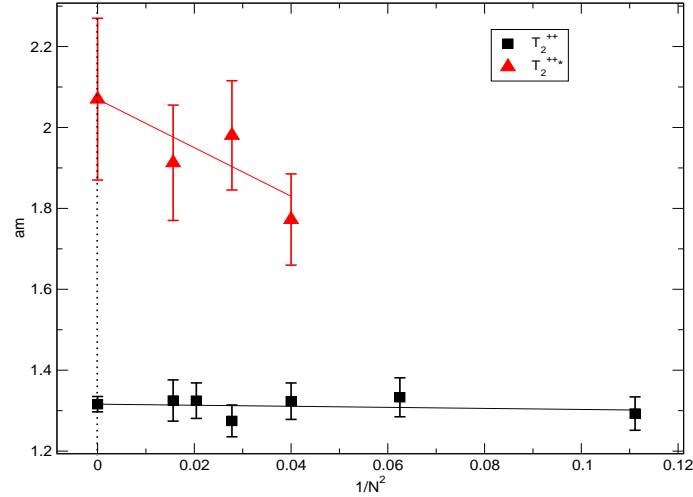


Figure 5.9: Ground state and first excited state in the T_2^{++} representation expressed in unit of the lattice spacing for all N in $[3, 8]$. The points in zero are the $N = \infty$ extrapolations done using the linear fits shown.

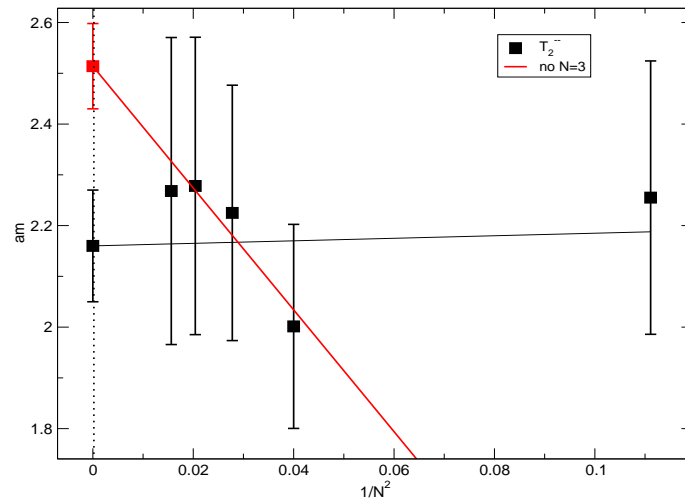


Figure 5.10: Ground state in the T_2^{--} representation expressed in unit of the lattice spacing for all N in $[3, 8]$. The points in zero are the $N = \infty$ extrapolations done using the linear fits shown, where the red one does not consider the point for $N = 3$. The red fit has the best χ^2 .

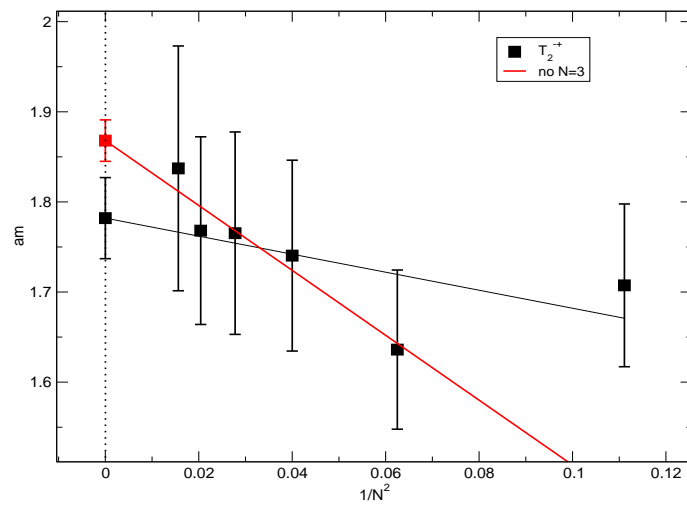


Figure 5.11: Ground state in the T_2^{++} representation expressed in unit of the lattice spacing for all N in $[3, 8]$. The points in zero are the $N = \infty$ extrapolations done using the linear fits shown, where the red one neglect the point for $N = 3$. The red fit has the best χ^2 .

6. *Conclusions and perspectives*

Glueballs have been investigated for over twenty years. They are a genuine non-perturbative effect coming from the quantization of a pure gauge theory. Their masses can be studied by numerical simulations and by modelling; the former method is used in this work. The pure $SU(N)$ Yang–Mills theory is regularized with a lattice cut-off [7] and correlators of glueball operators are measured with Monte–Carlo simulations. Lattice spectroscopy techniques allow us to extract the mass of states in the spectrum of the regularized theory. Since the wave-functions of such states cannot be known in other ways, we try to guess an approximation of them by constructing a large number of different operators.

A major breakthrough of this thesis is the realization of an automated procedure capable of constructing operators for all the quantum numbers of the lattice glueball states. This allows us, in principle, to obtain the masses in every symmetry channel. The only restriction on the number of operators created is given by the computational memory needed. Using this automated procedure, we have explored the spectrum of $SU(N)$ with $N = 3, 4, 5, 6, 7, 8$. Since we were able to measure glueball masses in all symmetry channels, our work goes beyond previous studies well known in the literature [49, 11] where only two channels were investigated. Moreover, the full range of $N \in [3, 8]$ has been considered. To do this we had to calculate for the first time the deconfining temperature for $SU(5)$ and $SU(7)$ in order to set the scale of our lattice simulations consistently for all values of N and this is another original contribution given by this work.

Our calculation has been performed at only one value of the lattice spacing in the asymptotic scaling region, were some features of the continuum spectrum should already be manifest. Continuum glueball states characterized by integer spin can split into different irreducible representations of the lattice symmetry group, and, when the full rotational invariance is dynamically restored, some lattice states are degenerate. We can observe that pattern between the E and the T_2 ; their ground states in all PC channels have the same masses within the errors and are expected to be the continuum spin 2 glueball. However, we are not claiming that at our lattice spacing the continuum symmetries are restored.

Despite our progresses, at our lattice spacing, only the low-energy part of the spectrum can be investigated and higher excited states are very difficult to extract due to the statistical noise of the numerical procedure. Some improvements can be used to enhance the signal in correlator

measures; one of the future developments of this work will be to use anisotropic lattices, with a smaller lattice spacing in the temporal direction, to obtain a finer resolution of the correlators. This will enable us to obtain a reliable continuum limit that includes a few excitations in each channel.

In the spectrum of glueballs in a finite box, other contributions can be found, from multi-glueball scattering states and from excitations with a non-trivial topology such as torelons. It is important to identify the unwanted states to obtain the low-lying single-particle spectrum with less uncertainty. We made a further step in this direction trying to find the signal of such states using suitably constructed operators.

Our analysis has shown that some states extracted do not possess a clear single-glueball interpretation, like the ground state in the A_2^{++} or the first excited state in the E^{++} (for almost all values of N). They clearly receive contributions from bi-torelon operators and we cannot trust them as glueball states. Moreover, all states in the A_1^{++} seem to receive contributions from operators that we expected to overlap onto scattering states. This is a completely new observation we obtain as a result of our study with a very large number of operators of different kind. Since it was not expected, it will be further investigated in a future analysis.

In conclusion, with our data we were finally able to provide an extrapolation of the spectrum at $N = \infty$ aiming to confirm and further improve the results of [49], but also to get in contact with large- N theoretical results coming from the string theory (supergravity) side of the AdS/CFT correspondence. We are confident that a real comparison between our lattice data and string theory calculations is possible, but we first need to extrapolate the spectrum of $SU(\infty)$ to its continuum limit. This will be the natural prosecution of this work.

Ringraziamenti

Alla fine di questo lavoro di tesi, e alla luce soprattutto di queste ultime settimane di stesura, non posso che rivolgere i miei più sentiti ringraziamenti ad Antonio e Biagio (in ordine alfabetico ovviamente); sin dall'inizio di questo mio percorso mi hanno aiutato e sostenuto, anche fisicamente, alla Dynamic Rock di Swansea, mentre volavo giù da 7a improbabili. Vorrei ringraziarli per avermi dato innanzitutto l'opportunità di lavorare nel dipartimento di fisica dell'Università di Swansea, dove ho trovato un gruppo di ricerca molto attivo e dove ho avuto la possibilità di seguire corsi e seminari di alto livello.

La riuscita di questo lavoro di tesi è stata possibile grazie al sostegno finanziario ricevuto dal Dipartimento di Fisica dell'Università degli Studi di Milano e dall'Università di Swansea; e anche grazie all'utilizzo del cluster del gruppo di fisica teorica a Swansea e a Wuppertal. In particolare voglio ringraziare Francesco Knechtli per averci permesso di utilizzare le risorse del cluster di Wuppertal, senza le quali sarebbe stato impossibile completare lo studio effettuato nel tempo a disposizione.

I miei ringraziamenti vanno anche al mio relatore Prof. Sergio Caracciolo, il quale è sempre stato un riferimento importante durante l'intero corso dei miei studi in fisica a Milano.

Dovrei ringraziare tante altre persone, tra Milano, Cesena, Swansea ed Edinburgo, che mi hanno sopportato e sostenuto da Gennaio ad oggi. Tra queste, una dedica speciale va alla mia famiglia ed alla mia ragazza, sempre presenti nei momenti in cui mi sono trovato in difficoltà.

Bibliography

- [1] Chen-Ning Yang and Robert L. Mills. Conservation of isotopic spin and isotopic gauge invariance. *Phys. Rev.*, 96:191–195, 1954.
- [2] H. Fritzsch and M. Gell-Mann. Current algebra: Quarks and what else? *eConf*, C720906V2:135–165, 1972, hep-ph/0208010.
- [3] Gerard 't Hooft. A planar diagram theory for strong interactions. *Nucl. Phys.*, B72:461, 1974.
- [4] Juan Martin Maldacena. The large N limit of superconformal field theories and supergravity. *Adv. Theor. Math. Phys.*, 2:231–252, 1998, hep-th/9711200.
- [5] Edward Witten. Anti-de Sitter space and holography. *Adv. Theor. Math. Phys.*, 2:253–291, 1998, hep-th/9802150.
- [6] Edward Witten. Anti-de Sitter space, thermal phase transition, and confinement in gauge theories. *Adv. Theor. Math. Phys.*, 2:505–532, 1998, hep-th/9803131.
- [7] Kenneth G. Wilson. Confinement of quarks. *Phys. Rev.*, D10:2445–2459, 1974.
- [8] K. Osterwalder and E. Seiler. Gauge Field Theories on the Lattice. *Ann. Phys.*, 110:440, 1978.
- [9] B. Berg and A. Billoire. Glueball Spectroscopy in Four-Dimensional SU(3) Lattice Gauge Theory. 1. *Nucl. Phys.*, B221:109, 1983.
- [10] M. Teper. The scalar and tensor glueball masses in lattice gauge theory. *Phys. Lett.*, B185:121, 1987.
- [11] Biagio Lucini, Michael Teper, and Urs Wenger. Glueballs and k-strings in SU(N) gauge theories: Calculations with improved operators. *JHEP*, 06:012, 2004, hep-lat/0404008.

-
- [12] M. Creutz. Monte Carlo Study of Quantized SU(2) Gauge Theory. *Phys. Rev.*, D21:2308–2315, 1980.
- [13] Christopher Michael and M. Teper. The Glueball Spectrum in SU(3). *Nucl. Phys.*, B314:347, 1989.
- [14] Colin J. Morningstar and Mike J. Peardon. The glueball spectrum from an anisotropic lattice study. *Phys. Rev.*, D60:034509, 1999, hep-lat/9901004.
- [15] I. Montvay and G. Munster. Quantum fields on a lattice. Cambridge, UK: Univ. Pr. (1994) 491 p. (Cambridge monographs on mathematical physics).
- [16] H. J. Rothe. Lattice gauge theories: An Introduction. *World Sci. Lect. Notes Phys.*, 74:1–605, 2005.
- [17] S Coleman. *Aspects of Symmetry of Symmetry*, chapter 8, pages 351–401. Cambridge University Press, 1985.
- [18] Y Makeenko. *Methods of contemporary gauge theory*. Cambridge monographs on mathematical physics. Cambridge University Press, 2002.
- [19] Aneesh V. Manohar. Large N QCD. 1998, hep-ph/9802419.
- [20] Ofer Aharony, Steven S. Gubser, Juan Martin Maldacena, Hiroshi Ooguri, and Yaron Oz. Large N field theories, string theory and gravity. *Phys. Rept.*, 323:183–386, 2000, hep-th/9905111.
- [21] Paolo Di Vecchia. Large N gauge theories and ADS/CFT correspondence. 1999, hep-th/9908148.
- [22] M. Caselle. Lattice gauge theories and the AdS/CFT correspondence. *Int. J. Mod. Phys.*, A15:3901–3966, 2000, hep-th/0003119.
- [23] Robert de Mello Koch, Antal Jevicki, Mihail Mihailescu, and Joao P. Nunes. Evaluation Of Glueball Masses From Supergravity. *Phys. Rev.*, D58:105009, 1998, hep-th/9806125.
- [24] Michael J. Teper. SU(N) gauge theories in 2+1 dimensions. *Phys. Rev.*, D59:014512, 1999, hep-lat/9804008.
- [25] Alexander M. Polyakov. Thermal Properties of Gauge Fields and Quark Liberation. *Phys. Lett.*, B72:477–480, 1978.
- [26] Leonard Susskind. Lattice Models of Quark Confinement at High Temperature. *Phys. Rev.*, D20:2610–2618, 1979.

-
- [27] C. DeTar and U. M. Heller. QCD Thermodynamics from the Lattice. 2009, 0905.2949.
- [28] Larry D. McLerran and Benjamin Svetitsky. Quark Liberation at High Temperature: A Monte Carlo Study of SU(2) Gauge Theory. *Phys. Rev.*, D24:450, 1981.
- [29] Biagio Lucini, Michael Teper, and Urs Wenger. The deconfinement transition in SU(N) gauge theories. *Phys. Lett.*, B545:197–206, 2002, hep-lat/0206029.
- [30] Biagio Lucini, Michael Teper, and Urs Wenger. The high temperature phase transition in SU(N) gauge theories. *JHEP*, 01:061, 2004, hep-lat/0307017.
- [31] Biagio Lucini, Michael Teper, and Urs Wenger. Properties of the deconfining phase transition in SU(N) gauge theories. *JHEP*, 02:033, 2005, hep-lat/0502003.
- [32] Benjamin Svetitsky and Laurence G. Yaffe. Critical Behavior at Finite Temperature Confinement Transitions. *Nucl. Phys.*, B210:423, 1982.
- [33] Murty S. S. Challa, D. P. Landau, and K. Binder. Finite size effects at temperature driven first order transitions. *Phys. Rev.*, B34:1841–1852, 1986.
- [34] A. M. Ferrenberg and R. H. Swendsen. New Monte Carlo Technique for Studying Phase Transitions. *Phys. Rev. Lett.*, 61:2635–2638, 1988.
- [35] Alan M. Ferrenberg and Robert H. Swendsen. Optimized Monte Carlo analysis. *Phys. Rev. Lett.*, 63:1195–1198, 1989.
- [36] Saumen Datta and Sourendu Gupta. Scaling and the continuum limit of gluo N_c plasmas. 2009, 0909.5591.
- [37] William H. Press. *Numerical recipes in C++: the art of scientific computing*. Cambridge University Press, 2 edition, 2002.
- [38] Bradley Efron. *The Jackknife, the Bootstrap and Other Resampling Plans*. Number 38 in C B M S - N S F Regional Conference Series in Applied Mathematics. S.I.A.M., Philadelphia, 1982.
- [39] M. Luscher. Selected topics in Lattice Field Theory. Lectures given at Summer School 'Fields, Strings and Critical Phenomena', Les Houches, France, Jun 28 - Aug 5, 1988.
- [40] M. Albanese et al. Glueball Masses and String Tension in Lattice QCD. *Phys. Lett.*, B192:163–169, 1987.
- [41] M. Teper. An Improved Method for Lattice Glueball Calculations. *Phys. Lett.*, B183:345, 1987.

-
- [42] Christopher Michael. The glueball spectrum from lattice gauge theory. *Acta Phys. Polon.*, B21:119, 1990.
- [43] Harvey B. Meyer. Glueball Regge trajectories. 2004, hep-lat/0508002.
- [44] Olle Häggström. Finite Markov Chains and Algorithmic Applications. Lecture's notes, January 2001.
- [45] A. D. Kennedy and B. J. Pendleton. Improved Heat Bath Method for Monte Carlo Calculations in Lattice Gauge Theories. *Phys. Lett.*, B156:393–399, 1985.
- [46] N. Cabibbo and E. Marinari. A New Method for Updating SU(N) Matrices in Computer Simulations of Gauge Theories. *Phys. Lett.*, B119:387–390, 1982.
- [47] Stephen L. Adler. An overrelaxation method for the Monte Carlo evaluation of the partition function for multiquadratic actions. *Phys. Rev.*, D23:2901, 1981.
- [48] William H. Press. *Numerical Recipes in FORTRAN 77: The Art of Scientific Computing*. Cambridge University Press, 2 edition, 1992.
- [49] B. Lucini and M. Teper. SU(N) gauge theories in four dimensions: Exploring the approach to $N = \infty$. *JHEP*, 06:050, 2001, hep-lat/0103027.
- [50] Harvey B. Meyer. The spectrum of SU(N) gauge theories in finite volume. *JHEP*, 03:064, 2005, hep-lat/0412021.
- [51] Anna Hasenfratz, Etelka Hasenfratz, and Peter Hasenfratz. Generalized roughening transition and its effect on the string tension. *Nucl. Phys.*, B180:353, 1981.
- [52] Michael Creutz, Michel Tytgat, Claudio Rebbi, and She-Sheng Xue. Lattice formulation of the standard model. *Phys. Lett.*, B402:341–345, 1997, hep-lat/9612017.
- [53] Michael Creutz. The standard model and the lattice. 1998, hep-lat/9804021.
- [54] Michael Creutz. Yang-Mills fields and the lattice. 2004, hep-lat/0406007.
- [55] Thomas DeGrand and Carleton E. Detar. Lattice methods for quantum chromodynamics. New Jersey, USA: World Scientific (2006) 345 p.
- [56] G. Munster and M. Walzl. Lattice gauge theory: A short primer. 2000, hep-lat/0012005.
- [57] Biagio Lucini, Michael Teper, and Urs Wenger. Topology of SU(N) gauge theories at T approx. 0 and T approx. T(c). *Nucl. Phys.*, B715:461–482, 2005, hep-lat/0401028.

-
- [58] B. Lucini, M. Teper, and U. Wenger. Features of SU(N) gauge theories. 2003, hep-lat/0309170.
- [59] B. Lucini, M. Teper, and U. Wenger. The deconfining phase transition in SU(N(c)) gauge theories. *Nucl. Phys. Proc. Suppl.*, 119:532–534, 2003, hep-lat/0208080.
- [60] B. Lucini and M. Teper. The $k = 2$ string tension in four dimensional SU(N) gauge theories. *Phys. Lett.*, B501:128–133, 2001, hep-lat/0012025.
- [61] B. Lucini and M. Teper. Confining strings in SU(N) gauge theories. *Phys. Rev.*, D64:105019, 2001, hep-lat/0107007.
- [62] J. Greensite. The confinement problem in lattice gauge theory. *Prog. Part. Nucl. Phys.*, 51:1, 2003, hep-lat/0301023.
- [63] G. 't Hooft. Large N. 2002, hep-th/0204069.
- [64] Y. Chen et al. Glueball spectrum and matrix elements on anisotropic lattices. *Phys. Rev.*, D73:014516, 2006, hep-lat/0510074.
- [65] Biagio Lucini. The large N limit from the lattice. *Few Body Syst.*, 36:161–166, 2005, hep-ph/0410016.
- [66] Makoto Natsuume. String theory and quark-gluon plasma. 2007, hep-ph/0701201.
- [67] G. Endrodi, Z. Fodor, S. D. Katz, and K. K. Szabo. The curvature of the QCD phase transition line. *PoS, LATTICE2008:205*, 2008, 0901.3018.
- [68] F. Karsch, E. Laermann, and M. Lutgemeier. Three-dimensional SU(3) gauge theory and the spatial string tension of the (3+1)-dimensional finite temperature SU(3) gauge theory. *Phys. Lett.*, B346:94–98, 1995, hep-lat/9411020.
- [69] B. Lucini, M. Teper, and U. Wenger. SU(N) gauge theories near T(c). *Nucl. Phys. Proc. Suppl.*, 129:569–571, 2004, hep-lat/0309009.
- [70] Claude W. Bernard et al. The equation of state for two flavor QCD at N(t) = 6. *Phys. Rev.*, D55:6861–6869, 1997, hep-lat/9612025.
- [71] C. Bernard et al. QCD equation of state with 2+1 flavors of improved staggered quarks. *Phys. Rev.*, D75:094505, 2007, hep-lat/0611031.
- [72] Michael Creutz. Gauge Fixing, the Transfer Matrix, and Confinement on a Lattice. *Phys. Rev.*, D15:1128, 1977.

-
- [73] Tom Banks, Leonard Susskind, and John B. Kogut. Strong Coupling Calculations of Lattice Gauge Theories: (1+1)-Dimensional Exercises. *Phys. Rev.*, D13:1043, 1976.
- [74] John B. Kogut and Leonard Susskind. Hamiltonian Formulation of Wilson's Lattice Gauge Theories. *Phys. Rev.*, D11:395, 1975.
- [75] Jean-Paul Blaizot, Edmond Iancu, and Anton Rebhan. Thermodynamics of the high-temperature quark gluon plasma. 2003, hep-ph/0303185.
- [76] Eric Braaten and Agustin Nieto. Free Energy of QCD at High Temperature. *Phys. Rev.*, D53:3421–3437, 1996, hep-ph/9510408.
- [77] L. Del Debbio, L. Giusti, M. Luscher, R. Petronzio, and N. Tantalo. Stability of lattice QCD simulations and the thermodynamic limit. *JHEP*, 02:011, 2006, hep-lat/0512021.
- [78] Carleton DeTar. Recent Progress in Lattice QCD Thermodynamics. *PoS*, LAT2008:001, 2008, 0811.2429.
- [79] Y. Aoki, Z. Fodor, S. D. Katz, and K. K. Szabo. The equation of state in lattice QCD: With physical quark masses towards the continuum limit. *JHEP*, 01:089, 2006, hep-lat/0510084.
- [80] G. Endrodi, Z. Fodor, S. D. Katz, and K. K. Szabo. The equation of state at high temperatures from lattice QCD. *PoS*, LAT2007:228, 2007, 0710.4197.
- [81] Adi Armoni, Biagio Lucini, Agostino Patella, and Claudio Pica. Orientifold Planar Equivalence: The Chiral Condensate. 2008, 0809.5015.
- [82] Michael Teper. Large N. 2008, 0812.0085.